NIK, A NOVEL REGULATOR OF MITOCHONDRIAL DYNAMICS AND INVASION IN HIGH-GRADE GLIOMA

A Dissertation

by

JIUNG JUNG

Submitted to the Office of Graduate and Professional Studies of
Texas A&M University
in partial fulfillment of the requirements for the degree of

DOCTOR OF PHILOSOPHY

Chair of Committee,	Raquel Sitcheran
Committee Members,	David W. Threadgill
	Kayla Bayless
	Vytas A. Bankaitis
Head of Program,	Warren Zimmer

May 2018

Major Subject: Medical Sciences

ABSTRACT

NF-κB inducing kinase (NIK, also known as MAP3K14) is a serine/threonine protein-kinase that is crucial for activation of the non-canonical NF-κB signaling pathway. Although NIK has been shown to promote tumorigenesis in several cancers by increasing cell proliferation and survival, the molecular mechanisms underlying the role of NIK in regulating glioma pathogenesis remain poorly understood. While NIK is described as being primarily cytosolic, in this study, we found that a discrete pool of NIK is predominantly localized to mitochondria in patient-derived glioma cells, ex vivo tumor tissue, and mouse embryonic fibroblasts (MEFs). Depletion of NIK using CRISPR/Cas9-mediated genome editing causes diminished invasion in three-dimensional collagen matrices and also results in morphological alterations of mitochondria, which appear entangled and clustered in perinuclear regions. Analysis of mitochondrial trafficking in living cells revealed that NIK promoted mitochondria velocity and subcellular distribution to the leading edge of migrating glioma cells. Importantly, NIK enhances mitochondrial recruitment of dynamin related protein 1 (Drp1), a key component of mitochondrial fission machinery, to promote mitochondrial fragmentation and glioma cell invasion. NIK interacts with Drp1 at mitochondria, rather than in the cytoplasm. Particularly, NIK accumulated transiently on dividing mitochondria, where it binds to Drp1 at mitochondrial constriction at fission sites. Notably, NIK regulation of mitochondrial dynamics, glioma cell invasion, and tumor growth requires its kinase activity, but occurs independently of its established downstream targets, IκB kinase (IKK) α/β and NF-κB activation. Additionally, NIK kinase activity is critical to promote phosphorylation of Drp1 at serine 616, which is important for its fission-promoting function. Our results establish a new paradigm for IKK-independent

NIK signaling at mitochondria and significantly expand the current dogma that NIK is mainly cytosolic and exclusively regulates NF-κB activity. Overall, these findings highlight the importance of NIK in tumor pathogenesis and invite new therapeutic strategies that attenuate mitochondrial dysfunction through inhibition of NIK.

DEDICATION

I would like to dedicate this dissertation to

all my family

for their love, encouragement, and support.

ACKNOWLEDGEMENTS

First, I would like to thank my supervisor, Dr. Raquel Sitcheran, for mentoring me. I greatly appreciate her thoughtful guidance, academic advice, and warm encouragement throughout my graduate studies. You certainly are a great mentor for me. I also wish to express my appreciation to the dissertation committee members, Dr. David W. Threadgill, Dr. Kayla Bayless, and Dr. Vytas A. Bankaitis, for sharing many ideas and valuable suggestions on my research that improved the quality of my dissertation work. I was so lucky to have dissertation advisers like you.

I would also like to thank all the current and alumni members in Dr. Sitcheran lab, Dong Whan Lee, Sowndharya Ravi, Michael Kamradt, Kassandra McFadden, Kathryn Pflug, Linda Herrera de Lechuga, Evan Cherry, Ashley Feil, Marianne Best, Fred Price, Asmita Upreti, and Zoe Alaniz for being awesome colleagues and friends during my unforgettable time in the Dr. Sitcheran lab. I really appreciate your willingness to help and share me reagents, ideas, and research experiences, it was great encouragement to me.

Finally, I am deeply thankful for my parents who have encouraged and unconditionally supported me. I would like to thank my wife and daughter, Jihye Lee and Olivia Jung, for always loving and supporting me. I couldn't have done my Ph.D. without you.

CONTRIBUTORS AND FUNDING SOURCES

This work was supported by a dissertation committee consisting of Professor Raquel Sitcheran, Professor Kayla Bayless, and Professor Vytas A. Bankaitis of the Department of Molecular and Cellular Medicine, and Professor David W. Threadgill of the Department of Veterinary Pathobiology.

Some analyses described in Chapter III were conducted in part by Dong Whan Lee, Sowndharya Ravi, Michael Kamradt, and Kassandra McFadden of the Department of Department of Molecular and Cellular Medicine and were published in Current Biology, December 19, 2016. All other work conducted for the dissertation was completed by the student independently.

This work was funded by grants from the NIH (R01NS082554), Cancer Prevention and Research Institute of Texas HIHR award (RP160842), and The Texas Brain and Spine Institute (2016 seed grant).

NOMENCLATURE

ADP	Adenosine diphosphate
ATP	Adenosine triphosphate
ATP	Adenosine triphosphate
BR3	BAFF receptor
BTICs	Brain tumor initiating cells
CD30L	CD30 ligand
CD40L	CD40 ligand
cIAP	Cellular inhibitor of apoptosis
CON	Control
DAMPs	Danger-associated molecular patterns
Drp1	Dynamin-related protein 1
ECM	Extracellular matrix
EDTA	Ethylenediaminetetraacetic acid
ER	Endoplasmic reticulum
ErbB2	Erb-B2 Receptor Tyrosine Kinase 2
ERK2	Extracellular-signal-regulated kinase 2
ETC	Electron transport chain
FADH2	Flavin adenine dinucleotide
Fis1	Mitochondrial fission 1 protein
Fn14	Fibroblast growth factor-inducible 14
GBM	Glioblastoma multiforme

GFP	Green fluorescent protein
HA	Hemagglutinin
HCI	Hydrochloric acid
IgG	Immunoglobulin G
IKKα/β	IkappaB kinase α/β
IL-1R	Interleukin 1 receptor
IMM	Mitochondrial membrane
IκB	IkappaB
LTβR	Lymphotoxin-β receptor
MAM	Mitochondria-associated membrane
MAVS	Mitochondrial antiviral signaling
MDV	Mitochondrial-derived vesicles
MEFs	Mouse embryonic fibroblasts
Mff	Mitochondria fission factor
Mfn1	Mitofusin 1
Mfn2	Mitofusin 2
MID49	Mitochondrial dynamics protein of 49 kDa
MID51	Mitochondrial dynamics protein of 51 kDa
Miro1	Mitochondrial Rho GTPase 1
mito-PAGFP	Mitochondrial matrix-targeted photoactivatable green fluorescent protein
MOM	Mitochondrial outer membrane
mtDNA	Mitochondrial DNA
mTOR	Mechanistic target of rapamycin

MTS	Mitochondrial targeting sequence
NADH	Nicotinamide adenine dinucleotide
NF-κB	Nuclear Factor-kappaB
NIK	NF-κB inducing kinase
OPA1	Optic Atrophy 1
OXPHOS	Oxidative phosphorylation
PAMPs	Pathogen-associated molecular patterns
PGAM5	Phosphoglycerate mutase family member 5
PLA	Proximity ligation assay
RHD	Rel homology domain
ROI	Regions of interest
ROS	Reactive oxygen species
SDS	Sodium dodecyl sulfate
SR-SIM	Superresolution-structured illumination microscopy
TLR4	Toll-like receptor 4
TNF	Tumor necrosis factor
TNFR	Tumor necrosis factor receptor
TRAF	TNF receptor-associated factor
TWEAK	Tumor necrosis factor-like weak inducer of apoptosis
WT	Wild type

TABLE OF CONTENTS

Page

ABSTRACT ii

DEDICATION iv

ACKNOWLEDGEMENTS v

CONTRIBUTORS AND FUNDING SOURCES vi

NOMENCLATURE vii

TABLE OF CONTENTS x

LIST OF FIGURES xiii

CHAPTER I INTRODUCTION 1

1.1 Glioblastoma multiforme (GBM) 1
1.2 NF-κB pathways 2
1.2.1 NF-κB 2
1.2.2 Canonical and non-canonical NF-κB pathway 3
1.3 NF-κB inducing kinase (NIK) 6
1.3.1 Structure and turnover of NIK 6
1.3.2 Roles for NIK in cancer 11
1.4 Mitochondria 12
1.4.1 Mitochondria and mechanisms regulating mitochondrial dynamics 12
1.4.2 Mitochondrial dynamics in cancer 13
1.4.3 Mitochondrial fission regulator, Dynamin-related protein 1 14
1.5 Dissertation goals 17

CHAPTER II METHODS AND MATERIALS 19

2.1 Cell culture and reagents 19
2.2 Reagents 19
2.3 Plasmids construction for NIK overexpression 20
2.4 CRISPR-Cas 9 gene knockout 20
2.5 Lentivirus production 21
2.6 Three-dimensional collagen invasion assay 21
2.7 Immunofluorescence staining 22
2.8 Human glioma ex-vivo tissue staining 23
2.9 Image acquisition 23
2.10 Flow cytometry 24
2.11 Quantification of mitochondrial number and size and tracking 24

Page

2.12 Subcellular fractionation 25
2.13 Immunoblot 25
2.14 Immunoprecipitation 26
2.15 RNA isolation, cDNA synthesis, and quantitative-RT-PCR 26
2.16 Mito-PAGFP fusion assay 27
2.17 ROS assay 28
2.18 Oxygen Consumption Assay 28
2.19 Monitoring mitochondrial constriction and division 28
2.20 In vitro kinase assay 29
2.21 Xenograft mouse models 29
2.22 In situ proximity ligation assay 29

CHAPTER III NIK REGULATES MITOCHONDRIAL DYNAMICS TO PROMOTE CELL INVASION INDEPENDENTLY OF IKK/NF-KB 31

3.1 Summary 31
3.2 Introduction 31
3.3 Results 33
3.3.1 NIK is localized to mitochondria in cancer cells and promotes invasion 33
3.3.2 NIK regulates mitochondrial subcellular localization and motility 47
3.3.3 NIK regulates mitochondrial morphology through promoting fission 51
3.3.4 NIK recruits Drp1 to mitochondria and influences its activity 56
3.3.5 Drp1 interacts with NIK, but not IKKα. 65
3.3.6 NIK requires Drp1 to promote TWEAK-induced invasion 70
3.3.7 NIK enhances the invasive potential of MEFs in the absence of IKK/NF-κB signaling 73
3.3.8 NIK regulates mitochondrial morphology by recruiting Drp1 independently of IKK/NF-κB 82

CHAPTER IV NIK REGULATES DRP1 PHOSPHORYLATION AND IS LOCALIZED TO SITES OF MITOCHONDRIAL FISSION 87

4.1 Summary 87
4.2 Introduction 87
4.3 Results 91
4.3.1 Kinase-dead NIK affects mitochondrial fission and invasion of glioma 91
4.3.2 Impaired kinase activity of NIK reduces tumor growth in vivo xenograft models of glioma 97
4.3.3 NIK-Drp1 interaction enriches at mitochondrial constriction sites 101
4.3.4 NIK promotes phosphorylation of Drp1 111

CHAPTER V CONCLUSIONS AND FUTURE DIRECTIONS 118

Page

5.1 NIK promotes tumor cell invasion by regulating mitochondrial dynamics..... 118
5.2 NIK regulates Drp1 phosphorylation and is recruited to mitochondria constriction sites..... 122

REFERENCES 129

LIST OF FIGURES

Page

Figure 1 NF-κB pathway can be activated via two major signal transduction pathways 5

Figure 2 Structure of human NIK protein 8

Figure 3 NIK protein sequence alignment 9

Figure 4 Posttranslational regulation of NIK 10

Figure 5 Role of Drp1 in mitochondrial fission 16

Figure 6 Analysis of NIK protein expression and invasive potential in BT25 and BT114 cells 37

Figure 7 Loss of NIK leads to decreased invasion potential in glioma cells 38

Figure 8 NIK is localized to mitochondria in glioma cells 39

Figure 9 NIK protein is enriched in both mitochondrial and cytosolic fractions 40

Figure 10 NIK co-localization with specific mitochondrial markers in glioma cells 41

Figure 11 NIK has not signnificant co-localization with markers for the ER and endosome in glioma cells 42

Figure 12 Ectopically overexpressed NIK is localized to mitochondria in glioma cells 43

Figure 13 NIK overexpression enhances invasion of glioma cells 44

Figure 14 NIK is localized to mitochondria of invasive breast cancer cells 45

Figure 15 NIK is localized to mitochondria of invasive pancreatic cancer cells 46

Figure 16 NIK regulates mitochondrial distribution 48

Figure 17 NIK regulates both velocity and run distance of mitochondria 49

Figure 18 NIK influences direction of mitochondrial movement 50

Figure 19 Super-resolution microscopy of mitochondrial morphology 52

Page

Figure 20 Loss of NIK results in a hyperfused mitochondrial network 53

Figure 21 Overexpression NIK leads to increase in mitochondrial fragmentation 54

Figure 22 Fusion analysis in BT25 glioma cells..... 55

Figure 23 Loss of NIK diminishes mitochondrial association of Drp1 58

Figure 24 Drp1 antibody validation and staining 59

Figure 25 NIK enhances Drp1 recruitment to mitochondria 60

Figure 26 Expression of mitochondria membrane proteins in cells with altered NIK expression 61

Figure 27 NIK affects phosphorylation of Drp1..... 62

Figure 28 Loss of NIK decrease the production of ROS 63

Figure 29 Loss of NIK reduces oxygen consumption 64

Figure 30 Drp1 colocalized with NIK but not IKKα in glioma cells 66

Figure 31 Drp1 colocalized with NIK in human glioma patient tumor..... 67

Figure 32 Drp1 interacts with NIK but not IKKα..... 68

Figure 33 Interaction between NIK and other Drp1-related mitochondrial dynamic regulators..... 69

Figure 34 NIK requires Drp1 to promote TWEAK-induced invasion 71

Figure 35 TWEAK-induced mitochondria fragmentation requires Drp1..... 72

Figure 36 NIK is localized to mitochondria in MEFs..... 75

Figure 37 NIK co-localization with different organelle markers in MEFs..... 76

Figure 38 NIK's downstream target, IKKα does not colocalize with mitochondrial marker in MEFs..... 77

Figure 39 NIK regulates invasive potential in MEFs 78

Page

Figure 40 NIK increases the invasive potential of IKK-knockout MEFs 79

Figure 41 Overexpression of NIK in ΔIKK MEFs does not affect downstream NF-κB 80

Figure 42 Overexpression of NIK in ΔIKK MEFs does not affect expression of the NF-κB target gene 81

Figure 43 NIK regulates mitochondrial morphology of MEFs in the absence of IKK/NF-κB signaling 83

Figure 44 NIK promotes mitochondrial fragmentation in MEFs 84

Figure 45 NIK contributes mitochondrial localization of Drp1 in IKK-knockout MEFs 85

Figure 46 NIK enhances Drp1 recruitment to mitochondria in IKK-knockout MEFs 86

Figure 47 Potential phosphorylation motifs of Drp1 for serine/threonine protein kinase NIK 90

Figure 48 Kinase-dead mutant of NIK was not able to promote the non-canonical NF-κB pathway 93

Figure 49 Loss of NIK kinase activity does not affect its mitochondrial localization 94

Figure 50 Loss of NIK kinase activity reduces their invasive potential in glioma cells 95

Figure 51 Kinase-dead mutant of NIK failed to restore mitochondria fission 96

Figure 52 Loss of NIK reduces xenograft tumor growth 98

Figure 53 Kinase activity of NIK is required for xenograft tumor growth 99

Figure 54 H&E staining of xenograft tumor 100

Figure 55 Validation of NIK-GFP fusion protein function 103

Figure 56 NIK accumulates at mitochondrial constriction sites in glioma cells 104

Figure 57 Interactions between NIK and Drp1 are predominantly localized in mitochondria 105

Figure 58 Validation of specificity of proximity ligation assay 106

Page

Figure 59 NIK–Drp1 interaction is independent of NIK kinase activity 107

Figure 60 NIK-Drp1 interaction accumulates at mitochondrial constriction sites in glioma cells 108

Figure 61 NIK recruits to mitochondrial constriction sites in COS-7 cells 109

Figure 62 NIK recruits to mitochondria and interacts with Drp1 at constriction sites in COS-7 cells 110

Figure 63 NIK influences phosphorylation of Drp1-S616 113

Figure 64 Kinase-dead mutant of NIK reduces phosphorylation of Drp1-S616 114

Figure 65 Kinase-dead mutant of NIK doesn't affect mitochondrial association of Drp1 115

Figure 66 Kinase activity of NIK is not required for Drp1 mitochondrial recruitment..... 116

Figure 67 NIK phosphorylates Drp1 in vitro 117

Figure 68 Model depicting NIK function in mitochondria 128

CHAPTER I

INTRODUCTION

1.1 Glioblastoma multiforme (GBM)

Glioblastoma multiforme (Glioblastoma) is the most malignant and aggressive primary tumors in the adult central nervous system (CNS). Glioblastoma originates from star-shaped glial cells including oligodendrocytes and astrocytes, which mainly provide support functions for neurons. According to the National Cancer Institute, the average annual incidence rate of glioblastoma is two to three per 100,000 adults per year and glioblastoma accounts for approximately 17 percent of all brain tumors in the United States. Despite development of effective treatments, current intervention such as surgery, radiation therapy, and chemotherapy for glioblastoma extend overall median survival only up to 1.5 years due to therapeutic resistance and tumor recurrence after surgical removal. Thus, glioblastoma is classified as a WHO Grade IV (Grade I-least malignant to Grade IV-most malignant).

As a hallmark, tumor heterogeneity at the genetic level within individual tumors contributes to distinct tumorigenic potential that significantly influence tumor progression and outcome of the tumor in response to treatment (Calderwood, 2013; Lawrence et al., 2013; Longo, 2012). Deregulation of intracellular signaling such as mechanistic target of rapamycin (mTOR), Erb-B2 Receptor Tyrosine Kinase 2 (ErbB2), and nuclear factor kappa B (NF-κB) in malignancies is frequently observed and allows cancers cells to acquire resistance to cell death and uncontrolled growth and proliferation (Guertin and Sabatini, 2007; Xia et al., 2014; Yu and Hung, 2000). In addition, the major characteristic of glioblastoma malignancy is diffuse invasion into adjacent normal brain tissue and migration to a significant distance from the primary tumor

area that is a fundamental step in metastasis (Valastyan and Weinberg, 2011; van Zijl et al., 2011). This characteristic is one of the most difficult challenges to therapeutically target. Therefore, a clear understanding of the cellular and molecular mechanisms underlying the tumor pathogenesis is crucial for the development of specific therapeutic strategies against malignant glioblastoma.

1.2 NF-κB pathways

1.2.1 NF-κB

About thirty years ago, NF-κB was discovered by Sen and Baltimore, as a transcription factor that specifically recognizes and binds to the enhancer element of the immunoglobulin kappa light-chain of activated B lymphocytes (Sen and Baltimore, 1986). NF-κB comprises a family of five transcription factors, which contains of NF-κB1 (p105/p50), NF-κB2 (p100/p52), RelA (p65), RelB, and c-Rel (Baldwin, 1996; Ghosh et al., 1998). Interestingly, these proteins share a highly conserved Rel homology domain (RHD) essential for nuclear localization, dimerization and DNA binding. Based on sequences C-terminal to the RH domain, the NF-κB proteins can be divided into two distinct classes. One class includes RelA, RelB, and c-Rel have a C-terminal transactivation domain, and the other class includes NF-κB1 p105 and NF-κB2 p100 proteins, which are characterized by inhibitory multiple ankyrin repeats at C-terminal regions, and undergo proteolytic processing to yield p50 and p52, respectively (Betts and Nabel, 1996; Fan and Maniatis, 1991; Heusch et al., 1999). Homodimeric complexes of p50 or p52 can repress transcription through binding to NF-κB elements of gene promoters, whereas RelA, RelB, and c-Rel contain transcription activation domains that interact with either p52 or p50 to

bind DNA and activate gene transcription (Hayden and Ghosh, 2012; Moynagh, 2005; Oeckinghaus and Ghosh, 2009).

NF-κB pathway can be activated by various stimuli, such as growth factors, cytokines, and reactive oxygen species (ROS), in various cells (Oeckinghaus et al., 2011; Siebenlist et al., 1994) (Fig. 1). Extensive studies have revealed that NF-κB pathway plays critical roles in immune, inflammatory, cell growth, differentiation, and apoptotic processes through regulating the expression of many genes (Aggarwal, 2004; Ghosh et al., 1998; May and Ghosh, 1998). Importantly, NF-κB signaling is constitutively activated in various tumor types (Jost and Ruland, 2007; Karin, 2006). The aberrant constitutive activation of NF-κB in human cancers contributes to malignant progression and therapeutic resistance (Jost and Ruland, 2007; Perkins, 2012). Therefore, a clear understanding of NF-κB functions underlying tumor pathogenesis is crucial for the development of specific therapy strategy against malignant tumor.

1.2.2 Canonical and non-canonical NF-κB pathway

Two distinct NF-κB signaling pathways are tightly controlled by a complex network of positive and negative regulatory elements at multiple levels (Fig. 1). The canonical NF-κB pathway is triggered by the activation of various cell surface receptors such as tumor necrosis factor receptor (TNFR), interleukin 1 receptor (IL-1R), pathogen-associated molecular patterns (PAMPs), some danger-associated molecular patterns (DAMPs), and Toll-like receptor 4 (TLR4) through binding with their proinflammatory ligands (Oeckinghaus et al., 2011; Shih et al., 2011). Under activating conditions with cytokines, inactive NF-κB1/RelA family members sequestered in the cytoplasm are release from inhibitory IkappaB (IκB) proteins through recruited IkappaB kinase complex (IKKα, IKKβ, and IKKγ)-mediated IκB phosphorylation, which results in

ubiquitination and proteasomal degradation of the IκB proteins. Consequently, the free NF-κB dimers translocate to the nucleus to activate expression of target genes (Oeckinghaus and Ghosh, 2009; Wertz and Dixit, 2010).

In contrast, the non-canonical NF-κB pathway is only activated by a subset of receptors including lymphotoxin-β receptor (LTβR), CD30 ligand (CD30L), CD40 ligand (CD40L), BAFF receptor (BR3), and Fibroblast growth factor-inducible 14 (Fn14) (Hayden and Ghosh, 2012; Razani et al., 2011; Sun, 2011). Upon stimulation with tumor necrosis factor (TNF) family cytokines, stabilized NF-κB inducing kinase (NIK) phosphorylates and activates IKKα homodimers, which leads to phosphorylation of sequestered NF-κB member, NF-kB2 p100 associated with RelB, and proteolytic processing of precursor protein p100 to generate mature p52 (Ling et al., 1998; Sun, 2017). Finally, the NF-κB p52/RelB complexes translocate to the nucleus, leading to transcription of target genes (Sun, 2012). Thus, unlike canonical NF-κB pathway, the non-canonical pathway is largely depending on NIK-mediated phosphorylation of IKKα to promote NF-κB2/p100 processing, which does not depend on IKKβ or IKKγ for degradation of the inhibitory IκB proteins.

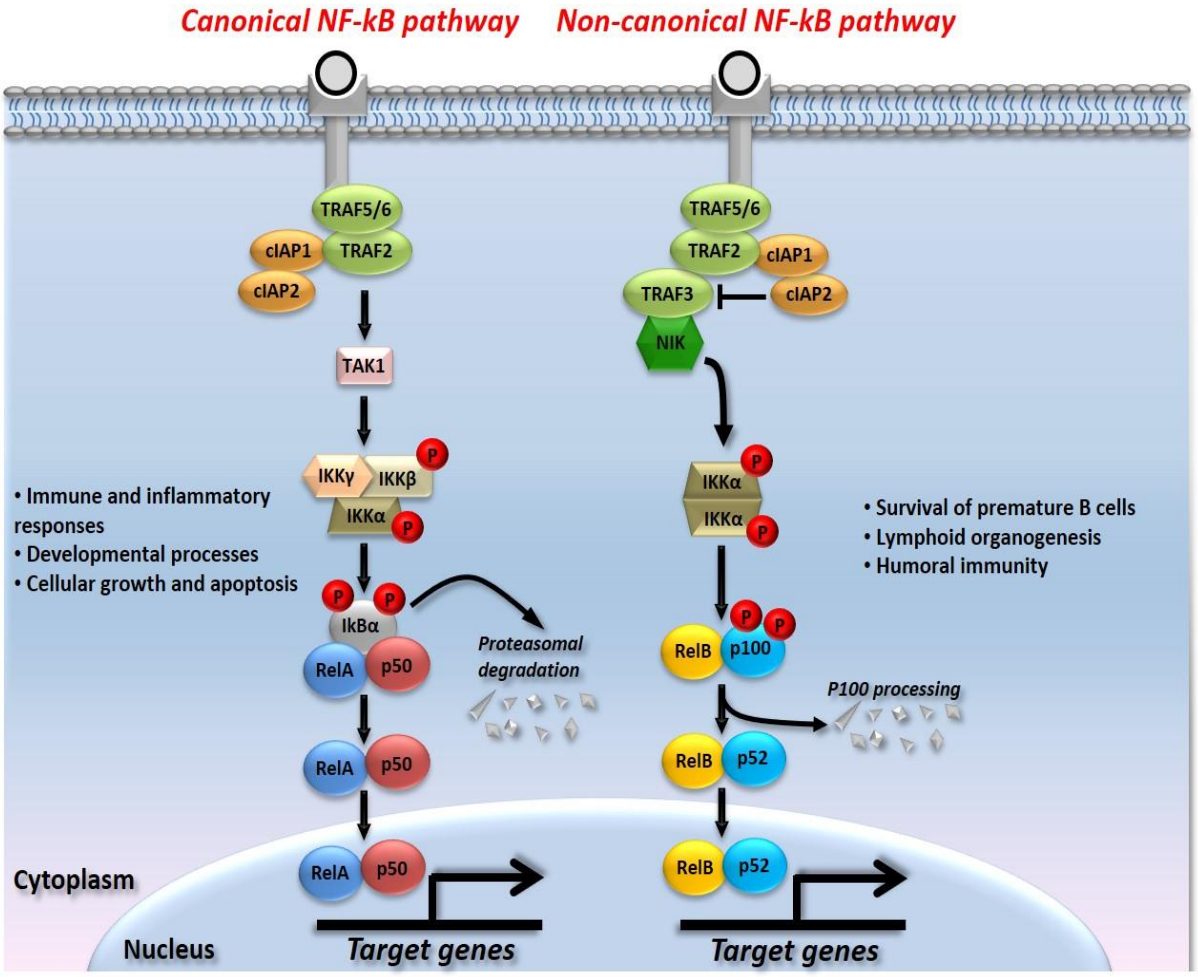

Figure 1. NF-κB pathway can be activated via two major signal transduction pathways. Canonical NF-κB pathway: under stimulated conditions, the IκB molecules are phosphorylated by the IKK complex, which leads to proteasomal degradation of IκB. RelA:p50 heterodimer are translocate to the nucleus, resulting in target genes expression involved in immune and inflammatory responses, developmental processes, cellular growth and apoptosis. Non-canonical NF-κB pathway: stabilized NIK by receptor ligation activates IKKα, which leads to processing of p100 to generate p52 and nuclear translocation of RelB:p52 heterodimers for activation of transcription of target genes involved in survival of premature B cells, lymphoid organogenesis, and humoral immunity.

1.3 NF-κB inducing kinase (NIK)

1.3.1 Structure and turnover of NIK

Non-canonical NF-κB pathway requires serine/threonine protein kinase NIK (also known as MAP3K14; mitogen-activated protein kinase kinase kinase 14), which phosphorylates IKKα and induces the processing of the precursor protein p100 into p52 and subsequently activates RelB-p52-driven NF-κB signaling. As a central regulatory component of the non-canonical NF-κB pathway, NIK has been extensively studied for its roles in regulating homeostasis and maturation of B cell and lymphoid organ development (Fagarasan et al., 2000; Hahn et al., 2016; Sasaki et al., 2008; Senftleben et al., 2001). The human NIK gene encodes 947 amino acid residues and is known to contain at least four functional domains: N-terminal TRAF3-binding domain (aa30 - aa120), a negative regulatory domain (aa121 - aa318), a central serine/threonine kinase domain (aa390 - aa660), and a C-terminal non-catalytic region (aa660 - aa947) (Liao G 2004; Xiao G 2000) (Fig.2). The sequence of NIK is highly conserved and identical to the corresponding amino acids of a variety of species (human NIK residues is >80% identical with mouse 84%, rat 85%, bovine 88%, and rabbit 87%) (Fig.3). Interestingly, a study examining the structure of NIK revealed that NIK activation doesn't require its inducible phosphorylation, rather it requires a catalytically important salt bridge between Lys429 and Glu440 to stabilize active conformation (Tao and Ghosh, 2012). In fact, NIK containing alanine mutations at Lys429 and Lys430 is unable to promote processing of p100 for activation of non-canonical NF-κB signaling (Sheng et al., 2012; Sylla et al., 1998).

Under resting conditions, NIK is constitutively ubiquitylated and degraded by K48-linked polyubiquitylation through E3 ligase complex including TNF receptor-associated factor (TRAF)2/3 and cellular inhibitor of apoptosis (cIAP)1/2, resulting very low intracellular

concentrations of NIK (Liao et al., 2004; Tao and Ghosh, 2012; Thu and Richmond, 2010) (Fig.4). After stimulation with TNF family cytokines such as a tumor necrosis factor-like weak inducer of apoptosis (TWEAK, also known as TNFSF12), NIK-TRAF3-TRAF2-cIAP complex is recruited to the receptor. Then, the receptor-induced ligase activity of TRAF2 results in K63-specific ubiquitination of cIAP, leading to K48-linked ubiquitination and proteasomal degradation of TRAF3 as a key NIK-associated protein. Consequently, stabilized and accumulated NIK activates non-canonical NF-κB pathway through phosphorylation of IKKα for triggering p100 processing (Hacker et al., 2012; Sun, 2010) (Fig.4).

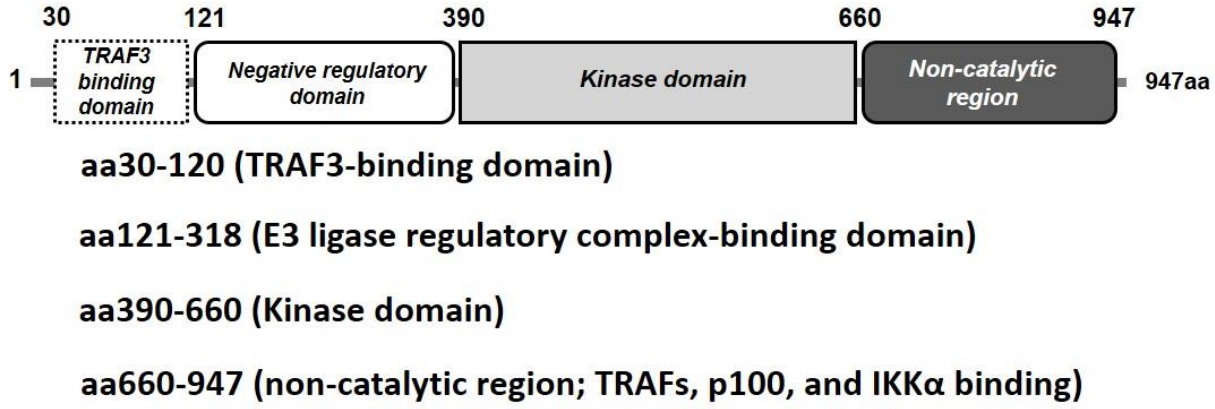

Figure 2. Structure of human NIK protein. Human NIK contains four main domains, including a TRAF3-binding domain, negative regulatory domain, kinase domain and non-catalytic domain.

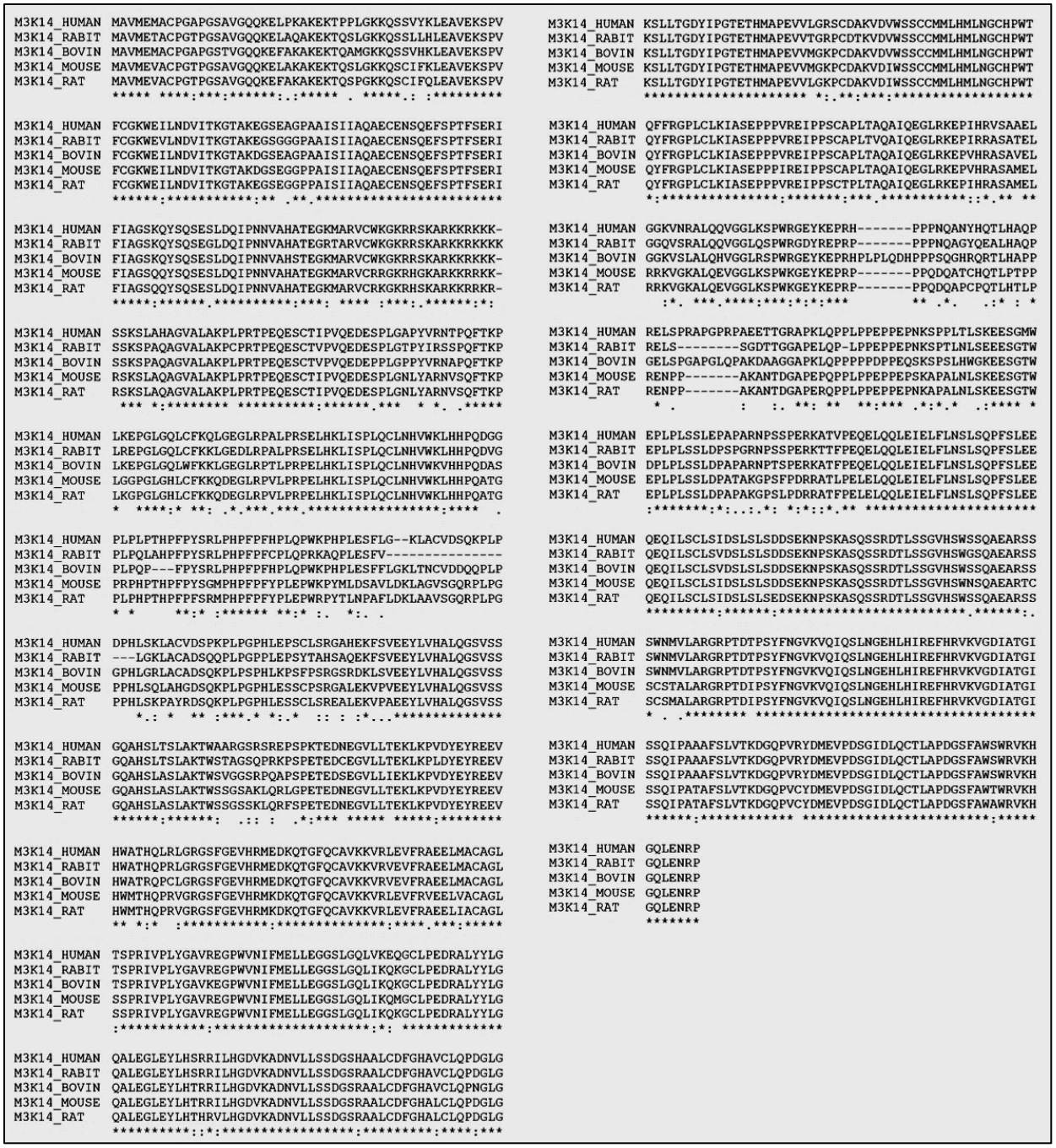

Figure 3. NIK protein sequence alignment. Amino acid sequences of NIK are highly conserved between species. Human - mouse 84%; - rat 85%; - bovine 88%; - rabbit 87%. The multiple sequence alignment analysis was done through ClustalX.

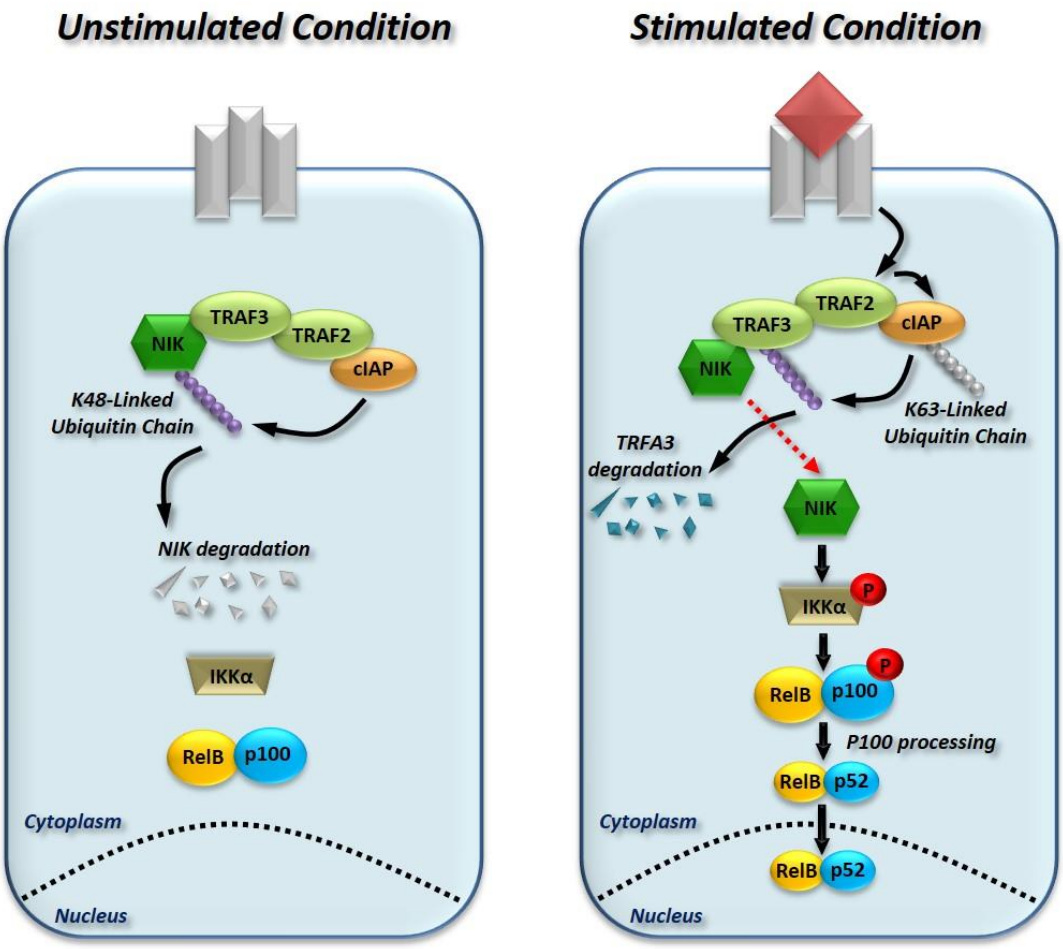

Figure 4. Posttranslational regulation of NIK. Under unstimulated conditions, the E3 ligase complex (TRAF2:TRAF3:cIAP1:cIAP2) direct ubiquitination and proteasomal degradation of NIK, resulting in low intracellular concentration of NIK below the threshold. Upon stimulation, NIK-E3 ligase complex is recruited to the receptor, leading to degradation of TRAF3 and release newly synthesized NIK. NIK-mediated phosphorylation of IKKα triggers the p100 processing and nuclear translocation of p52:RelB dimers for target gene expression.

1.3.2 Roles for NIK in cancer

Since NIK was originally identified as NF-κB-activating protein kinase interacting with TRAF2 (Natoli et al., 1997), many studies demonstrated that NIK is involved in many of the key cellular processes necessary for stem cell behaviors such as differentiation, development, and embryogenesis (Kajiura et al., 2004; Shinkura et al., 1999; Vaira et al., 2008; Yang et al., 2010; Yin et al., 2001). Aberrant activation of non-canonical NF-κB pathway comprising NIK-IKKα-p100 axis is commonly observed in human malignancies (Annunziata et al., 2007; Bennett et al., 2017; Cogswell et al., 2000; Keats et al., 2007; Nadiminty et al., 2008). Moreover, deregulation of the signaling pathway contributes to pathologic features of malignancies such as enhanced invasion, metastasis, and tumorigenicity (Ge et al., 2016; Tchoghandjian et al., 2013). Recently, there has been growing interest in roles of NIK in cancers. NIK is frequently overexpressed in human cancers including ovarian cancer, breast cancer, melanoma, pancreatic cancer, and lung cancer (Doppler et al., 2013; Saitoh et al., 2010; Thu et al., 2012; Uno et al., 2014; Yamamoto et al., 2013). NIK has been shown to promote tumorigenesis in cancers through its ability to promote cell proliferation and survival as anti-apoptotic and pro-survival functions (Thu et al., 2012; Xia et al., 2014). In particular, our previous studies have investigated the correlation between NF-κB pathway and invasiveness of glioma cells derived from surgical samples of GBM patients in a three-dimensional collagen I matrix. We observed that NIK-dependent non-canonical NF-κB pathway is significantly increased in highly invasive glioma cell lines compared to less invasive glioma cell lines (Cherry et al., 2015; Lee et al., 2013). More recently, we have shown that the ability of NIK to promotes glioma invasiveness is associated with cell shape changes including formation of extensive actin-rich membrane protrusions, termed invadopodia, which is related with degradation of the extracellular matrix (ECM) for tumor

migration and invasion (Duran et al., 2016). However, the role of NIK in CNS tumor pathogenesis, and the molecular mechanisms underlying NIK-mediated malignant characteristics in glioblastoma are still largely unknown.

1.4 Mitochondria

1.4.1 Mitochondria and mechanisms regulating mitochondrial dynamics

Since anatomist Von Kölliker first described granular structures in muscle cells in 1856, many scientists identified the organelle under the light microscope that was later named mitochondria by Benda in 1898 (Lehninger, 1964; Margulis, 1970). Mitochondria are double membrane-bound subcellular organelles found in the cytoplasm of nearly all eukaryotic cells and contain a small amount of their own DNA, known as mitochondrial DNA (mtDNA) that retains 13 of the most important oxidative phosphorylation (OXPHOS) genes for adenosine triphosphate (ATP) production. The mitochondrial ATP production depends on the electron transport chain (ETC) consisting of respiratory chain complexes I - IV within mitochondrial inner membrane (MIM), which pumps nicotinamide adenine dinucleotide (NADH) and flavin adenine dinucleotide ($FADH_2$) produced in the citric acid cycle and glycolysis. The ETC generates a proton gradient across the MIM to convert adenosine diphosphate (ADP) into energy molecule ATP for many vital cellular functions (Benard et al., 2010; Bhargava and Schnellmann, 2017).

Mitochondria are highly dynamic organelles that continuously fuse, divide, and migrate. The dynamics of mitochondrial morphology is tightly regulated by a balance between mitochondrial fusion and fission machineries that adapt to cellular metabolic demands during cell proliferation, differentiation, division and survival (Kageyama et al., 2012; Khacho et al., 2016; Mils et al., 2015). Fission results in mitochondrial fragmentation into short rods or spheres,

while fusion causes long filamentous mitochondrial morphology. These morphological changes of mitochondria also contribute to a quality control mechanism that preserve healthy mitochondria and remove damaged mitochondria (Ni et al., 2015; Twig et al., 2008). In mammalian cells, mitochondria fission is mediated by dynamin-related protein 1 (Drp1). The cytosolic Drp1 is recruited to mitochondria through binding with mitochondrial outer membrane (MOM) proteins including Mitochondrial fission 1 protein (Fis1), mitochondria fission factor (Mff), mitochondrial dynamics protein of 49 kDa (MID49) and 51 kDa (MID51), resulting in generating the constriction force for division of mitochondria (Elgass et al., 2013; Palmer et al., 2013). Mitochondrial fusion is mediated by three large GTPases including mitofusin 1 (Mfn1), mitofusin 2 (Mfn2) and Optic Atrophy 1 (OPA1). Mfn1 and Mfn2 are involved in MOM tethering of neighboring mitochondria to facilitate membrane fusion, while OPA1 is localized on MIM and facilitates MIM fusion (Zhang and Chan, 2007).

1.4.2 Mitochondrial dynamics in cancer

In early 1900s, physiologist Otto Warburg first suggested that mitochondria may play an important role in the development of cancer through constitutively upregulation of glucose metabolism, but not by OXPHOS, to produce most ATP even under anaerobic conditions for cell survival (Warburg et al., 1931). Warburg's observation is known as the ‘Warburg effect’ (enhanced aerobic glycolysis), and described that metabolic shift towards aerobic glycolysis in cancer cells increased glucose uptake to synthesize enough ATP for several proliferative and survival advantages. Aerobic glycolysis also known to causes local acidification of tumor microenvironment, which leads to changes in intracellular pH that facilitate tumor invasion (Swietach et al., 2007). In addition, increased ROS caused by impaired oxidative

phosphorylation in cancer lead to progression of the cancer (Singh et al., 2009; Weinberg et al., 2010). Therefore, metabolic imbalances and mitochondrial dysfunction are major hallmarks of cancer cells (Boland et al., 2013; Galluzzi et al., 2006).

The dynamic network, which includes changes in size and subcellular distribution of mitochondria, is tightly regulated through mitochondrial dynamic machinery (Chan, 2006). Alteration of mitochondrial dynamics caused by imbalance between mitochondrial fusion and fission events potentially contribute to dysregulation of various cellular processes, which have been implicated in tumorigenesis (Grandemange et al., 2009; Liesa et al., 2009; Liu et al., 2004; Maycotte et al., 2017). Interestingly, recent studies revealed that mitochondria in human invasive breast carcinoma and oncocytic thyroid tumors were more fragmented, compared to non-malignant tumors (Ferreira-da-Silva et al., 2015; Zhao et al., 2013). In these tumors, expression of mitochondrial fission regulator Drp1 is highly upregulated and its genetic and pharmacological inhibition suppressed cell migration and invasion. A similar phenotype that enhanced mitochondrial fragmentation and expression of Drp1 were also observed in brain tumor initiating cells (BTICs), compared with non-BTICs. Targeting Drp1 using genetic and pharmacological approaches inhibited tumor growth and induced apoptosis (Xie et al., 2015). Thus, current studies on cancer have shed light on physiological roles of mitochondria in cancer cells that emphasize the importance of mitochondrial dynamics. Nonetheless, the molecular mechanisms underlying relationships between mitochondrial dynamics and tumor invasion/migration are still poorly understood.

1.4.3 Mitochondrial fission regulator, Dynamin-related protein 1

Drp1 is a member of the dynamin family of GTPases that regulates mitochondrial fission

in mammals. Upon the initiation of fission, the GTPase is translocated from the cytosol to the mitochondrial outer membrane through binding to its mitochondrial receptors including Fis1, Mff, Mid49, and Mid51 (Loson et al., 2013; Smirnova et al., 2001). Membrane-bound Drp1 undergoes oligomerization, wraps around potential fission sites, and sequentially constricts the mitochondrial membrane in the presence of GTP (Ji et al., 2015; van der Bliek et al., 2013) (Fig.5). The activity of Drp1 can be controlled by post-translational modifications, such as phosphorylation, sumoylation, S-nitrosylation and ubiquitination (Elgass et al., 2013; Otera et al., 2013). Particularly, its activity is differently regulated by two major phosphorylation sites, serine 616 (S616) and serine 637 (S637) (Benard et al., 2010; Jahani-Asl and Slack, 2007; Taguchi et al., 2007). Phosphorylation at S616 of Drp1 promotes mitochondrial fission, whereas S637 phosphorylation resulted in loss of its activity. Furthermore, multiple serine/threonine protein kinases including cAMP-dependent protein kinase (PKA), calcium calmodulin-dependent protein kinase (CAMK), and cyclin-dependent kinase (CDK) have been identified to regulate Drp1 activity (Chang and Blackstone, 2007a; Cho et al., 2014; Strack et al., 2013). Recent studies revealed that extracellular-signal-regulated kinase (Erk2)-mediated phosphorylation at S616 of Drp1 promotes mitochondrial fission, contributing to mitogen-activated protein kinase (MAPK)-driven tumor growth (Kashatus et al., 2015; Serasinghe et al., 2015). Based on the observation that excessive mitochondrial fission with upregulated Drp1 activity in cancers, regulation of intracellular localization and phosphorylation of Drp1 should be a key regulatory approach to prevent tumor progression through controlling mitochondrial dynamics.

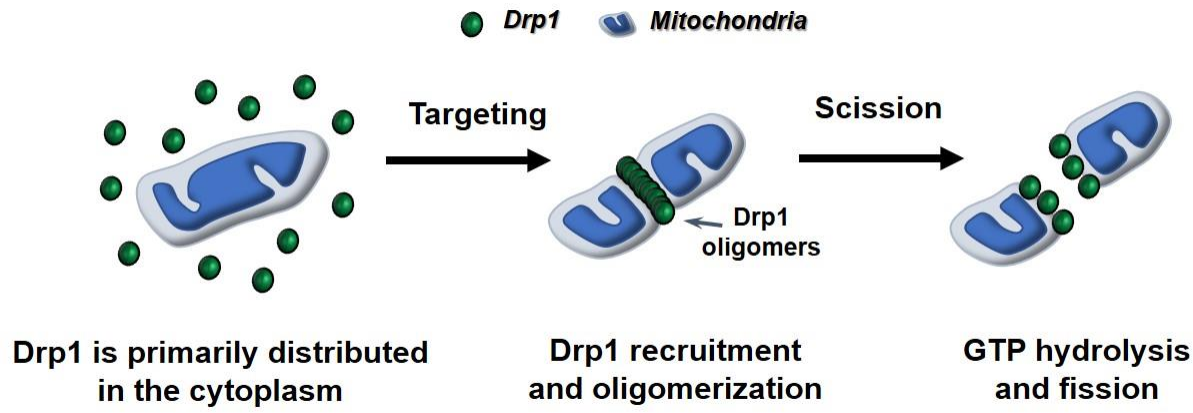

Figure 5. Role of Drp1 in mitochondrial fission. Mitochondrial fission requires the function of dynamin-related protein Drp1. Cytoplasm-localized Drp1 is recruited to pre-determined sites on mitochondrial outer membrane and oligomerized. The oligomerized Drp1 induces constriction of the fission site through GTP hydrolysis.

1.5 Dissertation goals

The NF-κB family of transcription factors is known to play crucial roles in the development of multiple malignancies through regulating inflammation, proliferation and survival (Ben-Neriah and Karin, 2011). In fact, constitutive activation of NF-κB signaling has been observed in various tumor types (Jost and Ruland, 2007; Karin, 2006). The NF-κB pathways are classified into two distinct pathways: canonical and the non-canonical pathway. Most studies investigating the effects of NF-κB signaling on tumorigenesis have been focused on the canonical signaling pathway, while roles of non-canonical NF-κB signaling pathway in cancers are very poorly understood. In particular, NIK as a central signaling component of the non-canonical pathway, undergoes constitutive proteasomal degradation and consequently results in biochemically undetectable levels of NIK in unstimulated normal cells. In contrast, NIK expression was significantly elevated in breast cancer, multiple myeloma and inflammatory diseases (Annunziata et al., 2007; Enzler et al., 2006; Yamaguchi et al., 2009). In our previous studies, we demonstrated that non-canonical NF-κB signaling can promote glioma tumor (Cherry et al., 2015), particularly NIK is both necessary and sufficient for glioma cell invasion through promoting extensive membrane branching and elongated invadopodia protrusions independently of canonical NF-κB signaling (Duran et al., 2016).

Mitochondria are specialized cellular compartments that are involved in various functions including energy production, apoptosis and cell proliferation. Altered mitochondrial dynamics by imbalance between fusion and fission is known to contribute to tumorigenesis. Importantly, canonical NF-κB proteins have been shown to be localized in mitochondria that regulate mitochondrial functions (Cogswell et al., 2003; Johnson et al., 2011). Moreover, non-canonical NF-κB signaling has been recently implicated in mitochondrial biogenesis and regulation of

mitochondrial network morphology (Laforge et al., 2016; Millet et al., 2013; Zeng et al., 2015). However, roles of NIK in regulating mitochondrial dynamics to promote tumor progression have never been explored. Given this information, we hypothesize that NIK is localized to mitochondria and regulates mitochondrial dynamics, which are required for acquisition of tumorigenic phenotype in glioma. This project will seek to address new roles of NIK, more specifically the molecular mechanisms controlling mitochondrial morphology associated with pathogenesis of tumor cells, and it may contribute to the development of new therapies for cancers.

CHAPTER II

METHODS AND MATERIALS*

2.1 Cell culture and reagents

BT25 and BT114 cell lines were obtained from human glioma patients as previously described (Kelly et al., 2009). These cell lines were maintained as spheroids in Neural Stem Cell (NSC) medium containing DMEM/F-12, 1X B-27 supplement minus Vitamin A, 1X Glutamax, 25 ng/ml EGF, 25 ng/ml bFGF and 1X Pen/Strep (Life Technologies). 293T cells were obtained from ATCC. IKK MEFs were a kind gift from Dr. Baldwin (originally from Dr. Verma). MEFs and HEK293T were cultured in DMEM medium with 10 % FBS and 1X Pen/Strep. MDA-MB231 and Panc1 were from ATCC (Manassas, VA) and cultured in RPMI medium with 10% FBS and 1X Pen/Strep. All cells were cultured at 37 °C with 95 % humidity and 5 % CO_2.

2.2 Reagents

For immunostaining, the following primary antibodies were purchased: NIK (ab191591 or ab7204, for Figure S2A); IKKα (ab32041); Tom20-AF647 (ab205487); Sec61A-AF488 (ab205794); Drp1 (ab56788) from Abcam, Cambridge, MA, USA and Drp1 (8570S); p-Drp-S616 (CST4494) from Cell Signaling Technology, Danvers, Ma, USA and Tim50 (sc-393678) from Santa Cruz Biotechnology, Dallas, Tx, USA. For immunoblot analyses, the following antibodies were obtained: MFF (ab81127); Fis1 (ab156865); Opa1 (ab157457) from Abcam and

* Part of this chapter is reprinted with permission from "NIK/MAP3K14 Regulates Mitochondrial Dynamics and Trafficking to Promote Cell Invasion." By Jung JU, Ravi S, Lee DW, McFadden K, Kamradt ML, Toussaint LG, Sitcheran R, 2016. Current Biology, 26, 3288-3302, Copyright 2016 by Elsevier Ltd.

IKKα (CST2682); IKK (CST2684); NIK (CST4994); Drp1 (CST8570); CoxIV (CST11967); Tom20 (CST42406); NFKB2 (CST4882); Mfn-1 (CST14739); Mfn-2 (CST11925) from Cell Signaling Technology. The following antibodies were purchased from Santa Cruz Biotechnology: GAPDH (sc137179), and β-actin (sc69879). The following antibodies were obtained from Cell Signaling Technology: p-Drp-S637 (CST4867S); p-Drp-S616 (CST3455S) for Flow Cytometry. Cellight® Mitochondria-RFP, BacMam 2.0 (Mito-RFP, C10601) was purchased from Life Technologies, Grand Island, NY, USA. MG132 (#2194S) was purchased from Cell Signaling Technology. Collagen type I (#354249) was purchased from Corning, Corning, NY, USA. rhTWEAK (#310-06) was obtained from PeproTech, Rocky Hill, NY, USA.

2.3 Plasmids construction for NIK overexpression

Human (hNIK) or mouse (mNIK) cDNA was cloned into pLenti6-V5-DEST (Addgene, Cambridge, MA) using the GATE-WAY™ Cloning System (Invitrogen). Luciferase (Promega, Madison, WI) coding sequences were subcloned into pLenti6-v5-DEST (Invitrogen) and served as a control vector for NIK overexpression.

2.4 CRISPR-Cas 9 gene knockout

NIK: Oligos encoding sg RNAs for human NIK (sgNIK-1: GCUCCUUCGGAGAGGUGCAC, sgNIK-2: GAAAGCGUCGCAGCAAAGCC, sgNIK-3: AGUACCGAGAAGAAGUCCAC) and sgRNAs for mouse NIK (sgNIK-4: AGGAUGGGGCAUUCCGCUGU sgNIK-5: UGGAGCGCAUGCACCAGGUA, sgNIK-6: AGUAUCGAGAAGAGGUCCAC) were cloned into Lenti-CrispR-v2 (Addgene) respectively.

BT25, WT MEFs, IKK MEFs, Panc1 and MDA-MB231 cells were transduced with a mixture of lentiviruses carrying the three mice or human sgRNAs. Loss of NIK expression was confirmed by immunoblot, pPCR and/or immunofluorescence microscopy analysis of puromycin-resistant cells. BT25-sgNIK cells and sgNIK-MEFs, single colony cells were isolated by serial dilution and experiments were repeated with at least two clones. Panc1-sgNIK and MDA-MB231-sgNIK cells were analyzed as mixed clones. For controls, cells were transduced with empty LentiCrispR-V2. Drp1: Oligos encoding sgRNAs for human Drp1 (sgDrp-1: GUUCCCACUACGACGAUUUG, sgDrp1-2: GCUGCCUCAAAUCGUCGUAG, sgDrp1-3: GUGACAAUUCCAGUACCUCU) were cloned into Lenti-CrispR-v2. BT25 cells were transduced with a mixture of three lentiviruses carrying the human sgRNAs and selected against puromycin then subjected to screen Drp1 null by serial dilution.

2.5 Lentivirus production

Twenty-four μg of lentiviral plasmids and 72 g of polyethyleneimine were used to transfect 293T cells. After 3 days of transfection, viral supernatant was harvested and filtered through 0.45 μM syringe filter. After filtration, viral particles were concentrated 20-fold to 500 μl using Lenti-X Concentrator (#631231, Clontech, Mountain View, CA), and 100 μl of concentrated virus were used to infect cells. Stably transduced cells were selected for 72 h in medium containing 0.6 μg/ml puromycin or 3 μg/ml blasticidin (Invitrogen).

2.6 Three-dimensional collagen invasion assay

Invasion assays were performed as previously described (Cherry et al., 2015; Lee et al., 2013). Briefly, collagen type I (Corning, NY) was diluted to 2 mg/ml in DMEM/F-12 medium

(1X Pen/Strep) and matrices polymerized in 96-well plates. 4 x 10^5 cells cultured in NSC or NSC+10 % serum were seeded in triplicate in 100µl DMEM/F-12 (1x Pen/Strep, 1X Glutamax) without growth factors or serum. Cells were fixed with 3 % glutaraldehyde solution after 48 hours of invasion and stained with 0.1 % toluidine blue. Invasion density was quantified by counting cells below the plane of the monolayer by bright-field light microscopy using a 10 X 10 ocular grid at 10X or 20X magnification corresponding to a 1 mm^2 field. Numbers in at least three equivalent, random fields were counted (n = 3 wells each) and normalized to the corresponding control. All experiments were performed at least three times.

2.7 Immunofluorescence staining

2 x 10^4 cells were seeded in 8 well chamber slides (#80827, Ibidi, Munich, Germany) or on coverslips in the presence of 0.5 % FBS and allowed to adhere for 4 hours. Cells were transfected with Mito-RFP (for mitochondrial labelling, Invitrogen, C10508) for 16 h, fixed with 4 % paraformaldehyde, permeabilized for 20 minutes with 0.3 % Triton X-100 in PBS, and blocked 30 min at room temperature with 5 % serum corresponding to secondary antibody host. Cells were incubated overnight in 0.1 % Triton X-100, 1 % BSA in PBS at 4 °C with primary antibody. Cells were then incubated in 1 % BSA for 1 h at room temperature with secondary antibody Alexa Fluor 488 (A11008) or Alexa Fluor 594 (A11005) from Life Technologies. Dual immunostaining was performed sequentially; cells were incubated with the first primary antibody in 1 % BSA overnight at 4 °C, washed three times with PBS and incubated with the corresponding secondary antibody in 1 % BSA for 1 h at room temperature in dark. After washing three times with PBS, cells were blocked for a second time with corresponding host serum (5 %) for 30 minutes at room temperature. Cells were then incubated with the second

primary antibody from a different species, followed by the appropriate secondary antibody. For immunostaining with two rabbit antibodies, we used either commercially pre-labeled antibodies, or custom-labeled antibodies generated with an antibody labeling kit (Invitrogen, A20181). The pre-labeled antibody was always used last. Cells were counter stained with the nuclear stain DAPI (Invitrogen, P36931), and phalloidin (Invitrogen, A22287) as indicated.

2.8 Human glioma ex-vivo tissue staining

The use of de-identified human glioblastoma tissue samples were approved by the Institutional Review Boards (IRBs) of both St. Joseph Regional Health Center, Bryan, TX (IRB2012-001) and Texas A&M University (IRB2014-0318D). Ex-vivo tissue was immediately snap-frozen in OCT on dry ice. Sections of human glioma biopsy samples were fixed with 4 % paraformaldehyde and immunostained with antibodies specific for NIK, IKKα and Drp1 (see immunofluorescence staining above).

2.9 Image acquisition

Images were acquired with a Nikon TI A1R inverted confocal microscope with CFI60 Plan Apochromat Lambda 60x oil immersion objective lens. The Zeiss ELYRA S.1 super-resolution microscope with a Plan Apochromat 63x objective/1.4 NA oil objective was used for super-resolution microscopy. Images were acquired with the following scan parameters: a "frame" scan mode of 1024 x 1024 pixels with a 16 bit depth and a grating of 3 rotations. For imaging the mitochondria, 561 nm excitation was used and emission was collected with a BP 570-620 nm filter. Fluorescence intensity was collected using a sCMOS pco.edge EMCCD camera with exposure time set to 100 ms.

2.10 Flow cytometry

Cells were harvested and washed 2 times by adding HBSS, centrifuged at 2000 rpm for 5 min and aliquoted 3 x 10^5 cells in FACS tubes. Cells were fixed using cold 4 % paraformaldehyde for 10 min, permeabilized using 0.3 Triton X-100 for 15 min at room temperature and blocked 30 min at room temperature with corresponding 5 % host serum. Cells were immunostained for an hour in 0.1 % Triton X-100, 1 % BSA at 4 °C using either NIK-specific antibody (ab191591), pDRP S637 (4867S), or pDRP S616 (3455S). After three times wash with HBSS, cells were incubated in secondary antibody (AF488 or AF594, Invitrogen) for 30 min in the dark and wash with HBSS. Finally, cells were resuspended in 300 μL HBSS and analyzed using BD LSR Fortessa™ X-20 cell analyzer (BD Biosciences, San Jose, CA). At least 10,000 events were measured. Data were analyzed using Flow Jo V-X (Flowjo Llc, Ashland, OR).

2.11 Quantification of mitochondrial number and size and tracking

All Mito-RFP images were taken on a Nikon TI A1R inverted confocal microscope or Nikon Eclipse Ti microscope with similar contrast and at the same magnification. Each particle in individual cells was outlined and measured for mitochondrial number and average size utilizing particles analyzer in ImageJ (NIH) (Dagda et al., 2009). BT25 cells were plated on 8 well chamber slides with a glass bottom and incubated with CellLight Mitochondria-RFP (Mito-RFP) BacMam reagent (C10601). After 18 hr, time-lapse imaging was performed every 10 s for 5 min, and movies of mitochondria were acquired at a rate of 5.2 frames per second using a Nikon TI A1R inverted confocal microscope with 60x Plan-Apochromat lenses and Stage-top

incubator system. NIS Elements software (Nikon) with tracking module was used to track and analyze movement of single mitochondria.

2.12 Subcellular fractionation

Cultured cells were washed twice with ice-cold PBS and scraped in 2 ml of ice-cold PBS. After removing supernatants following centrifugation at 800 xg for 5 min, pellets were resuspended and homogenized in homogenization buffer (10 mM HEPES-KOH, pH 7.5, 0.25 M sucrose) by passing a 27-gauge needle 10 times. Post-nuclear supernatants were collected by centrifugation at 1,000 xg for 10 min and then, heavy membrane fraction was separated from the resultant supernatant by centrifugation at 8,000 xg for 10 min at 4 ˚C. The pellets of heavy membrane fraction as mitochondria enriched fraction were washed with buffer and solubilized in 100 μl of solubilization buffer (50 mM Tris-HCI [pH 8.8], 5 mM EDTA, 1 % SDS). The remaining supernatants as cytosol fraction were centrifuged again at 16,000 xg for 10 min at 4 ˚C to remove any remain membrane fraction.

2.13 Immunoblot

Cells were lysed in RIPA lysis buffer (Pierce, Rockford, 89900) with protease/phosphatase inhibitor cocktail (Thermo Scientific, 78440). Equal amounts of protein were mixed with NuPage 4X LDS sample buffer (Invitrogen, NP0008) containing reducing agent and denatured at 100 ˚C for 7 min. Proteins were separated on 8 % - 12 % SDS-PAGE and transferred to nitrocellulose membranes (Bio-Rad, #162-0115). The membranes were blocked for 1 h with 5 % non-fat dry milk in 0.1 % Tween-20/TBS (TBST) or Odyssey blocking buffer (LI-COR Biosciences, 927-40000) and incubated with primary antibodies diluted in blocking buffer

at 4 °C overnight. After washing in TBST, membranes were incubated with goat anti-rabbit IRDye800CW (LI-COR Biosciences, 926-32211), goat anti-mouse IRDye680 (LI-COR Biosciences, 926-68070) or goat anti-rabbit HRP conjugate (Thermo Scientific, 31460) diluted in blocking buffer and incubated for 1 hour at room temperature. The blots were washed with TBST and developed using Chemiluminescent HRP Substrate (EMD Millipore, WBKLS0100) for detection of HRP or an Odyssey Infrared Imaging system (LI-COR Biosciences) for detection of IRDye fluorescent dyes.

2.14 Immunoprecipitation

Cells were lysed with in RIPA lysis buffer with Protease/Phosphatase Inhibitor Cocktail. 500 μg of proteins from each sample were incubated with 5 μg of Drp1 antibody (Abcam, 56788), Tim50 antibody (Santa Cruz, 393678), PGAM5 antibody (Abcam, 126534), Miro1 antibody (Abcam, 211363), control mouse IgG (Santa Cruz, 2025) or Rabbit IgG (Cell Signaling Technology, 2729) covalently bound to protein A magnetic beads (Life Technologies, 10001D) for 18 hr at 4 °C on a rotator. Beads were collected using a magnetic stand and washed four times with ice-cold RIPA buffer followed by boiling in 1 × LDS sample buffer containing reducing agent for 7 min at 100 ˚C. Proteins were separated on 8 % ~ 12 % SDS-PAGE followed by western blot using appropriate antibodies.

2.15 RNA isolation, cDNA synthesis, and quantitative-RT-PCR

Total RNA was isolated from cells by Purelink™ RNA Mini Kit (Life Technologies). cDNA was synthesized from 1 μg total RNA using iScript reverse transcription supermix (Bio-Rad, Hercules, CA) following the manufacturer's protocol. Quantitative RT-PCR was performed

using iTaq Universal SYBR Green Supermix (Bio-Rad) with StepOnePlus Real-Time PCR System (Applied Biosystems, Foster City, CA). The following primers were used: human NIK, 5'-CTAGTGCATGCTCTGCAAGG-3' and 5'-TGAGTTTCTCAGTGAGCAGGA-3'; mouse NIK, 5'-CCAGAATCGTCCCTCTCTAT-3' and 5'-GACAGCCCATTTGCTTTATG-3'; mouse MMP9 5'-GATC CCC AGA GCG TCATTC-3' and 5'-CCACC TTG TTC ACC TCA TTTTG-3'; human GAPDH, 5'-GAAGGTGAAGGTCGGAGTC-3' and 5'-GAAGATGGTGATGGGATTTC-3'; mouse GAPDH, 5'-CTTTGTCAAGCTCATTTCCTGG-3' and 5'-TCTTGCTCAGTGTCCTTGC-3'. Expression of mRNA was normalized to either GAPDH expression levels. All experiments were performed at least three times with three replicates per sample.

2.16 Mito-PAGFP fusion assay

BT25 cells were plated on μ-Slide 8 well chamber slides with a glass bottom (ibidi) and cotransfected with mito-PAGFP (Addgene, #23348) and pDsRed2-Mito (Addgene, #55838). After 24 hr, cells were imaged on a Nikon TI A1R inverted confocal microscope with 100x Plan-Apochromat lenses and Stage-top incubator system including heated stage and carbon dioxide chamber. A region of interest (ROI) of approximately 4 μm-wide was selected and activated by a short pulse of 405 nm laser. Imaging of post-activation was obtained immediately by the 488 nm laser and subsequent images were taken every 15 min for a total of 45 min. The dilution of mito-PAGFP fluorescence in time-lapse images was analyzed by measuring the pixel intensities using ImageJ (NIH).

2.17 ROS assay

Cellular Reactive oxygen species (ROS) levels were assayed using the CellROX Green reagent (Thermo Fisher, C10444) diluted 1:500 for 30 minutes at 37 °C. At least 10,000 events were measured and data was analyzed using Flow Jo V-X (Flowjo Llc, Ashland, OR).

2.18 Oxygen Consumption Assay

1.5 x 10^4 cells were seeded in triplicate in black clear bottom 96 well plates (Corning, CLS3603) in 150 µL NSC media containing 10% FBS and were allowed to adhere at 37 °C overnight. 10 µL of Mito-ID Extracellular O2 Sensor probe (ENZ-51045-K100) from Enzo Life Sciences (Farmingdale, NY) was reconstituted in PBS was added to each well and 2 drops of Mito-ID HS Oil was added to seal each well. The cells were then immediately analyzed with a Cytation 3 plate reader (Biotek, Winooski, VT). Reads were taken every 20 minutes over the course of 7 hours. All graphs and statistical data were analyzed using GraphPad Prism (GraphPad Software Inc., San Diego, CA, USA).

2.19 Monitoring mitochondrial constriction and division

BT25 cells and COS-7 cells expressing GFP-NIK, mCherry-Drp1 (Addgene, #49152), and mito-BFP (Addgene, #49151) were plated on µ-Slide 8 well chamber slides with a glass bottom (ibidi). After 18 hr, time-lapse images were acquired every 5 s for 2 min on Nikon TI A1R inverted confocal microscope with 60x Plan-Apochromat lenses and Stage-top incubator system. The diffuse cytosolic images were threshold-adjusted by subtracting background signal in the cytosol.

2.20 In vitro kinase assay

GST-Drp1$^{518–736}$ (Kashatus et al., 2015) was expressed in E. coli BL21 and purified using glutathione-sepharose-4B (GE Healthcare, #17075601). The GST fusion protein eluted from the beads via glutathione (Sigma-Aldrich, G4251) was dialyzed against PBS. 500 ng GST-Drp1 was incubated with cell lysates of transfected 293T cells (NIK wild-type and NIK$^{K429A/K430A}$) or HA-NIK (wild-type and mutant K429A/K430A)-bound beads in 25 µl 1× Kinase Buffer (Cell Signaling Technology, 9802) and 20 µM ATP for 15 min at 37 °C. The kinase assay was terminated by the addition of LDS sample buffer containing reducing agent for 7 min at 100 ˚C and resolved by SDS-Page.

2.21 Xenograft mouse models

All animal experiments were done in compliance with IACUC, AAALAC and Texas A&M Health Science Center Biosafety guidelines using an IACUC-approved Animal Use (Protocol # 2015-0330). For orthotopic tumor inoculations, cells were labeled using a DiD Cytoplasmic Membrane dye (Biotium, abs/ em=644/665). $5x10^5$ cells in 3 µl PBS medium were injected into the right striatum of 4 - 6 week old CD-1 nude mice. Tumor formation was imaged using an In Vivo FX Imaging System (Carestream, Rochester, NY). Injections were done using 3 - 4 animals for each cell type.

2.22 In situ proximity ligation assay

The in situ Proximity ligation assay (PLA) was performed according to the manufacturer's instructions, using the Duolink PLA reagents (Sigma-Aldrich, Louis, MO, USA). BT25 control and BT25-sgNIK cells were fixed in 4 % paraformaldehyde for 20 min and

permeabilized for 20 minutes with 0.3 % Triton X-100 followed by blocking at room temperature for 30 min. Cells were incubated with primary antibodies against NIK (Abcam, ab191591), Drp1 (Abcam, ab56788), PGAM5 antibody (Abcam, 126534) or control mouse IgG (Santa Cruz, 2025) for 18 hours at 4°C, followed by washing and incubation with the Duolink® In Situ PLA® Probe Anti-Rabbit PLUS and Anti-Mouse MINUS (Sigma-Aldrich, DUO92002, DUO92004). After ligation and amplification using DUO92008 Duolink® In Situ Detection Reagents Red (Sigma-Aldrich, DUO92008), the cells were counterstained with DAPI and Tom20-AF647 (Abcam, ab205487) and red PLA signals were visualized under a TI A1R inverted confocal microscope (Nikon).

CHAPTER III

NIK REGULATES MITOCHONDRIAL DYNAMICS TO PROMOTE CELL INVASION INDEPENDENTLY OF IKK/NF-KB*

3.1 Summary

Although the role of NIK in immunity is well established, its relevance in cancer is just emerging. Here we describe novel functions for NIK in regulating mitochondrial dynamics and motility to promote cell invasion. We show that NIK is localized to mitochondria in cancer cell lines, ex vivo tumor tissue, and MEFs. NIK recruits Drp1 to promote mitochondrial fission and subcellular distribution to the leading edge of migrating cells. Consistent with a role for NIK in regulating mitochondrial dynamics, we demonstrate that Drp1 is required for NIK-dependent, cytokine-induced invasion. Importantly, using MEFs, we demonstrate that the established downstream mediators of NIK signaling, IκB kinase α/β (IKK α/β) and NF-κB, are not required for NIK to regulate cell invasion, Drp1 mitochondrial localization, or mitochondrial fission. Taken together, these findings reveal a previously unknown pool of NIK protein that is localized to mitochondria in cancer cells and regulates mitochondrial dynamics, motility and cell invasion independently of the IKK/NF-κB signaling cascade.

3.2 Introduction

NIK, the central kinase activating the non-canonical NF-κB pathway, has been shown to

*Part of this chapter is reprinted with permission from "NIK/MAP3K14 Regulates Mitochondrial Dynamics and Trafficking to Promote Cell Invasion." By Jung JU, Ravi S, Lee DW, McFadden K, Kamradt ML, Toussaint LG, Sitcheran R, 2016. Current Biology, 26, 3288-3302, Copyright 2016 by Elsevier Ltd.

contribute to tumorigenesis in several cancers through regulating cell proliferation and survival (Thu and Richmond, 2010; Xia et al., 2014). However, the molecular mechanisms by which NIK stimulates tumor growth have not been fully elucidated. Our previous work demonstrated that non-canonical NF-κB signaling is significantly increased in highly invasive glioma tumor lines, compared to less invasive glioma lines (Cherry et al., 2015; Lee et al., 2013). More recently, we have shown that the ability of NIK to promote glioma invasiveness is associated with cell shape changes, including formation of invadopodia pseudopodial membrane protrusions and cell size (Duran et al., 2016). Why is cell size shown to positively correlate with the expression of NIK? Cell size correlates with the proliferative potential and metabolic demands of cancer cells (Dolfi et al., 2013). Large cell size correlates with mitochondria abundance that is associated with cancer progression (Grupp et al., 2013; Yamamoto et al., 2014). Interestingly, tumor cell migration and invasion have been linked to regulation of mitochondrial dynamics, and more specifically, to alterations in the balance between mitochondrial fission and fusion (Caino and Altieri, 2015; Desai et al., 2013; Ferreira-da-Silva et al., 2015; Zhao et al., 2013). Indeed, cancer cells often exhibit a fragmented mitochondrial phenotype (Arismendi-Morillo, 2009; Inoue-Yamauchi and Oda, 2012; Rehman et al., 2012). During cancer cell migration, mitochondria are redistributed to the leading edge containing invadopodia, a subcellular region requiring high energy due to extensive cytoskeletal and focal adhesion remodeling during cell movement (Caino and Altieri, 2015). Consistent with these observations, the mitochondria-associated fission protein Drp1 has been shown to promote tumor migration, invasion and pathogenesis (Senft and Ronai, 2016).

Regulation of NIK, a constitutively active kinase (Liu et al., 2012), occurs primarily at the post-translational level. In unstimulated cells, NIK is rendered inactive through its

association with a TRAF-cIAP complex that catalyzes its ubiquitination and continuous proteasome-dependent degradation in the cytosol (Sun, 2012). Activation of NIK is achieved through disassembly of the degradation complex, resulting in stabilization and accumulation of NIK protein (Sun, 2010). Once stabilized, NIK phosphorylates and activates IKKα, which in turn phosphorylates p100, triggering proteolytic processing to p52 and nuclear translocation of p52-RelB non-canonical NF-κB transcription factors (Razani et al., 2011; Sun, 2010). The predominant, physiological function of NIK is to activate IKKα and non-canonical NF-κB signaling, but NIK can also induce IKKα-dependent, canonical NF-κB signaling, particularly when NIK is overexpressed, or aberrantly stabilized (Odqvist et al., 2013; Oeckinghaus et al., 2011; Ramakrishnan et al., 2004). Functions for IKK-independent NIK signaling have not been described to date.

Generally, subcellular localization of a protein can provide crucial information about its function. While NIK is known to be present mainly in the cytoplasm and quickly translocates into the nucleus, in this study, we identified novel protein pools of NIK localized at the mitochondria that functions independently of IKK/ NF-κB to promote mitochondrial fragmentation and tumor cell invasion.

3.3 Results

3.3.1 NIK is localized to mitochondria in cancer cells and promotes invasion

Proteomics analysis has revealed an enrichment of mitochondrial proteins in invadopodia (Attanasio et al., 2011), and recent cell-biological studies have shown a re-distribution of mitochondria to the leading edge of cells during migration (Desai et al., 2013). These observations suggest that mitochondria move to distal cell protrusions and sites of active cell

invasion. In light of our recent findings that NIK promotes invasion of glioma cells and induces cell shape changes, including pseudopodia/invadopodia formation (Duran et al., 2016), we sought to determine whether NIK plays a role in these processes using a highly invasive (BT25) and a minimally invasive (BT114) glioma cell line derived from human glioma patients that express high and low levels of NIK, respectively (Fig. 6) (Cherry et al., 2015). We first investigated NIK's role in BT25 cells and employed small guide (sg) RNAs in combination with the CrispR/Cas9 gene editing system in BT25 cells to generate tumor cells lacking a functional NIK gene (BT25-sgNIK) (Duran et al., 2016). Loss of NIK significantly attenuates invasion in three-dimensional collagen matrices compared with control cells, and invasion was restored with expression of the highly conserved, murine NIK (BT25-sgNIK+rescue) (Fig. 7).

To visualize mitochondria, we transfected BT25 control, BT25-sgNIK and BT25-sgNIK+rescue cells with the mitochondrial marker CellLight Mitochondria-RFP (Mito-RFP) (Kilgore et al., 2013). Confocal fluorescence microscopy revealed that mitochondria extended throughout the cell body to sites distal from the nucleus (Fig. 8A). However, in the absence of NIK (BT25-sgNIK cells), Mito-RFP staining appeared collapsed within the perinuclear region of cell, which had minimal cytoplasmic processes (Fig. 8B), while expression of murine NIK in NIK knockout cells (BT25 sgNIK+rescue) restored distal mitochondrial extensions, similar to control (Fig. 8C). Interestingly, when we performed NIK immunostaining to confirm alterations in NIK expression, we observed a striking co-localization of NIK with Mito-RFP in untreated BT25 control cells (Fig. 8A and D). Minimal NIK immunostaining was observed in BT25-sgNIK cells, demonstrating specificity of the antibody (Fig. 8B), and re-expression of murine NIK (BT25 sgNIK+rescue cells) restored NIK mitochondrial staining (Fig. 8C and D). For detection of endogenous NIK protein by immunoblot, cells were treated with TWEAK (to induce

NIK/non-canonical NF-κB signaling) (Cherry et al., 2015) and the proteasome inhibitor MG132 (to stabilize NIK for more facile detection). NIK protein was present in both mitochondrial-enriched (M) and cytosolic (C) cell fractions of TWEAK/MG132-treated BT25 control cells and BT25 sgNIK+rescue cells. (Fig. 9). However, while mitochondrial NIK was readily detected by immunostaining, cytosolic NIK was not detectable, suggesting that antibody epitope availability differs in the cytosolic and mitochondrial compartments. NIK protein was not detected by immunoblotting in either fraction from BT25-sgNIK cells, confirming NIK knockout, as well as antibody specificity (Fig. 9).

Given the close association of mitochondria with other organelles, particularly the endoplasmic reticulum (ER), as well as a recent report describing localization of a small fraction of NIK to endosomes in endothelial cells (Jane-wit et al., 2015), we examined NIK subcellular localization in more detail in BT25 glioma cells. Triple-immunostaining experiments showed that NIK immunostaining overlapped extensively with mitochondrial protein CoxIV, but not the ER protein Calnexin (Fig. 10A). Consistent with this observation, NIK showed extensive co-localization with the mitochondrial outer membrane protein Tom20 (Fig. 10B), but not the ER protein Sec61, or the endosomal protein Rab5 (Fig. 11A and B).

We next confirmed NIK's function in mitochondria using gain-of-function studies in BT114 glioma cells. Interestingly, BT114 control cells displayed a mitochondrial phenotype that resembled BT25-sgNIK cells, with a concentration of Mito-RFP signal in the perinuclear region (compare Fig.12A to Fig. 8B). Overexpression of human NIK (BT114-hNIK) robustly increased invasion, compared to BT114 control cells (Fig. 13A and B). Furthermore, BT114-hNIK cells exhibited increased Mito-RFP staining throughout distal regions of the cell (Fig.12B). Though much weaker than BT25 cells, NIK immunostaining signal similarly colocalized with Mito-RFP

in BT114 control cells (Fig.12A). We were unable to detect any NIK in untreated BT114 cells (without TWEAK/MG132) by immunoblotting (Fig.12D). However, ectopically expressed NIK protein was observed in both mitochondrial and cytosolic fractions of BT114-hNIK cells (Fig.12D).

To test whether mitochondrial localization of NIK, as well as its effect on mitochondrial intracellular distribution, was restricted to glioma cells, we performed immunostaining and invasion assays in MDA-MB231 breast cancer cells and Panc1 pancreatic cancer cells. As with glioma cell lines, we observed co-localization of NIK and Mito-RFP in both MDA-MB231 and Panc1 cells (Fig. 14A and 15A; top panels), and NIK immunostaining was lost in CrispR-Cas9 mediated NIK knockout cells (Fig. 14A and 15A; lower panels), similar to BT25 knockout cells. Moreover, loss of NIK in MDA-MB231-sgNIK and Panc1-sgNIK cells resulted in condensed, perinuclear mito-RFP staining and significantly diminished invasive potential (Fig. 14 and 15). Together, these data identify a previously unknown pool of NIK protein that localizes to mitochondria in several different cancer cells and demonstrate a strong correlation between mitochondrial NIK expression and cell invasion.

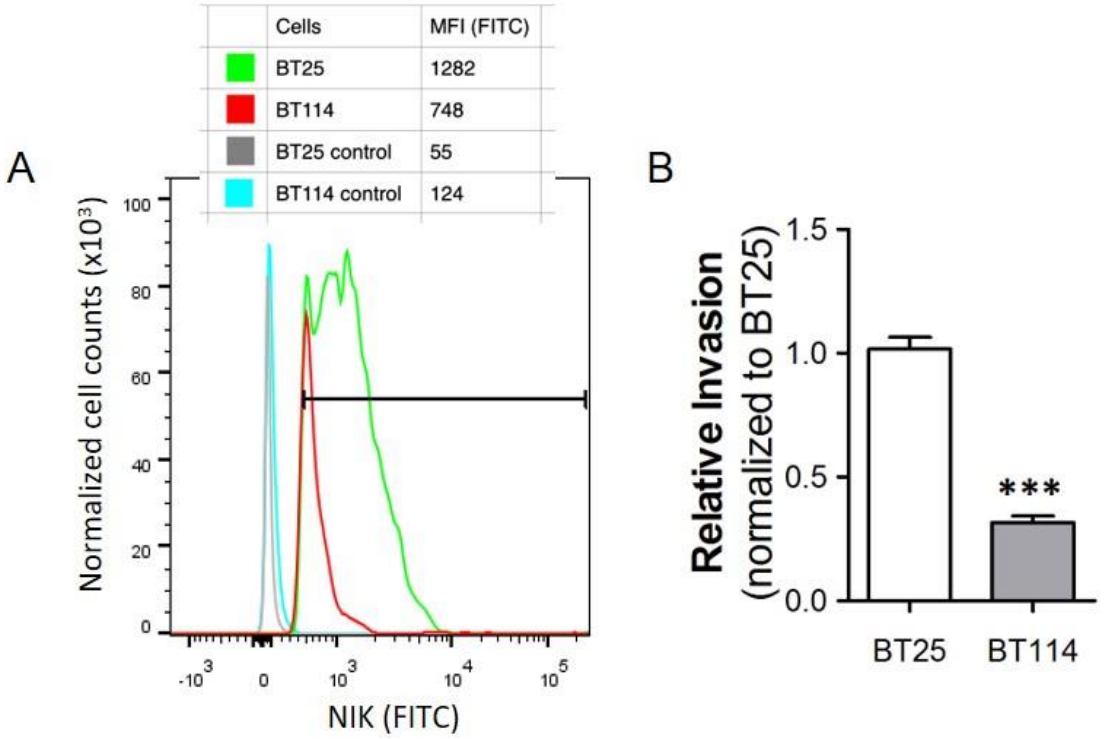

Figure 6. Analysis of NIK protein expression and invasive potential in BT25 and BT114 cells. (A). Flow cytometry analysis was performed on fixed, permeabilized cells using NIK antibody and anti-rabbit AF-488. Results demonstrate that NIK is more highly expressed in BT25 cells compared with BT114 cells. Mean Fluorescence Intensity (MFI) of FITC signal is indicated. (B) Equal numbers (40,000 cells) of BT25 and BT114 cells were allowed to invade three-dimensional collagen matrices for 48 hours. Cells were fixes, stained and invading cells were counted from at least 3 random 10X fields from each replicate sample (n=3). Representative data from one experiment is shown (n>6). Results demonstrate that BT25 cells are significantly more invasive compared with BT114 cells. Statistics *** $p<0.001$, unpaired t-test.

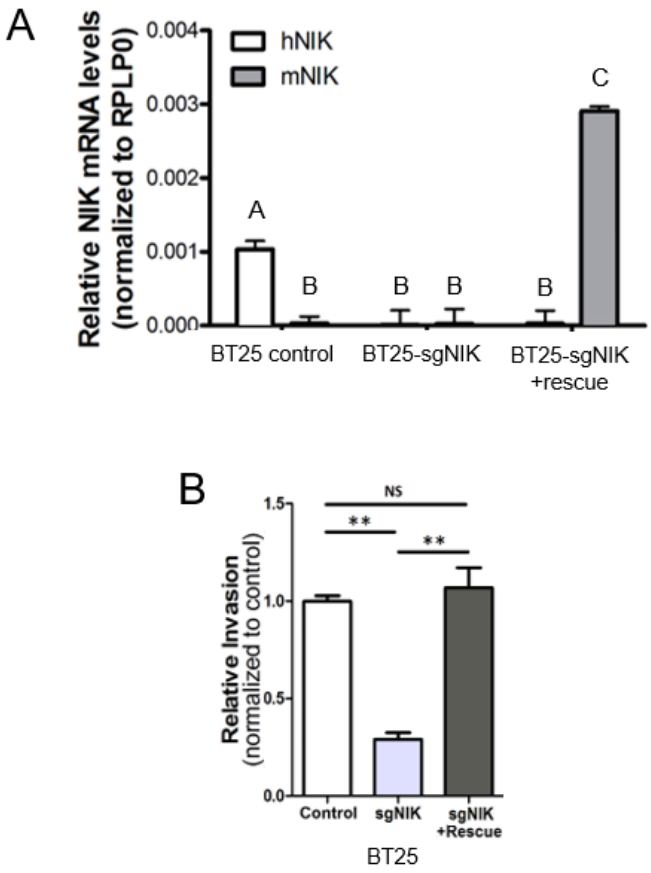

Figure 7. Loss of NIK leads to decreased invasion potential in glioma cells. (A) Quantitative RT-PCR (qPCR) analysis of human and mouse NIK expression in human glioma cells: BT25 control, BT25-sgNIK and BT25-sgNIK cells expressing mouse NIK (sgNIK+rescue). For this and all subsequent experiments, representative data from at least three independent experiments are shown. Graph shows mean values ± SD (n=3). Different letters indicate statistically significant differences: for A vs. B, $p<0.001$; for A/B vs. C, $p<0.0001$. (B) NIK expression correlates with invasive potential in three-dimensional collagen invasion assays. Relative invasion reflects numbers of invading cells normalized to control and data are represented as mean ± SD. ** $p<0.001$ for sgNIK vs. control and sgNIK vs. sgNIK+rescue, one-way ANOVA.

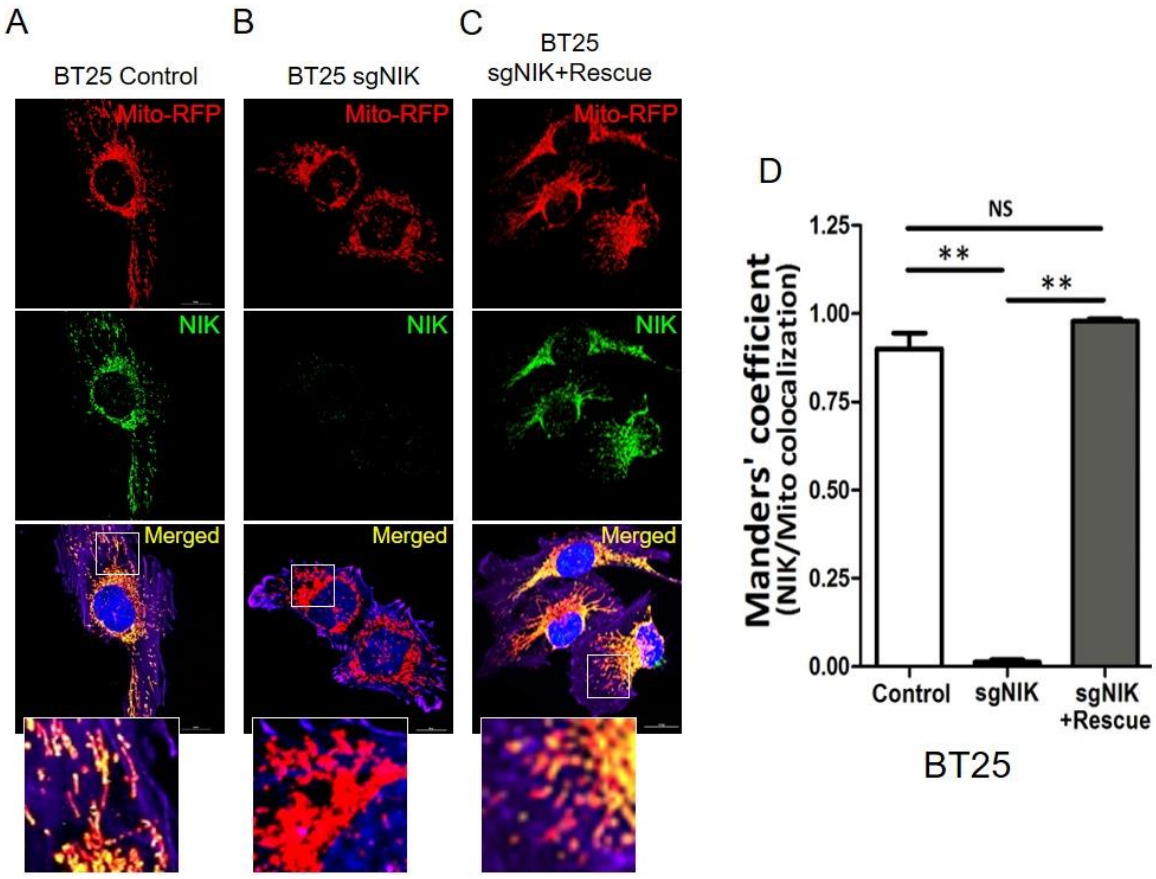

Figure 8. NIK is localized to mitochondria in glioma cells. (A) Immunofluorescence images of BT25 control, (B) BT25-sgNIK and (C) BT25-sgNIK+rescue cells transfected with Mito-RFP (red) and immunostained for NIK (green), and DAPI (blue). Images marked with white squares are amplified and shown in the bottom. Scale bar, 10 μm. (D Bar graph showing Manders' coefficients (fraction of NIK in co-localization with Mito-RFP) for co-localization of NIK and mitochondria (C - E). Data are mean ± SD (n=12). ** $p<0.01$ for sgNIK vs. control and sgNIK vs. sgNIK+rescue, one-way ANOVA.

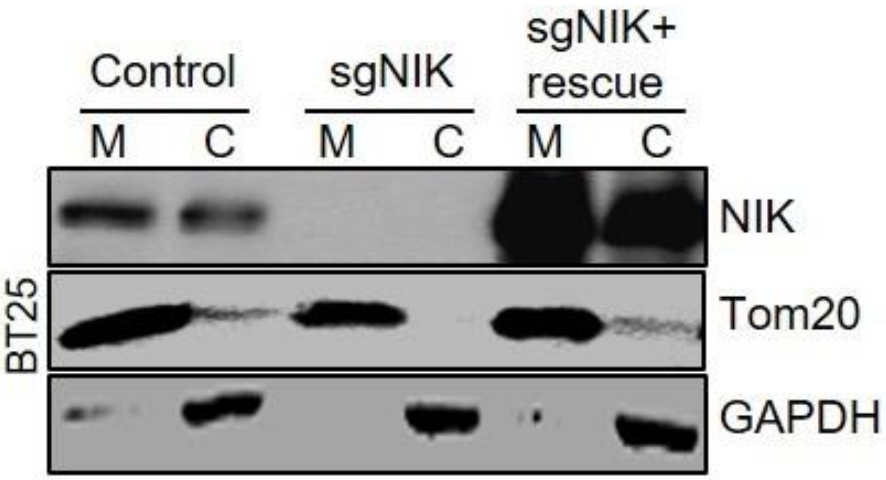

Figure 9. NIK protein is enriched in both mitochondrial and cytosolic fractions. Immunoblot analysis of mitochondrial-enriched (M) and cytosolic (C) fractions prepared from BT25 control, BT25-sgNIK and BT25-sgNIK+rescue cells pretreated with TWEAK (10 ng/ml) and MG132 (5 μM) to stabilize NIK for facile detection and to confirm loss of protein in sgNIK cells. Four times the volume equivalent of mitochondrial-enriched fraction versus cytosol fraction was loaded (mitochondrial-enriched/cytosol = 4:1). Blots were probed with indicated antibodies.

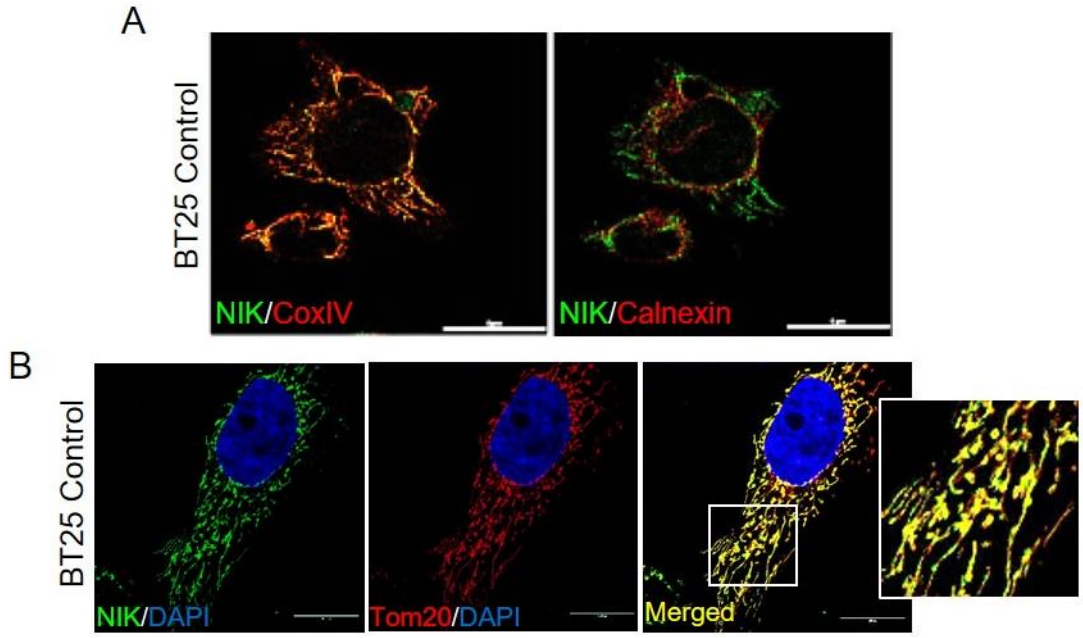

Figure 10. NIK co-localization with specific mitochondrial markers in glioma cells. (A) Representative confocal immunofluorescence images of BT25 cells sequentially triple-stained with antibodies specific for mitochondrial marker CoxIV (red; AF564), endoplasmic reticulum marker calnexin (red; AF647) and polyclonal NIK (green; Abcam ab7204). NIK-specific antibody was pre-labeled with AF488. Left panel shows merged overlay (yellow-orange) of NIK (green) and CoxIV (red). Right panel shows the same cell with merged overlay of NIK (green) and calnexin (pseudo-colored red). Scale bar, 10 µm. (B) Representative confocal immunofluorescence images of BT25 glioma cells immunostained for NIK (green; Abcam ab191591) and pre-labeled antibody specific for Tom20-AF647 (pseudo-colored red, upper panels). Images marked with white squares are amplified and shown in the bottom. Scale bar, 10 µm.

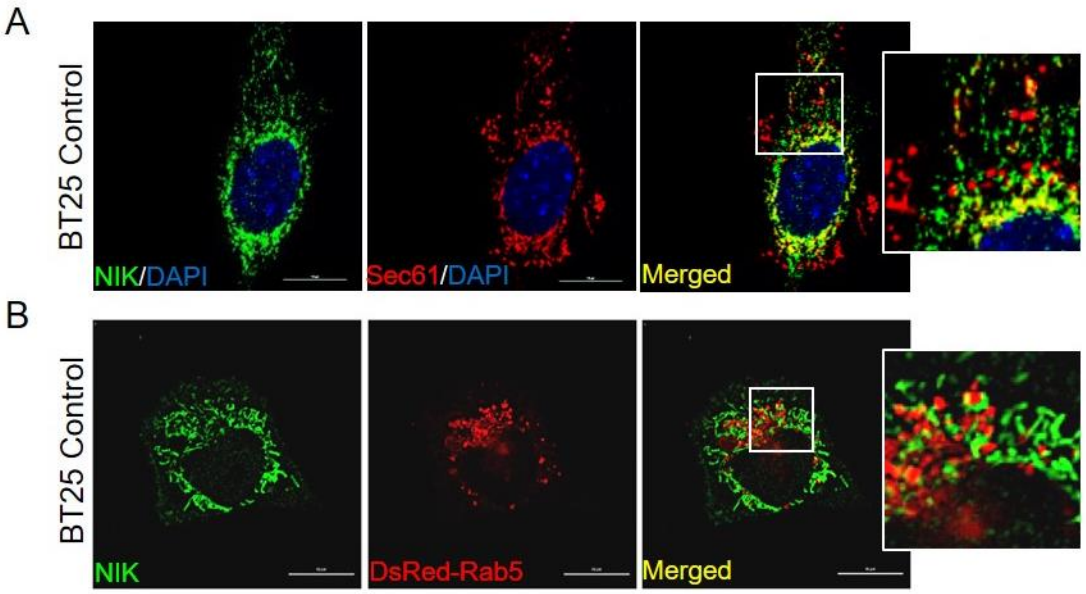

Figure 11. NIK has not signnificant co-localization with markers for the ER and endosome in glioma cells. (A) Representative confocal immunofluorescence images of BT25 glioma cells immunostained for NIK (AF564, pseudo-colored green) and pre-labeled antibody specific for Sec61A-AF488 (pseudo-colored red), and DAPI (blue). Images marked with white squares are amplified and shown in the bottom. Scale bar, 10 μm. (B) Representative immunofluorescence confocal microscopy images of BT25 cells transfected with dsRed-Rab5 and then fixed and stained with an antibody specific to NIK (green). Images marked with white squares are amplified and shown in the bottom. Scale bar, 10 μm.

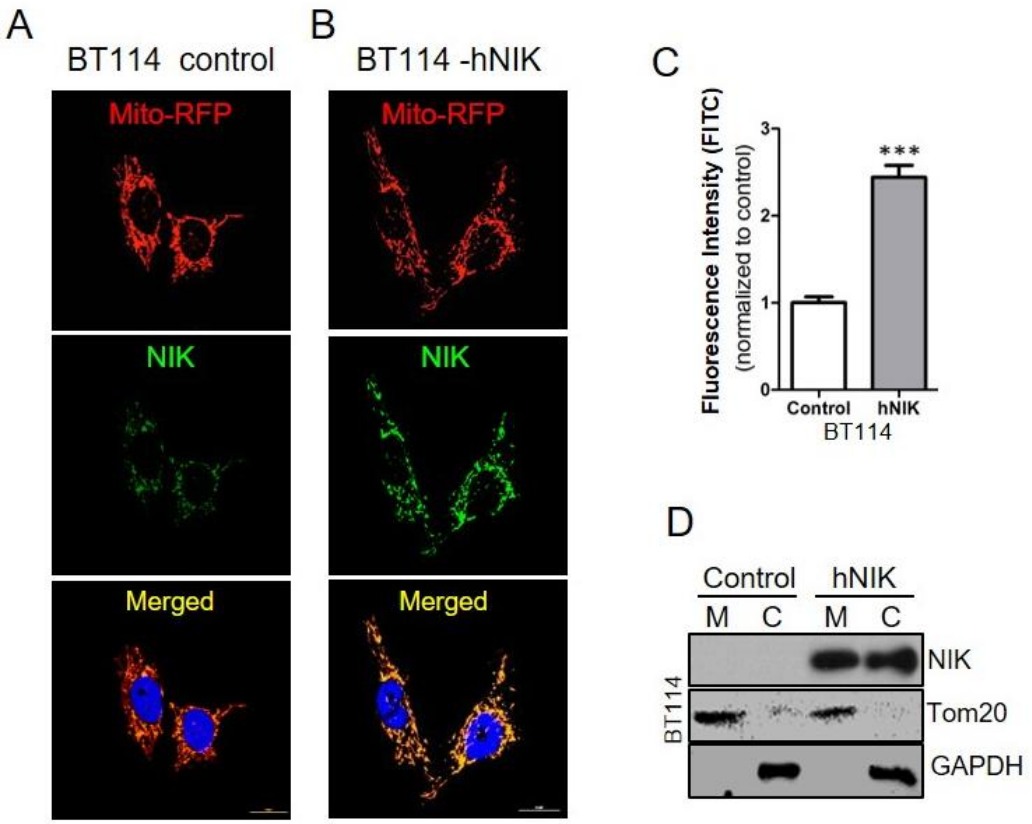

Figure 12. Ectopically overexpressed NIK is localized to mitochondria in glioma cells. (A) Representative confocal immunofluorescence images are shown of BT114 control and (B) BT114-hNIK cells transfected with Mito-RFP and then immunostained for NIK (green), and DAPI (blue). (C) Bar graph showing results from measurements of mean fluorescent intensity of NIK staining in BT114 control (A) and BT114-hNIK cells (B) normalized to control and represented as mean ± SEM (n=30). *** $p<0.001$, unpaired t-test. (D) Immunoblot analysis of cell fractions prepared from untreated BT114 control and BT114- hNIK using the indicated antibodies. (mitochondrial-enriched/cytosol = 4:1 in volume equivalents).

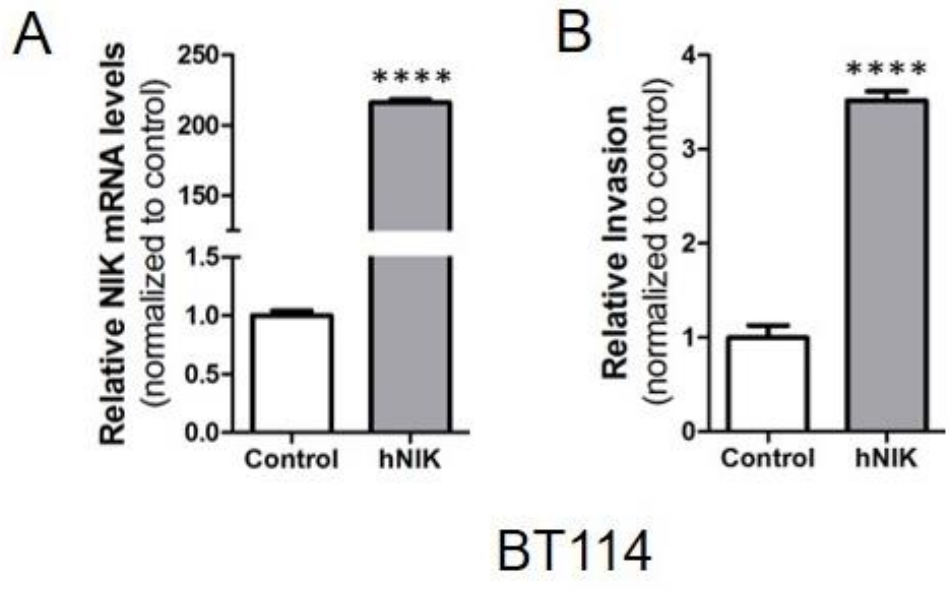

Figure 13. NIK overexpression enhances invasion of glioma cells. (A) qPCR analysis of NIK expression in BT114 control and BT114-hNIK cells. Data are represented as mean ± SD. **** $p<0.0001$, unpaired t-test (n=3). (B) Quantification of three-dimensional collagen invasion assays comparing BT114 control and BT114-hNIK cells. Data are represented as mean ± SEM. *** $p<0.001$, unpaired t-test (n=3).

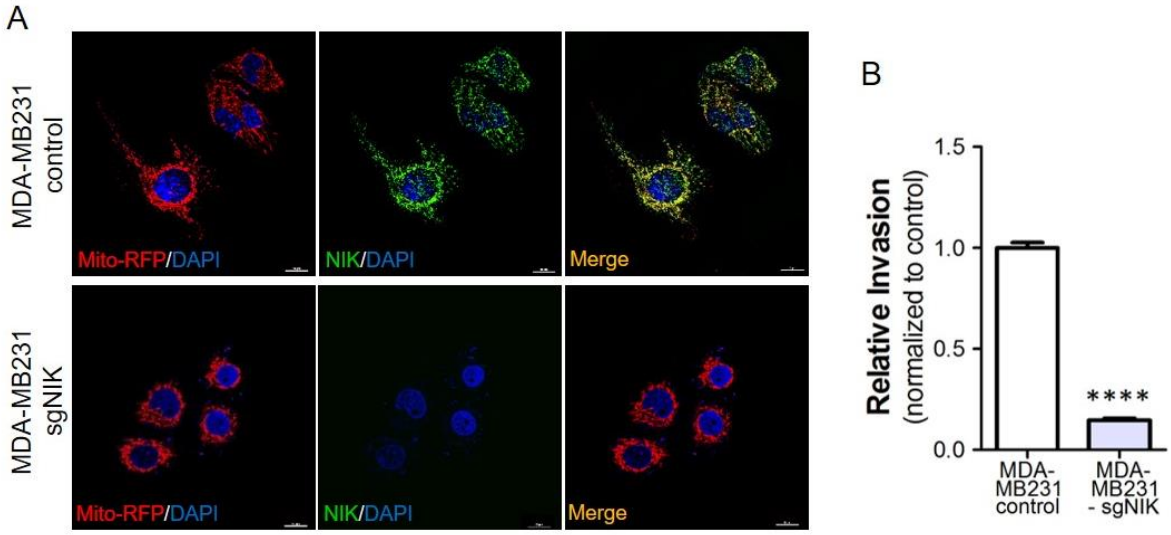

Figure 14. NIK is localized to mitochondria of invasive breast cancer cells. (A) MDA-MB231 control cells (upper panel) and MDA-MB231 NIK knockout cells (sgNIK, lower panel) were transfected with Mito-RFP and then stained for NIK (green) and DAPI (blue). Representative confocal immunofluorescence images are shown. (B) NIK promotes the invasive potential of breast and pancreatic cancer cells. Quantification of three-dimensional collagen invasion assays comparing MDA-MB231 control and MDA-MB231-sgNIK (left panel). Relative invasion reflects numbers of invading cells normalized to control from at least three independent experiments, each with $n \geq 3$ for each cell type. For MDA-MB231 control vs. sgNIK: **** $p<0.0001$, unpaired t-test.

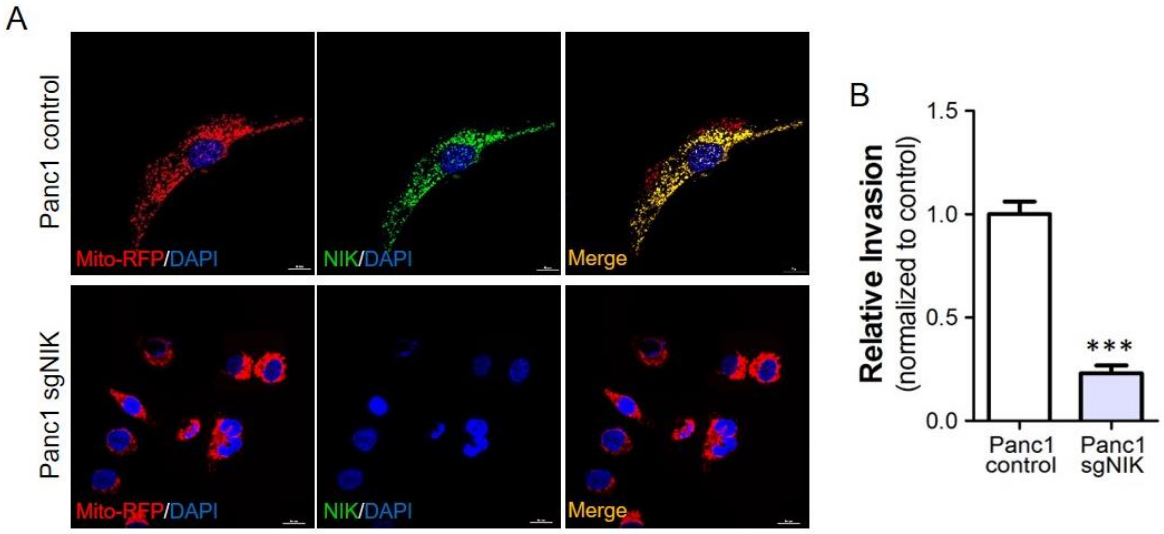

Figure 15. NIK is localized to mitochondria of invasive pancreatic cancer cells. (A) Panc1 control cells (upper panel) and Panc1 NIK knockout cells (sgNIK, lower panel) were transfected with Mito-RFP and then stained for NIK (green) and DAPI (blue). No NIK signal is observed in Panc1-sgNIK cells. (B) NIK promotes the invasive potential of breast and pancreatic cancer cells. Quantification of three-dimensional collagen invasion assays comparing Panc1 control and Panc1-sgNIK cells (right panel). Relative invasion reflects numbers of invading cells normalized to control from at least three independent experiments, each with $n \geq 3$ for each cell type. For Panc1 control vs. sgNIK: ***$p<0.001$, unpaired t-test.

3.3.2 NIK regulates mitochondrial subcellular localization and motility

To analyze NIK's role in mitochondria clustering in more detail, we quantified intracellular mitochondrial distribution in BT25, BT25-sgNIK and BT25-sgNIK+rescue cells. Fluorescence intensity plots demonstrated that mitochondria in BT25 control cells extended from the nucleus to the distal edge of cells (Fig. 16A and D). Mitochondria in cells lacking NIK extended less than half the distance of those organelles in control cells, and remained collapsed in the perinuclear region (Fig. 16B and D). As expected, NIK overexpression (BT25-sgNIK+rescue cells) restored the presence of mitochondria from the nucleus to the distal edge, similar to control cells (Fig. 16C and D). To determine whether the accumulation of perinuclear mitochondria was associated with decreased mitochondria motility during cell migration, we performed live cell imaging and particle-tracking analysis of Mito-RFP-labeled mitochondria (watch the video linked; BT25 control cell http://www.cell.com/cms/attachment/2118002281/2085729692/mmc2.mp4; BT25-sgNIK cell http://www.cell.com/cms/attachment/2118002281/2085729693/mmc3.mp4; BT25-sgNIK+rescue cell http://www.cell.com/cms/attachment/2118002281/2085729694/mmc4.mp4). Results from these experiments revealed that the velocity and overall distance traveled by mitochondria was significantly compromised in BT25-sgNIK cells, and these defects were restored by re-expression of NIK (BT25-sgNIK+rescue cells; Fig. 17). Moreover, mitochondria in BT25 control and BT25-sgNIK+rescue cells exhibited predominantly anterograde movement and directional migration towards the cell periphery, whereas mitochondria in BT25-sgNIK cells exhibited seemingly random patterns of both anterograde and retrograde movement (Fig. 18). These data indicate that NIK regulates velocity and directional migration of mitochondria, resulting in subcellular distribution of mitochondria to the periphery of regions of the cells.

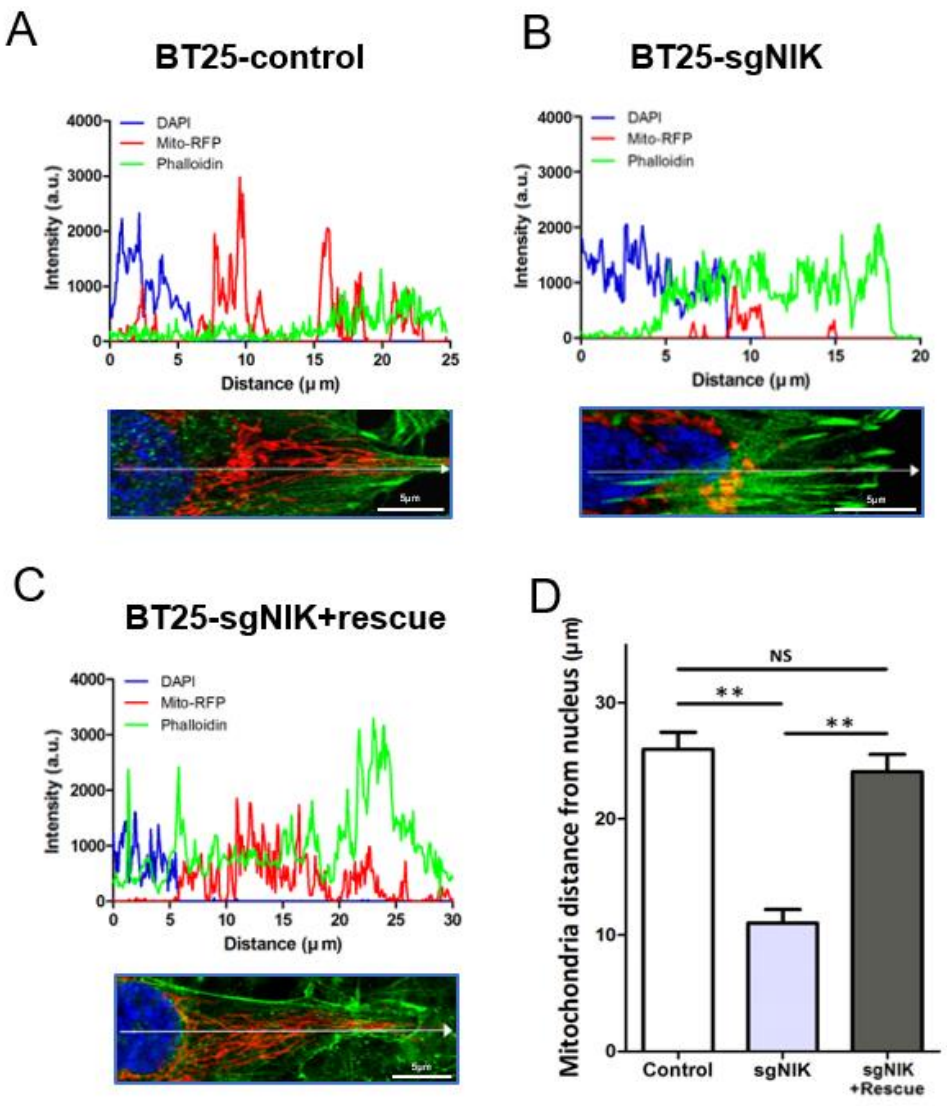

Figure 16. NIK regulates mitochondrial distribution. Fluorescence intensity profile plot of BT25 control (A), BT25-sgNIK (B), and BT25-sgNIK+rescue cells (C). Graphs show the immunofluorescence intensity, expressed in arbitrary units (a.u.), of Mito-RFP (red), DAPI (blue) and Phalloidin (green) along the line arrow in lower images. Scale bar, 5 μm. (D) Bar graph shows quantification of distance from the nucleus to mitochondria. Data are represented as mean ± SD (n>10). ** p<0.01 for sgNIK vs. control and sgNIK vs. sgNIK+rescue, one-way ANOVA.

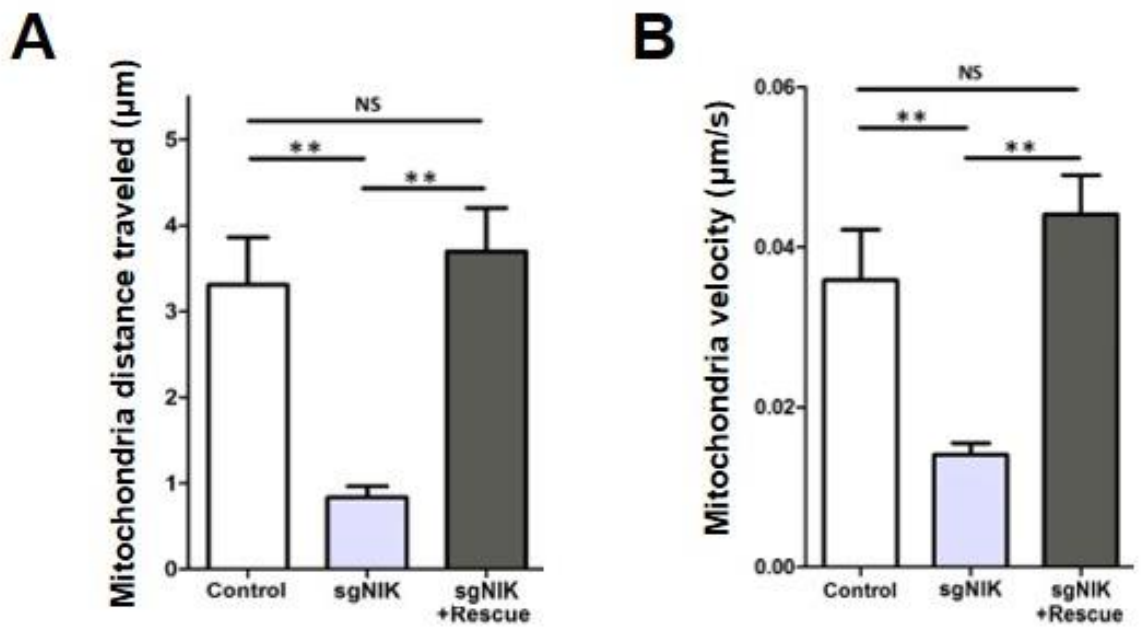

Figure 17. NIK regulates both velocity and run distance of mitochondria. Plot of run length (A) and velocity (B) of mobile mitochondria in the cells expressing Mito-RFP as supplementary material Movie S1. Data are represented as mean ± SD. of randomly selected mitochondria shown in different colors (n > 10 cells, respectively).

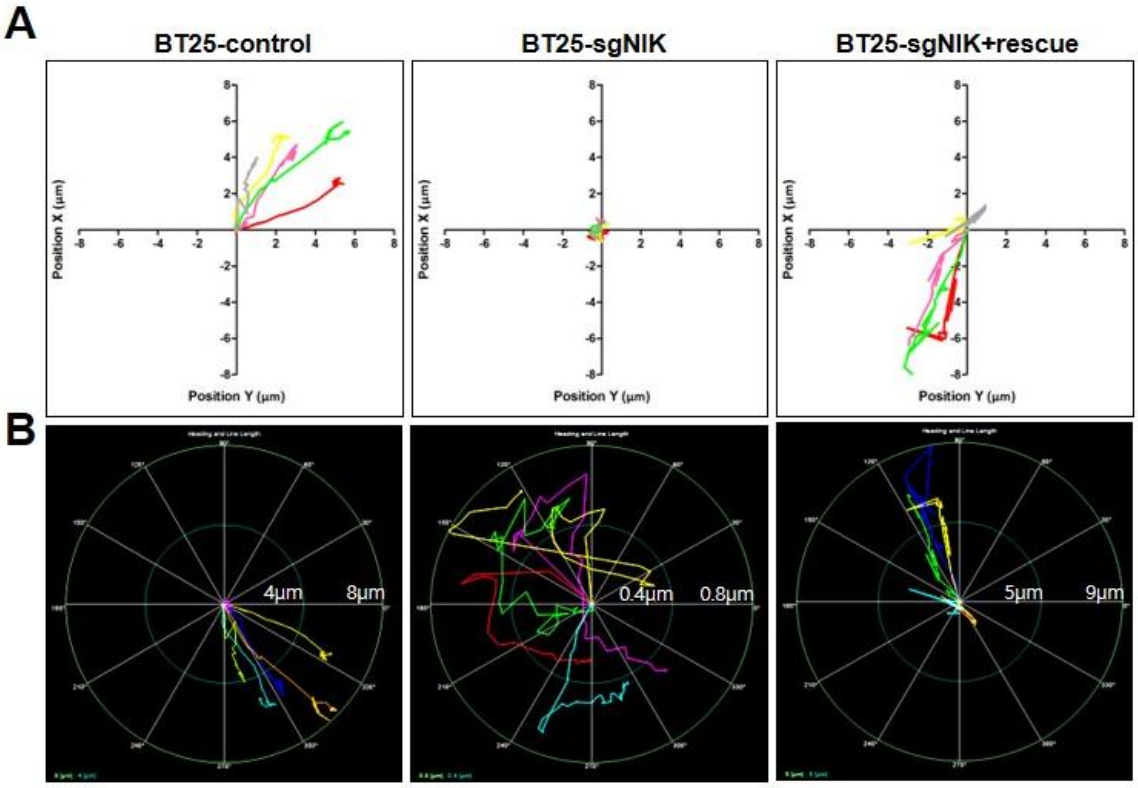

Figure 18. NIK influences direction of mitochondrial movement. (A) Vector paths of single mitochondria observed during live-cell imaging representing the tracks and (B) direction of mitochondria movement. The intersection point of X the Y axis is starting point of each mitochondria.

3.3.3 NIK regulates mitochondrial morphology through promoting fission

We next performed superresolution-structured illumination microscopy (SR-SIM) of Mito-RFP-labeled BT25 cells. Results from these experiments demonstrated that mitochondria in BT25 control cells were fragmented and punctate, forming elongated tracks throughout the cytoplasm that extended towards the cell periphery (Fig. 19A). In BT25-sgNIK cells, however, mitochondria were more tangled, fused and condensed within the perinuclear region (Fig. 19B), a phenotype that was reversed by mNIK overexpression (Fig. 19C). We also performed particle analysis of Mito-RFP staining using ImageJ, which revealed that while the number of mitochondria was significantly decreased in cells lacking NIK (BT25-sgNIK cells) compared to corresponding control cells, mitochondria size increased (Fig. 20). Conversely, NIK overexpression (BT114-hNIK cells) was associated with increased number and decreased size of mitochondria (Fig. 21).

Lastly, to determine whether the increased mitochondrial size in BT25-sgNIK cells reflected altered mitochondrial dynamics, we examined mitochondrial fusion in live cells using a mitochondrial matrix-targeted photoactivatable green fluorescent protein (mito-PAGFP)-based assay (Karbowski et al., 2014). Fluorescence intensity in specific regions of interest (ROIs) had very similar rates of dissipation in BT25 control and BT25-sgNIK cells (Fig. 22), demonstrating that mitochondrial fusion is not significantly impaired in the absence of NIK. Together, these results strongly suggest a role for NIK in promoting mitochondrial fission leads to mitochondrial dynamics.

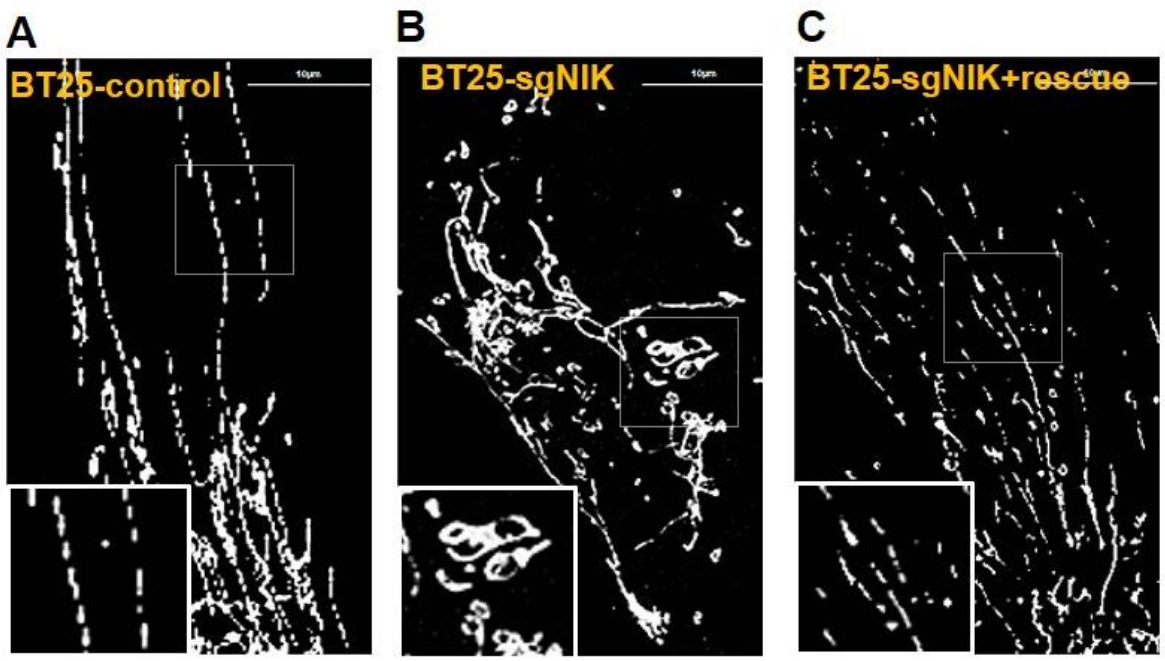

Figure 19. Super-resolution microscopy of mitochondrial morphology. (A) Super-resolution structured illumination microscopy (SR-SIM) was performed with the following cells expressing Mito-RFP: BT25 control, (B) BT25-sgNIK, and (C) BT25-sgNIK+rescue. Images marked with white squares are magnified and shown in the bottom. Scale bar, 10 μm.

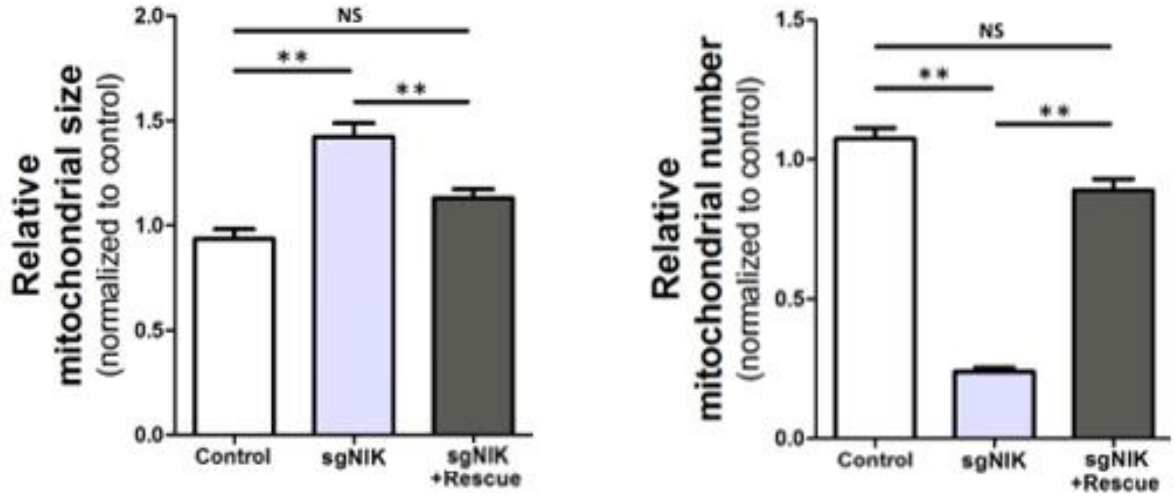

Figure 20. Loss of NIK results in a hyperfused mitochondrial network. Mitochondrial number and size in BT25 control, BT25-sgNIK, and BT25-sgNIK+rescue were quantified using the Analyze Particles function in ImageJ software. Data are represented as mean ± SD. ** $p<0.01$ for sgNIK vs. control and sgNIK vs. sgNIK+rescue, one-way ANOVA ($n > 100$, respectively).

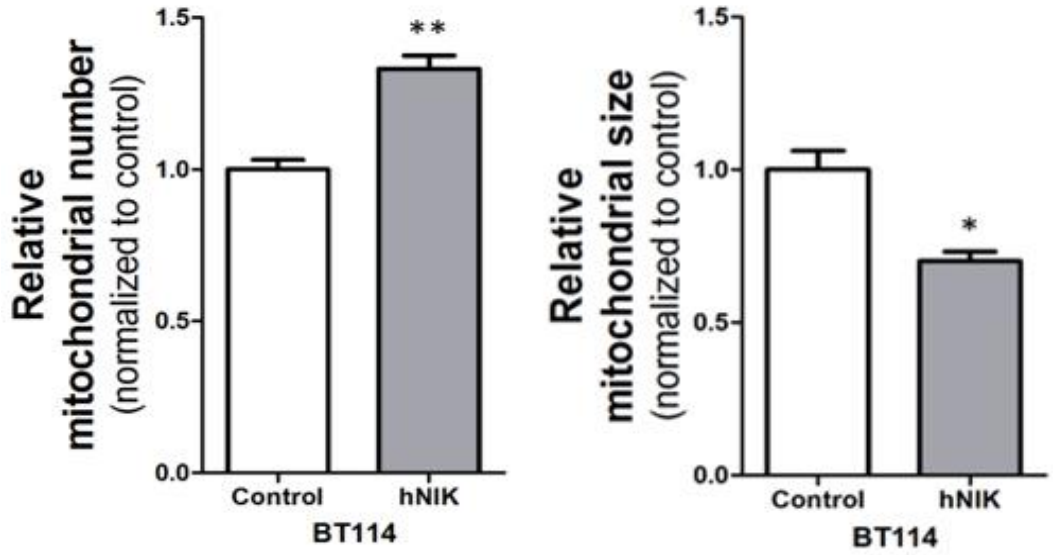

Figure 21. Overexpression NIK leads to increase in mitochondrial fragmentation. Mitochondrial number and size in BT114 control and BT114-hNIK were quantified using the Analyze Particles function in ImageJ software (±SEM **$p<0.01$; *$p<0.05$, using unpaired Student's t-test, N=47 and 27 cells, respectively).

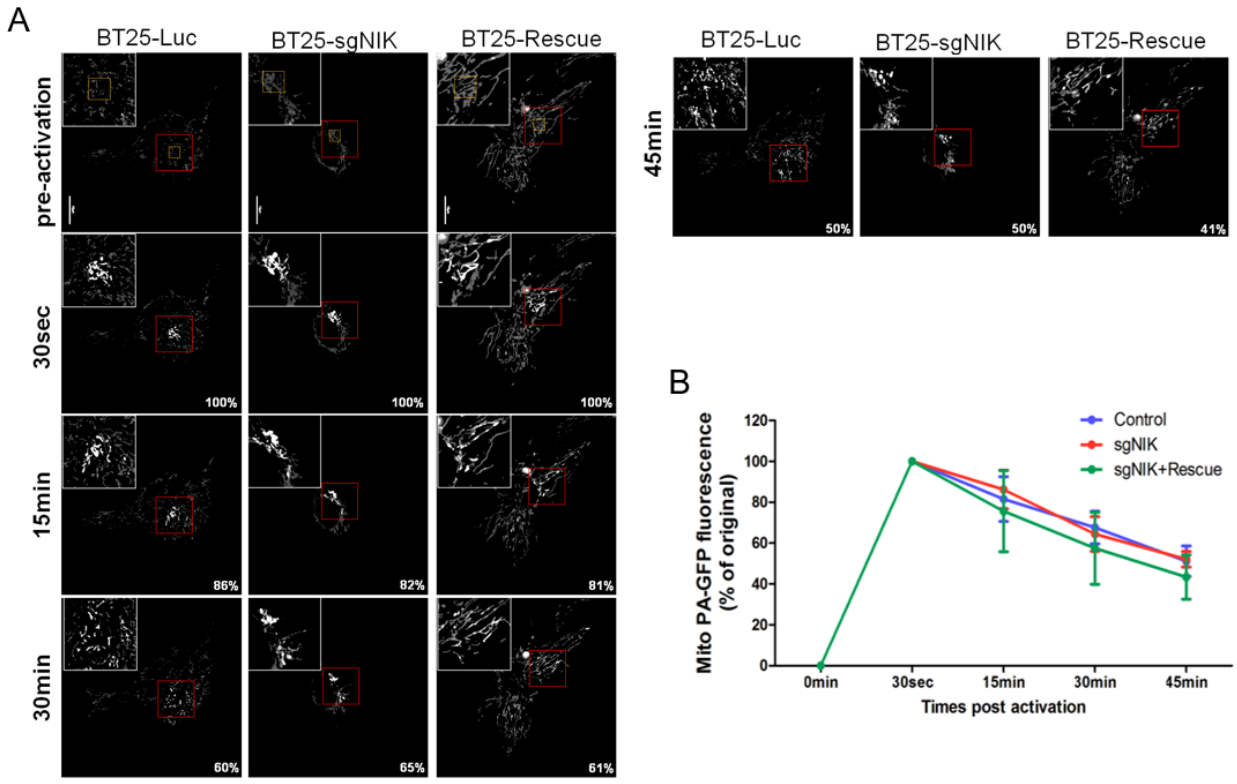

Figure 22. Fusion analysis in BT25 glioma cells. (A) Fusion analysis in BT25 cells. BT25 control, BT25-sgNIK, and BT25-sgNIK+rescue cells were co-transfected with mito-PAGFP (green) and pDsRed2-Mito (red). The mito-PAGFP was photoactivated with a 405 nm laser, and images were acquired with 15 min intervals for 45 min after activation. Percentage of GFP fluorescence intensity of a regions of interest (ROI) at different time points was normalized by the highest intensity. Representative images from at least three independent experiments are visualized as grayscale. Same trends were consistently observed in each experiment. Scale bar, 10 µm. Inserts are magnifications of the boxed regions. (B) Selected mitochondrial regions were analyzed for their PAGFP fluorescence intensity (mean ± SD, one-way ANOVA, N= 6 cells, respectively). There was no significant difference between the dilution rates of BT25 control, BT25-sgNIK, and BT25-sgNIK+rescue cells.

3.3.4 NIK recruits Drp1 to mitochondria and influences its activity

The GTPase Drp1 is a cytosolic factor that is recruited to the mitochondria where it promotes mitochondrial fission (Smirnova et al., 2001). To investigate whether Drp1 expression and subcellular localization is regulated by NIK, we performed immunostaining experiments. Drp1 broadly observed in the cytosol as a punctate signal and also colocalized with Mito-RFP in BT25 control cells (Fig. 23A). Intriguingly, Drp1 association with Mito-RFP was significantly diminished in BT25-sgNIK cells, but was restored in BT25-sgNIK+rescue cells (Fig. 23B, C, and D). No Drp1 staining was observed in BT25 cells expressing small guide RNAs for CrispR-Cas9 mediated knockout of Drp1 (BT25-sgDrp1 cells), verifying antibody specificity (Fig. 24A and B). A second Drp1 antibody, whose specificity was also verified, primarily recognized mitochondrial but not cytosolic Drp1, and also showed loss of Drp1 mitochondrial co-localization in BT25sgNIK cells (Fig. 24C).

Biochemical fractionation and immunoblot analyses confirmed that Drp1 was present in both cytosolic and mitochondria-enriched fractions of BT25 control cells (Fig. 25). In contrast, BT25-sgNIK cells exhibited diminished Drp1 protein levels specifically in the mitochondrial-enriched fraction (Fig. 25). Again, levels of mitochondrial Drp1 were restored in BT25-sgNIK+rescue cells (Fig. 25), demonstrating that the observed effects in BT25-sgNIK cells are mediated by NIK. The expression of other mitochondrial dynamic regulators, including Mff, Fis1, Opa1, and Mfn1/2 were not significantly altered in BT25-sgNIK cells compare to the control cells, whereas expression levels of the proteins in BT114-hNIK cells were slightly raised (Fig. 26A and B). Additionally, Tom20 levels were not affected in mitochondrial fractions of BT25-sgNIK cells (Fig. 25). These results suggest that mitochondria membrane protein topology is not grossly altered, and that NIK specifically regulates Drp1 mitochondrial localization.

Drp1 is regulated by posttranslational modification, including phosphorylation at serine residues 616 (Drp1-P616) and 637 (Drp1-P637), which enhances and inhibit its fission-promoting activity, respectively (Chang and Blackstone, 2007b; Taguchi et al., 2007). To investigate the potential regulation of Drp1 activity by NIK, we examined Drp1 phosphorylation in cells with altered NIK expression using flow cytometry. In BT25-sgNIK cells, Drp1-P616 levels decreased along with a concomitant increase in Drp1-P637, when compared to BT25 control cells (Fig. 27A and B), suggesting that NIK enhances the fission-promoting activity of Drp1. Similar to cells lacking Drp1, loss of NIK also exhibited differences in other mitochondrial functions, including a decrease in production of reactive oxygen species (ROS) and oxygen consumption (Fig.28 and 29). Taken together, these results indicate that NIK regulates Drp1 mitochondrial recruitment and activity to promote mitochondrial fission.

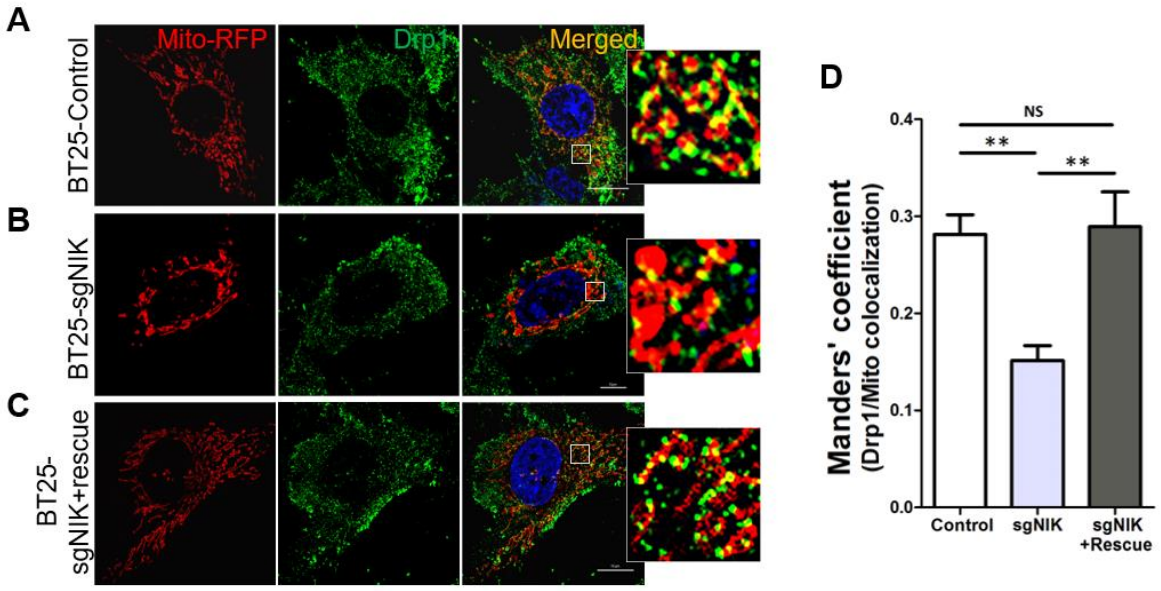

Figure 23. Loss of NIK diminishes mitochondrial association of Drp1. (A) BT25 control (upper panel), (B) BT25-sgNIK (middle panel) and (C) sgNIK+rescue cells (lower panel) were transfected with Mito-RFP to visualize mitochondria (red) and then immunostained for Drp1 (green), and DAPI (blue). Areas within white squares are amplified and shown on the right. Scale bar, 10 μm. (D) Bar graph showing Manders' coefficients for co-localization of Drp1 and Mito-RFP (A - C). Data are mean ± SD (n>8). ** $p<0.01$ for sgNIK vs. control and sgNIK vs. sgNIK+rescue, one-way ANOVA.

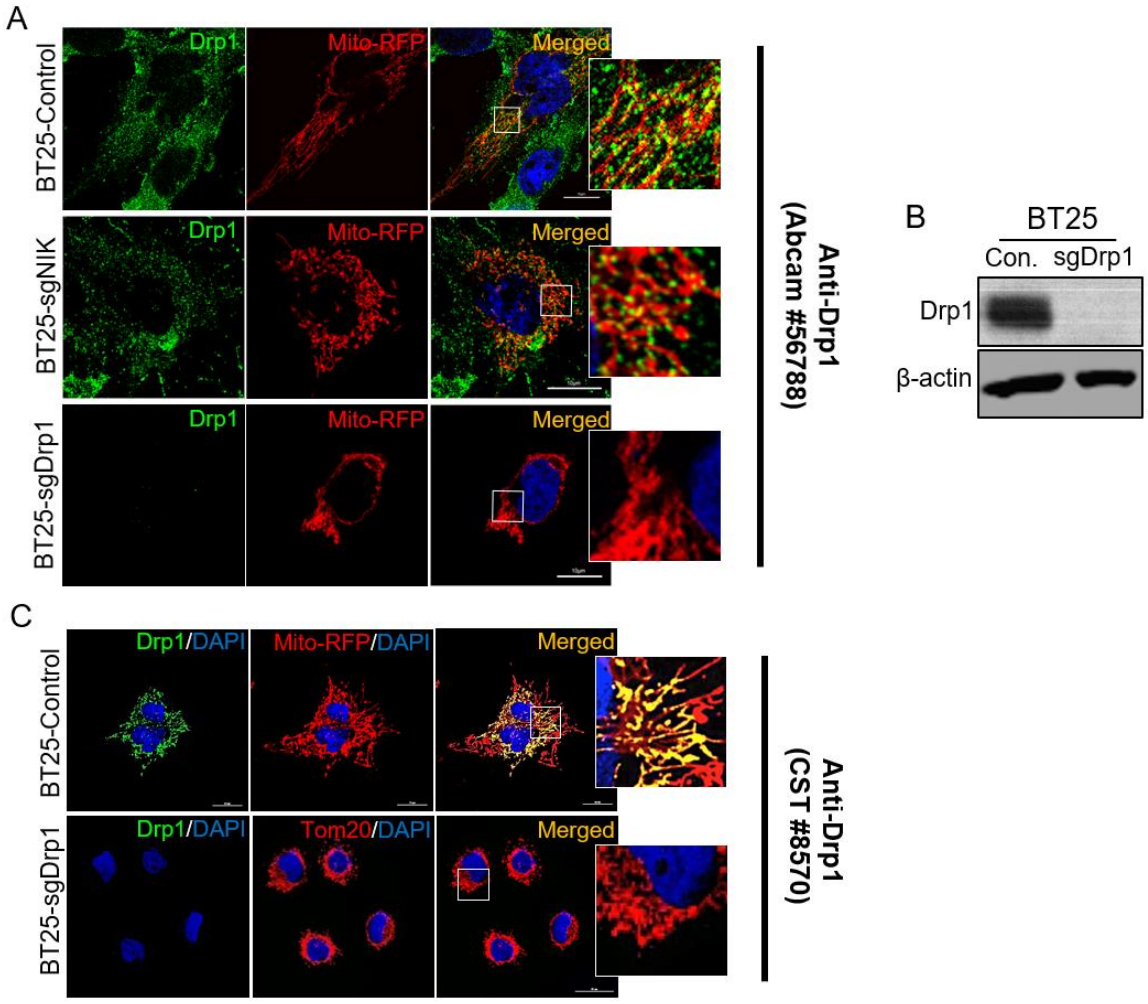

Figure 24. Drp1 antibody validation and staining. (A) BT25 control (upper panel), BT25-sgNIK (middle panel) and sgDrp1 (lower panel) cells were transfected with Mito-RFP to visualize mitochondria (red) and then immunostained with a Drp1 antibody against endogenous Drp1 (Abcam #56788; green), and DAPI (blue). Images marked with white squares are amplified and shown in the right. Scale bar, 10 μm. (B) Immunoblot analysis of whole cell lysates prepared from BT25 control and BT25-sgDrp1 cells were probed with Drp1 and β-actin-specific antibodies, as indicated. **(C)** BT25 control (upper panel) cells were transfected with Mito-RFP (red) and then immunostained with a Drp1 antibody (CST #8570; green), and DAPI (blue). sgDrp1 (lower panel) cells were immunostained with a Drp1 antibody against endogenous Drp1 (CST #8570; green), mitochondrial marker Tom20 and DAPI (blue). Images marked with white squares are amplified and shown in the right. Scale bar, 10 μm.

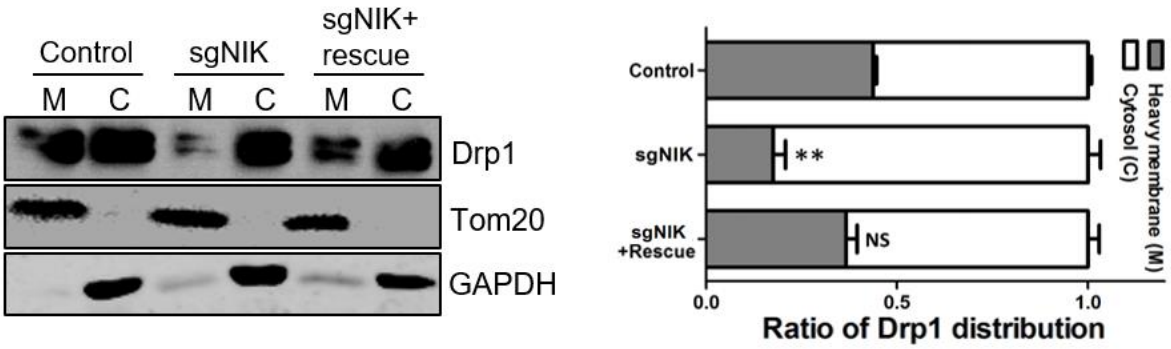

Figure 25. NIK enhances Drp1 recruitment to mitochondria. Immunoblot analysis of mitochondrial-enriched (M) and cytosolic (C) fractions prepared from BT25 control, BT25-sgNIK and BT25-sgNIK+rescue cells was performed with indicated antibodies. Results are representative of 5 separate experiments. Right bar graph shows quantification of the ratio of Drp1 in cytosolic and mitochondria-enriched fractions. Mean ± SD (n>4). ** $p<0.01$ for sgNIK vs. control and sgNIK vs. sgNIK+rescue, NS: not significant, one-way ANOVA.

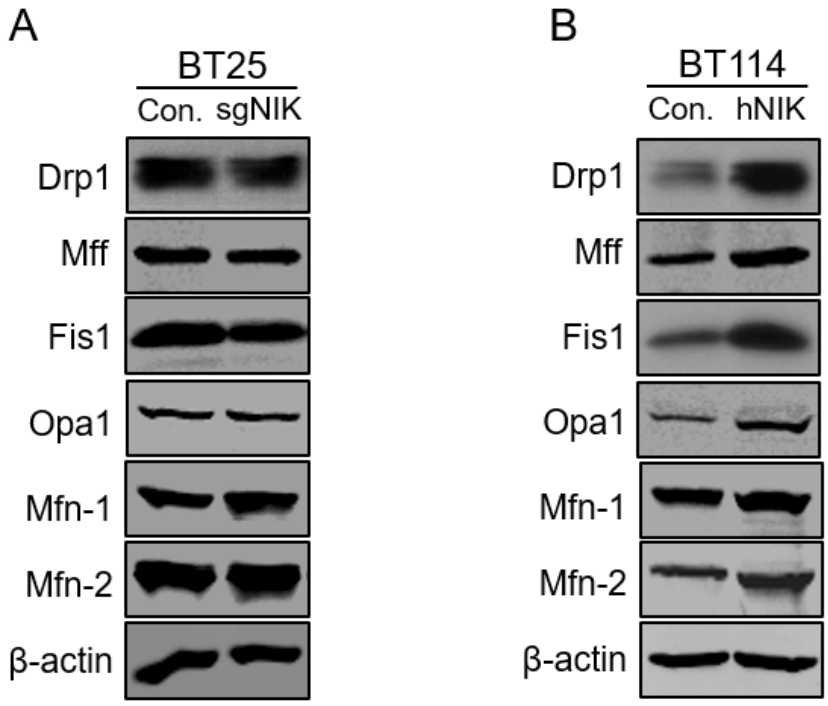

Figure 26. Expression of mitochondria membrane proteins in cells with altered NIK expression. (A) Immunoblot analysis of whole cell lysates prepared from untreated BT25 control and sgNIK cells for endogenous mitochondrial fission proteins: Drp1, Mff, and Fis1; mitochondrial fusion proteins: Opa1, Mfn-1, and Mfn-2. β-actin is often used as a loading control. (B) Immunoblot analysis of whole cell lysates prepared from untreated BT114control and hNIK cells for endogenous mitochondrial fission proteins: Drp1, Mff, and Fis1; mitochondrial fusion proteins: Opa1, Mfn-1, and Mfn-2. β-actin is often used as a loading control.

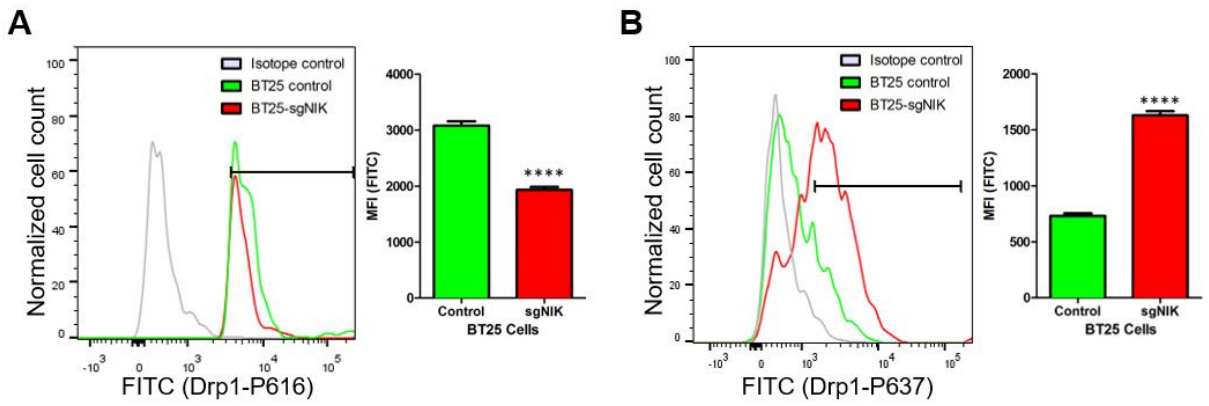

Figure 27. NIK affects phosphorylation of Drp1. Flow cytometric histogram measuring levels of (A) Drp1-PS616 and (B) Drp1-PS637 in BT25 control (green), sgNIK (red). Isotype control (grey). Right bar graph shows mean fluorescence intensity (MFI) values for control and sgNIK cells. At least 10,000 events were analyzed. Data are represented as mean ± SEM. **** $p<0.0001$, unpaired t-test.

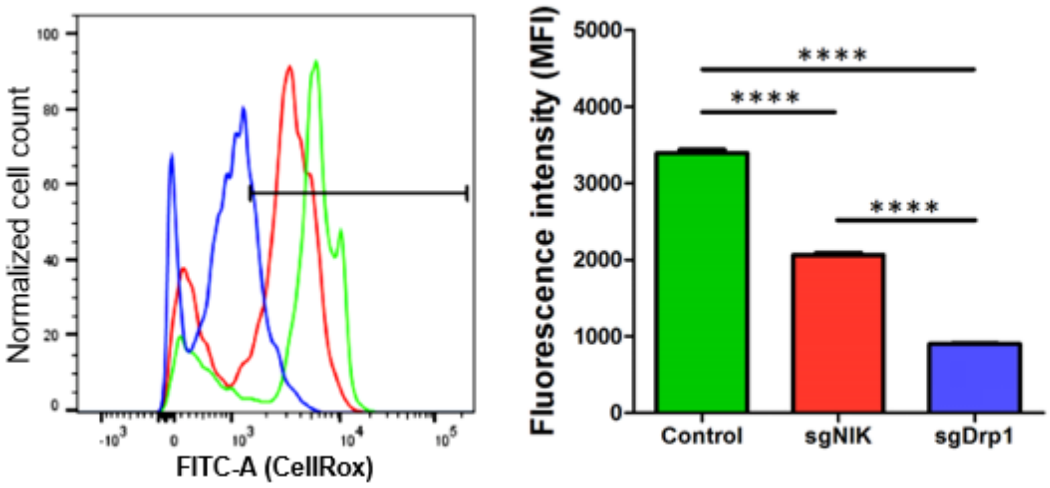

Figure 28. Loss of NIK decrease the production of ROS. Cellular reactive oxygen species (ROS) was analyzed using CellRox reagent and performing flow cytometry in live cells BT25 control (green), sgNIK (red) and sgDrp1 (blue) treated with Cell Rox reagent. At least 10,000 events were analyzed. Right bar graph shows mean fluorescence intensity (MFI) values from CellRox assy in (A). **** indicates significance of mean ± SEM p<.0001 as analyzed by a one-way ANOVA.

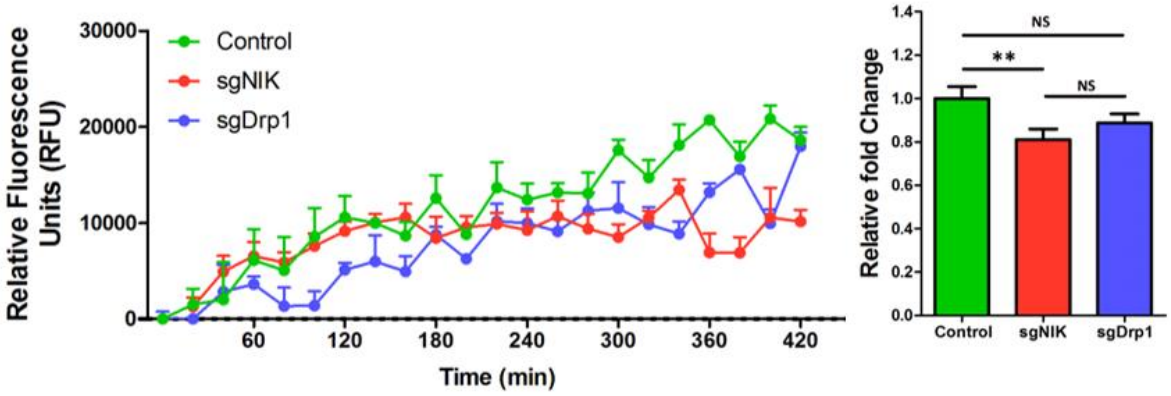

Figure 29. Loss of NIK reduces oxygen consumption. Time course analysis of the change in extracellular O2 consumption using a Mito-ID kit (ENZO life sciences). Higher fluorescence intensity indicates increased O2 consumption. Reads were taken every 20 minutes over the course of 7 hours. Right bar graph shows fold change in total extracellular O2 consumption over 7 hours. Data are represented as mean ± SD ** $p<0.01$ (n=3) as analyzed by a one-way ANOVA. NS: not significant.

3.3.5 Drp1 interacts with NIK, but not IKKα.

To examine the distribution of NIK and Drp1 within mitochondria, we performed co-immunostaining experiments in BT25 glioma cells. Drp1 immunoreactivity colocalized with that of NIK (Fig. 30A), but did not significantly overlap with IKKα, the primary direct downstream target of NIK (Fig. 30B and C). Similarly, we observed that NIK, but not IKKα, colocalized with Drp1 in patient-derived ex vivo glioma tissue (Fig. 31A and B). These data show that mitochondrial localization of NIK is an intrinsic property of primary human cancer cells, and not simply a phenotype observed in cancer cell lines in vitro. To determine whether the co-localization of Drp1 and NIK immunostaining reflected a direct interaction, we performed immunoprecipitation experiments for Drp1 in BT114 control and BT114-NIK overexpressing cell. Results from these experiments indeed showed that Drp1 exists in a complex with NIK (Fig. 32). However, the Drp1 does not interact with IKKα, which is widely known as a NIK-binding protein for activating non-canonical NF-κB pathway. Additionally, NIK does not bind to other Drp1-related mitochondrial dynamic regulators including phosphoglycerate mutase family member 5 (PGAM5) (Xu et al., 2015) and mitochondrial Rho GTPase 1 (Miro1) (Saotome et al., 2008) as well as a negative control, inner mitochondrial protein Tim50 (Tim 50) (Fig. 33). Thus, these data have suggested the existence of physical interaction between NIK and Drp1 in glioma cells.

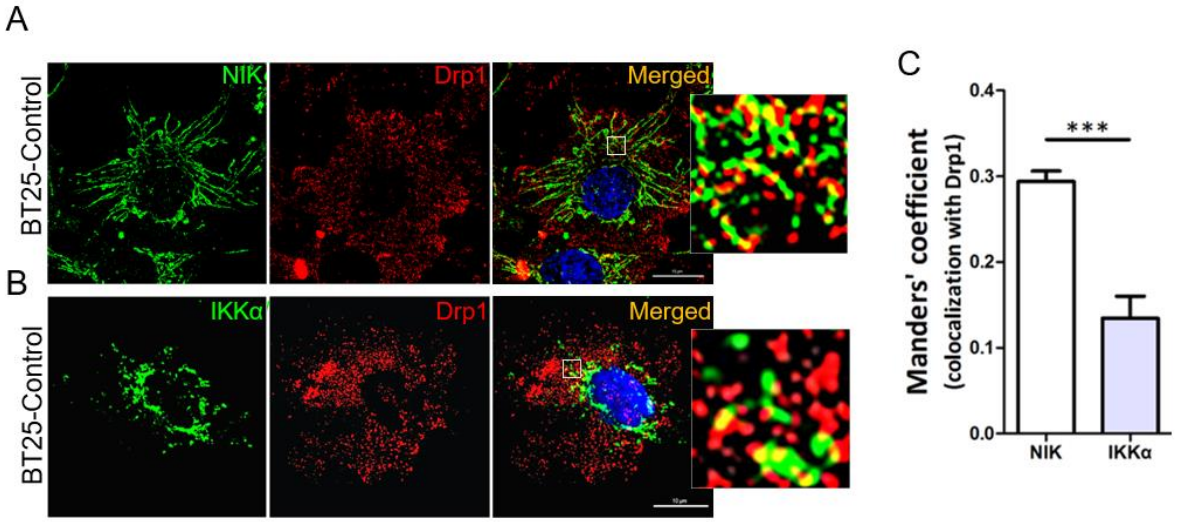

Figure 30. Drp1 colocalized with NIK but not IKKα in glioma cells. (A) BT25 control cells were immunostained for NIK (green), Drp1 (red), and DAPI (blue). Images marked with white squares are amplified and shown in the right. Scale bar, 10 μm. (B) BT25 control cells were immunostained for IKKα (green), Drp1 (red), and DAPI (blue). Images marked with white squares are amplified and shown in the right. Scale bar, 10 μm. (C) Bar graph showing Manders' coefficients for co-localization of Drp1 and NIK or IKKα (A and B). Data are mean ± SEM (n=9). *** $p<0.001$, unpaired t-test.

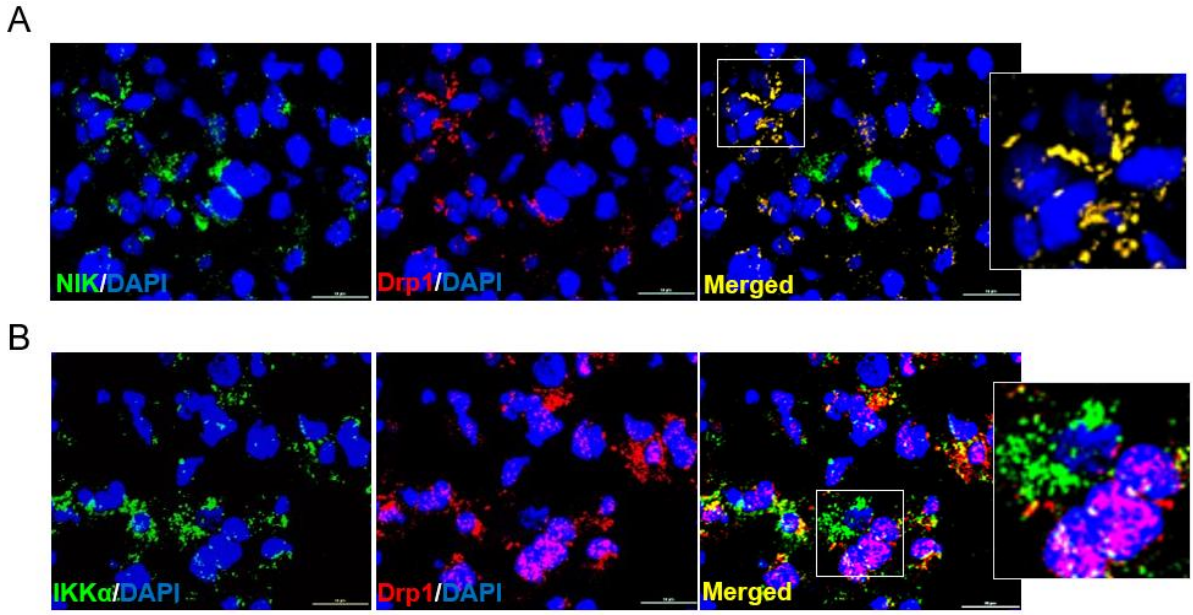

Figure 31. Drp1 colocalized with NIK in human glioma patient tumor. (A) Human glioma patient tumor sections were stained for NIK (green) and Drp1 (red), and DAPI (blue); upper panel. Representative images from 1 of 4 patient samples is shown. Images marked with white squares are amplified and shown in the right. Scale bar, 10 μm. (B) Adjacent tumor sections were stained with IKKα (green), Drp1 (red), and DAPI (blue); lower panel. Images marked with white squares are amplified and shown in the right. Scale bar, 10 μm.

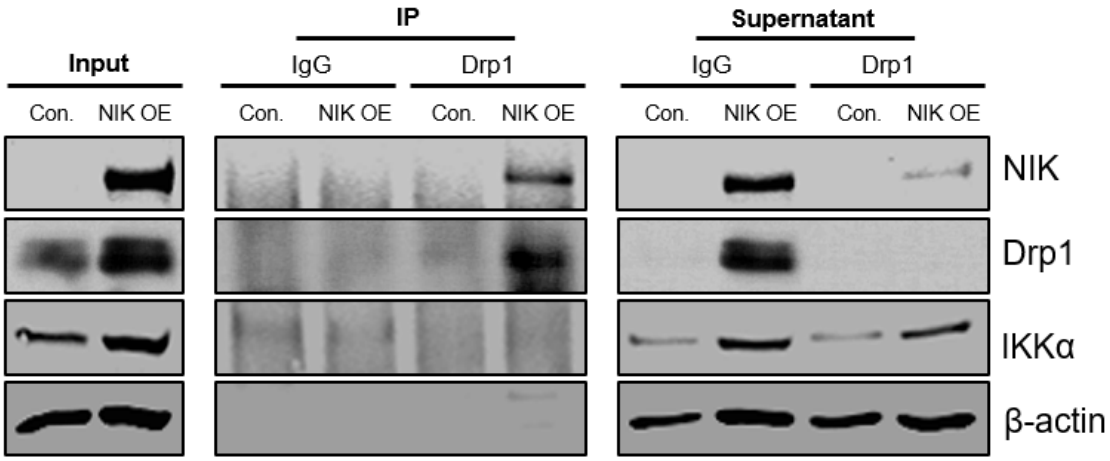

Figure 32. Drp1 interacts with NIK but not IKKα. BT114 control (Con.) and BT114-hNIK cell (NIK OE) lysates were subjected to immunoprecipitation (IP) with control immunoglobulin G (IgG) or a Drp1 antibody against endogenous Drp1. The immunoprecipitates were analyzed by immunoblotting with the indicated antibodies.

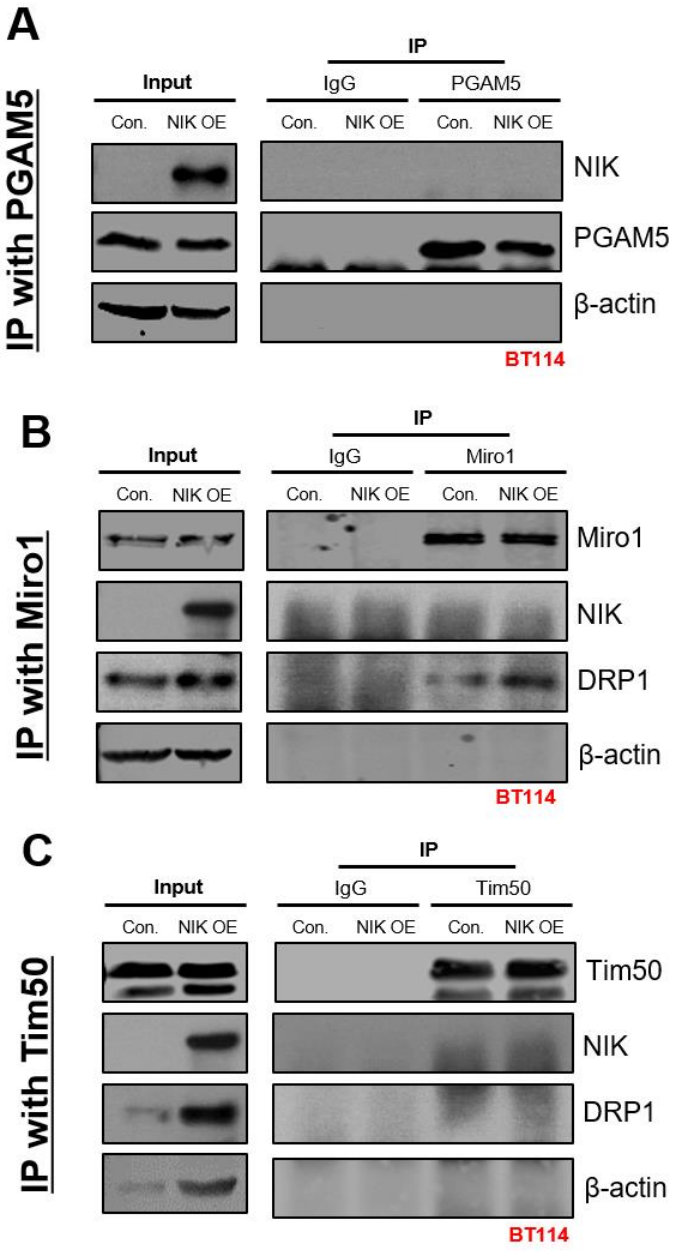

Figure 33. Interaction between NIK and other Drp1-related mitochondrial dynamic regulators. BT114 control (Con.) and BT114-hNIK cell (NIK OE) lysates were subjected to immunoprecipitation (IP) with control IgG, (A) PGAM5, (B) Miro1or (C) Tim50 antibody. The immunoprecipitates were analyzed by immunoblotting with the indicated antibodies.

3.3.6 NIK requires Drp1 to promote TWEAK-induced invasion

We have previously demonstrated that low, endogenous concentrations of the tumor inducing cytokine TWEAK (10 ng/ml) induces NIK expression and promotes NIK-dependent invasion (Cherry et al., 2015; Duran et al., 2016). Indeed, TWEAK treatment increases invasion of BT25 cells to a similar extent as NIK overexpression, which is further potentiated by TWEAK (Fig. 34). As expected, loss of NIK (sgNIK) almost completely abrogates both basal and TWEAK-induced invasion (Fig. 34) (Duran et al., 2016), and this loss was rescued by NIK overexpression (sgNIK+NIK). To directly assess whether NIK acts through Drp1, we measured invasion of TWEAK treated BT25-sgDrp1 cells. Indeed, these cells showed strongly attenuated invasion, phenocopying BT25-sgNIK cells (Fig. 34). TWEAK was still able to increase invasion in these cells, but to significantly lower levels than in BT25 cells. More importantly, NIK overexpression in BT25-sgDrp1 had no effect on TWEAK-induced invasion (Fig. 34). Visualization and quantification of mito-RFP-labeled mitochondria revealed that while TWEAK increased the number of small, punctate mitochondria in BT25 control cells (Fig. 35A and C), it had no effect on BT25-sgDrp1 cells, which also exhibited collapsed, fused mitochondria, similar to BT25-sgNIK cells (Fig. 35B and C). Together, these results suggest that Drp1 activity and mitochondrial fission are important downstream mediators of NIK-dependent, TWEAK-induced cancer cell invasion.

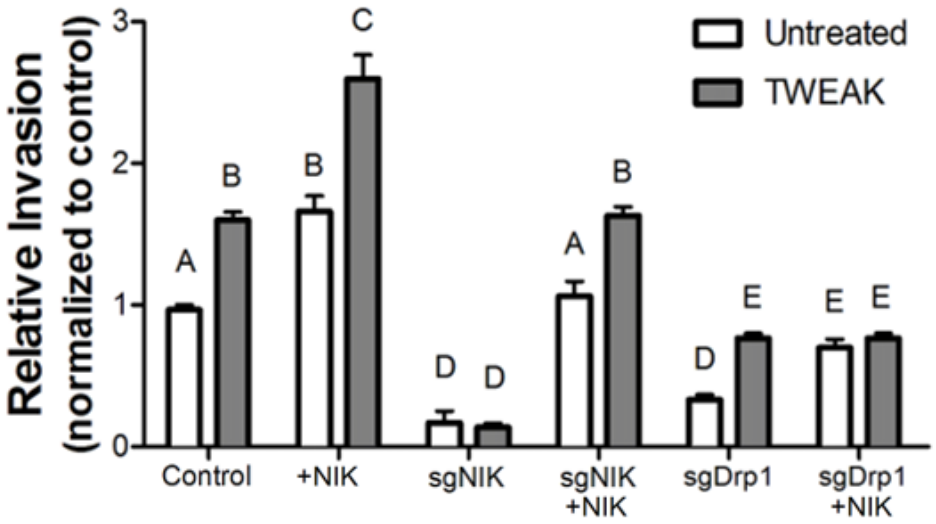

Figure 34. NIK requires Drp1 to promote TWEAK-induced invasion. Quantification of three-dimensional collagen invasion assays. The indicated cells were allowed to invade three-dimensional collagen matrices in the absence or presence of the TWEAK (10 ng/ml). Data are represented as mean ± SD (n=3). Different letters represent statistically significant differences (A vs. B: ***p<0.001; A/B vs. D, A vs. B and C vs. E: ****p<0.0001; D vs. E: *p<0.05; two-way ANOVA).

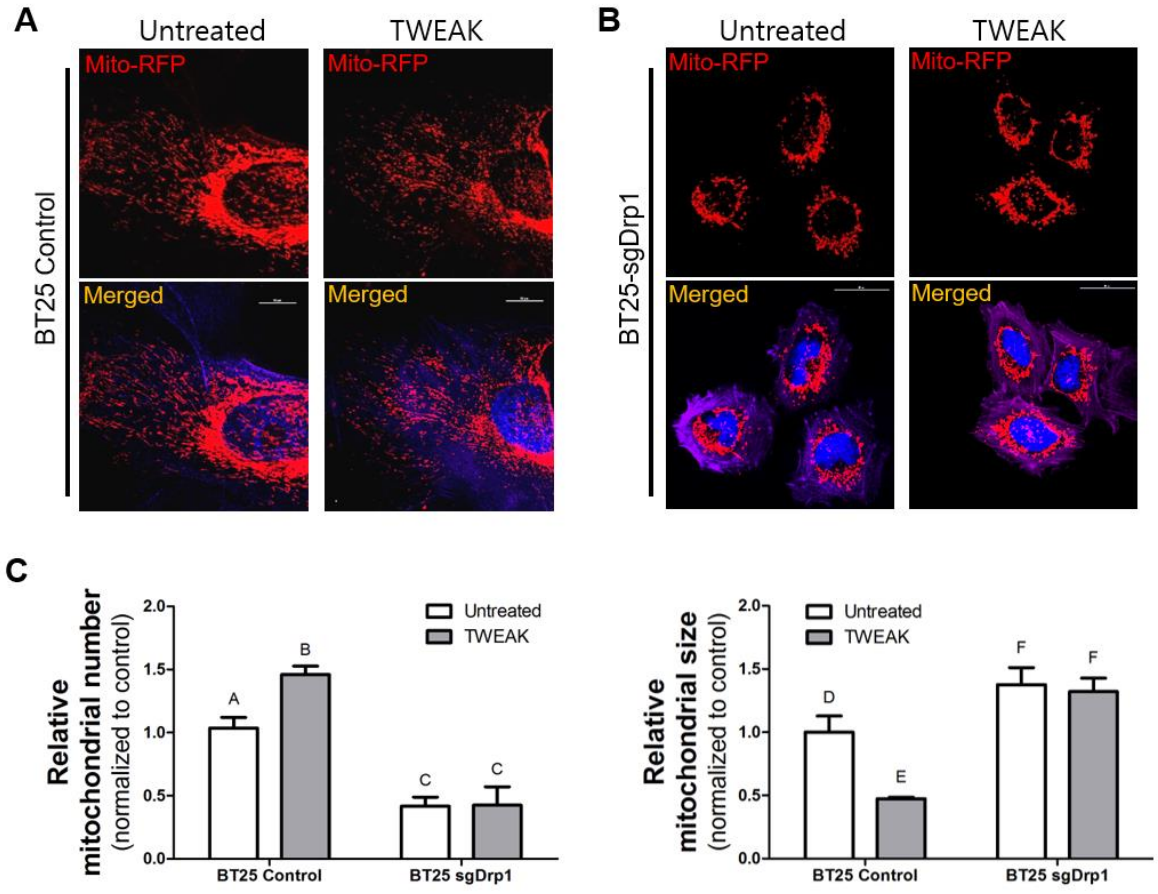

Figure 35. TWEAK-induced mitochondria fragmentation requires Drp1. Representative immunofluorescence images of (A) BT25 control and (B) BT25-sgDrp1 (right) cells in the absence or presence of the TWEAK (10 ng/ml) were transfected with Mito-RFP (red) and stained with DAPI (blue) and phalloidin (purple). Scale bar, 10 μm. (C) Mitochondrial number and size in BT25 control and BT25-sgDrp1 cells were quantified using the Analyze Particles function in ImageJ software. Data are represented as mean ± SD (n=14). Different letters represent statistically significant differences (D vs. F: *p<0.05; A vs. B and D vs. E: **p<0.01; A/B vs. C and E vs. F: ***p<0.001; one-way ANOVA).

3.3.7 NIK enhances the invasive potential of MEFs in the absence of IKK/NF-κB signaling

Lack of significant co-localization or interaction between IKK and Drp1 in glioma cells (Fig. 30B, 31B, and 32) led us to investigate whether NIK functions independently of IKK in the mitochondria. To do so, we took advantage of MEFs, which have the ability to undergo invasion in three-dimensional collagen matrices (Duran et al., 2016; Mierke et al., 2010), similar to glioma cells. Additionally, MEFs derived from IKKα/β null mice (Li et al., 2000) (referred to as ΔIKK-MEFs) provide a genetic tool to assess NIK function in the absence of IKK proteins and downstream NF-κB signaling. Immunofluorescence experiments in MEFs revealed that NIK broadly colocalized with Mito-RFP and Tom20 (Fig. 36A and 37A) and had minimal overlap with the ER protein Sec61 (Fig. 37B) in MEFs, similar to BT25 cells. As expected, MEFs in which NIK was knocked out using sgRNA-mediated CrispR/Cas9 genome editing (sgNIK MEFs) lacked any NIK protein, both by immunostaining and immunoblot analyses (Fig. 36A and B). Immunoblot experiments also demonstrated that NIK is present in mitochondrial-enriched MEF cell fractions (Fig. 36B). Similar to glioma cells, little, if any, co-localization of IKKα with Mito-RFP or NIK was observed in MEFs (Fig. 38A and B).

Compared to WT MEFs, sgNIK MEFs exhibited substantially diminished invasion in collagen matrices and overexpression of human NIK (hNIK) in WT MEFs increased invasion (Fig. 39A and B). While ΔIKK-MEFs are somewhat less invasive than WT MEFs (Fig. 40A), additional deletion of NIK (sgNIK-ΔIKK MEFs) further attenuated invasion in three-dimensional collagen matrices (Fig. 40B). Overexpression of hNIK in ΔIKK MEFs (sgNIK-ΔIKK MEFs+rescue) increased invasion (Fig. 40C). Importantly, hNIK overexpression in ΔIKK-MEFs did not activate downstream NF-κB signaling, assessed by the lack of any increase in p100 processing to p52, p65 (S536) phosphorylation or nuclear accumulation of p65, RelB or

p52 under basal or cytokine (TWEAK)-induced conditions (Fig. 41). Furthermore, ΔIKK MEFs overexpressing NIK did not exhibit increased expression of the NF-κB target gene MMP9 (Fig. 42A and B) (Fukuyama et al., 2007; Li et al., 2009; Raychaudhuri et al., 2007). Together, these data clearly show that mitochondrial localization of NIK is a common event in both malignant and non-malignant cells. The NIK-dependent invasive potential of MEFs is uncoupled from IKK/NF-κB signaling.

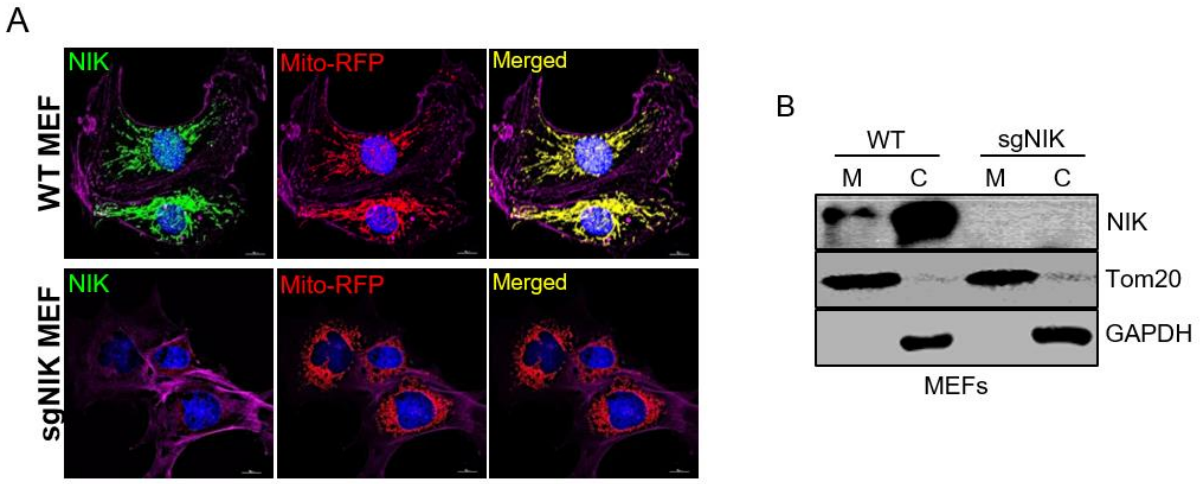

Figure 36. NIK is localized to mitochondria in MEFs. (A) Representative immunofluorescence confocal images of WT and NIK knockout (sgNIK MEFs) that were transfected with Mito-RFP (red) to visualize mitochondria, then fixed and immunostained for NIK (green), DAPI (blue) and phalloidin (purple). Scale bar, 10 μm. (B) Immunoblot analysis of mitochondrial-enriched (M) and cytosolic (C) fractions prepared from WT and sgNIK MEFs pretreated with TWEAK (10 ng/ml) and MG132 (5 μM) to stabilize NIK for facile detection and to confirm loss of NIK in sgNIK MEFs. Blots were probed with indicated antibodies. (mitochondrial-enriched/cytosol = 4:1 in volume equivalents).

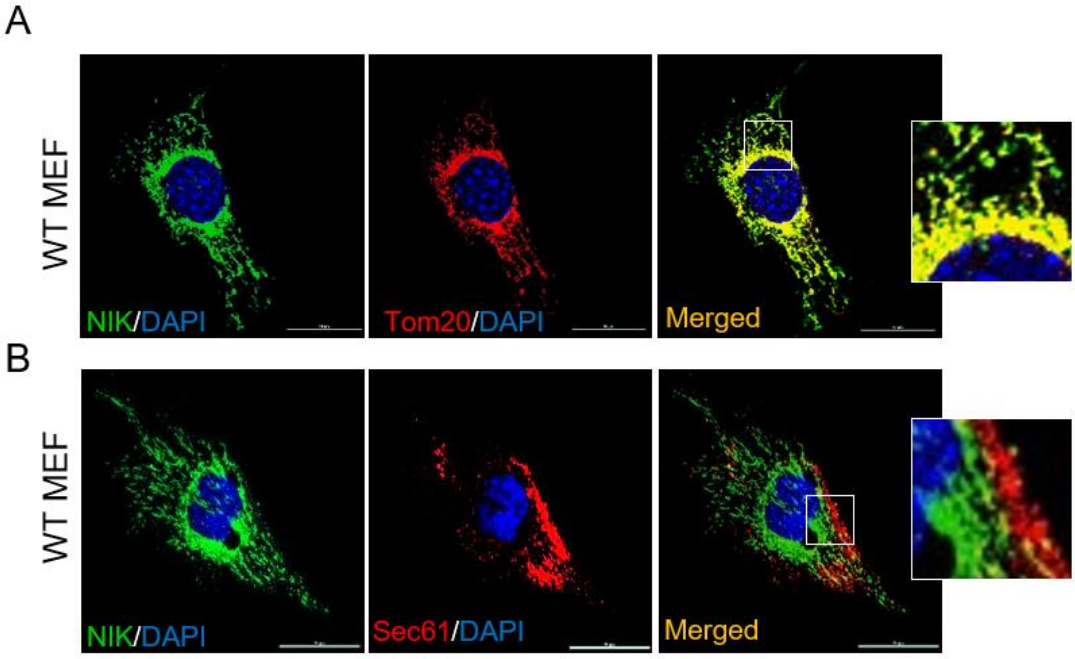

Figure 37. NIK co-localization with different organelle markers in MEFs. (A) Representative immunofluorescence confocal images of WT MEFs immunostaining for NIK (green), pre-conjugated Tom20-AF647 (pseudo-colored red), and DAPI (blue). (B) WT MEFs were immunostained for NIK (pseudo-colored green), Sec61A-AF488 (pre-conjugated, pseudo-colored red), and DAPI (blue). Scale bar, 10 μm.

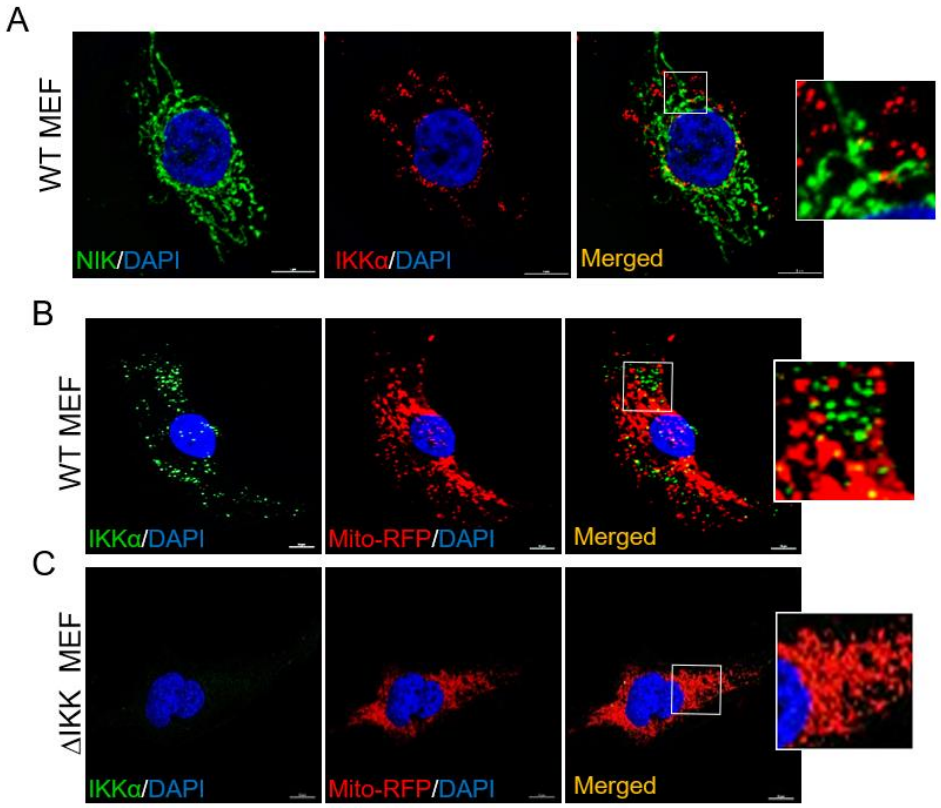

Figure 38. NIK's downstream target, IKKα does not colocalize with mitochondrial marker in MEFs. (A) WT MEFs were immunostained for NIK (green), IKKα (red), and DAPI (blue). (B) WT MEFs and (C) ΔIKK MEFs were immunostained for IKKα (green), Mito-RFP(red), and DAPI (blue). Images marked with white squares are amplified and shown in the right. Scale bar, 10 μm.

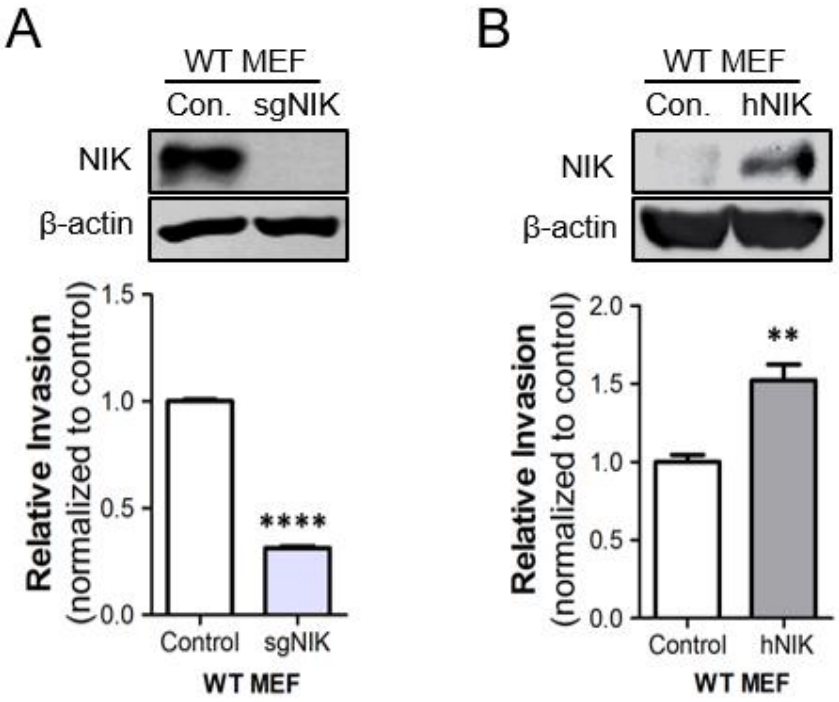

Figure 39. NIK regulates invasive potential in MEFs. (A) Immunoblot analysis of whole cell lysates prepared from WT MEFs (control for sgNIK) and sgNIK MEFs or (B) WT MEFs expressing control vector (control for overexpression) and hNIK were probed with NIK- and actin-specific antibodies, as indicated. Cells were pre-treated with TWEAK and MG132. The bar graph shows Quantification of three-dimensional collagen invasion assays comparing parental WT MEFs and sgNIK MEFs or WT MEFs-vector control and WT-hNIK. Relative invasion reflects numbers of invading cells normalized to each control from at least 3 independent experiments, each with $n \geq 3$ for each cell type. ** $p<0.01$; **** $p<0.0001$, unpaired t-test.

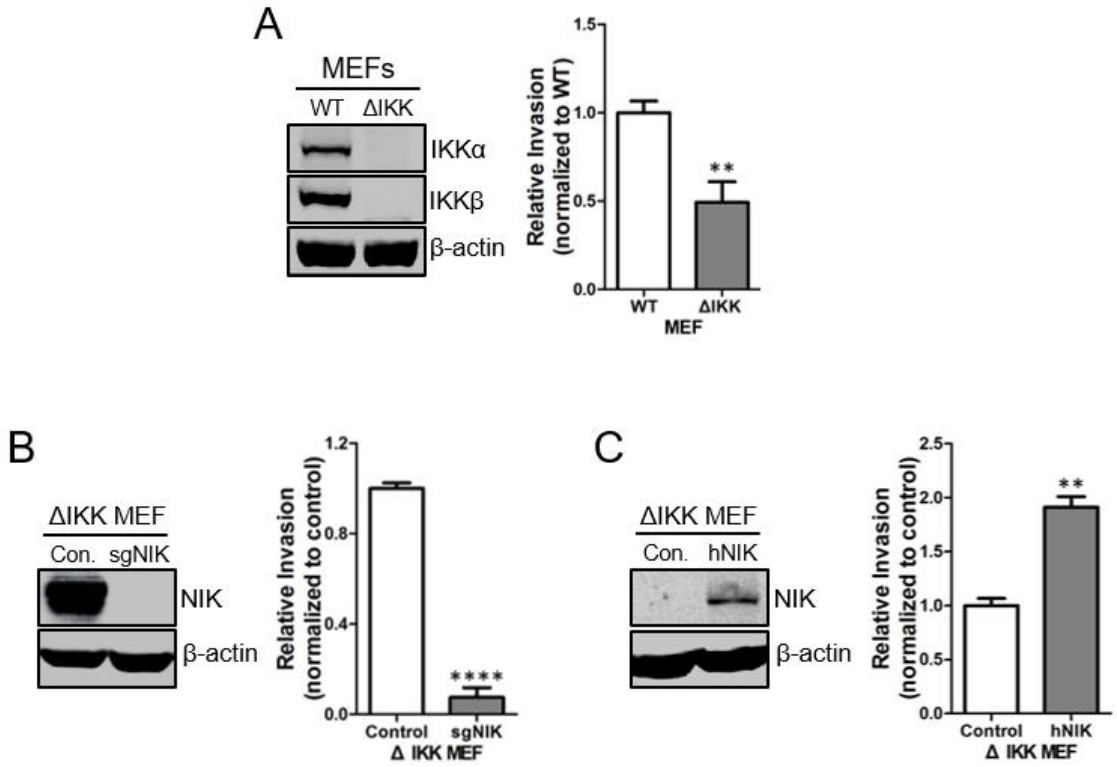

Figure 40. NIK increases the invasive potential of IKK-knockout MEFs. (A) (Left) Immunoblot analysis of whole cell lysates prepared from untreated WT MEFs and ΔIKK MEFs were probed with indicated antibodies. (Right) Quantification of three-dimensional collagen invasion assays comparing WT MEFs and ΔIKK MEFs. ** $p<0.01$ (n=3), unpaired t-test. (B) (Left) Immunoblot analysis of whole cell lysates prepared from ΔIKK MEFs (control) or NIK knockout (sgNIK-ΔIKK MEFs) were probed with indicated antibodies. Cells were pre-treated with TWEAK and MG132. (Right) Quantification of three-dimensional collagen invasion assays comparing ΔIKK MEFs and sgNIK-ΔIKK MEFs; **** $p<0.0001$(n=3), unpaired t-test. (C) (Left) Immunoblot analysis of whole cell lysates from untreated ΔIKK MEFs expressing vector (control) or hNIK was performed with indicated antibodies. (Right) Quantification of three-dimensional collagen invasion assays comparing ΔIKK MEFs expressing vector control or hNIK; ** $p<0.01$(n=3), unpaired t-test.

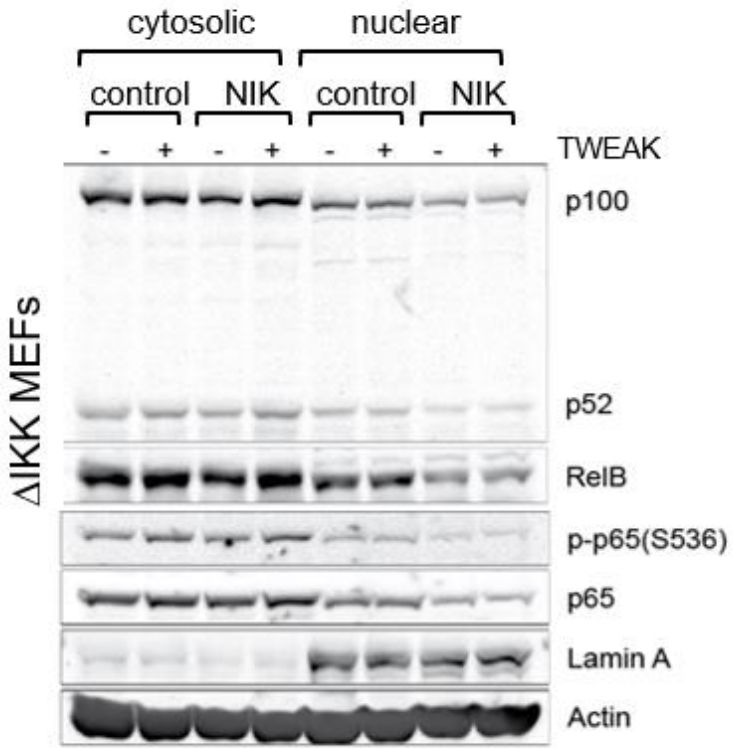

Figure 41. Overexpression of NIK in ΔIKK MEFs does not affect downstream NF-κB. Western blot analysis of cytosolic and nuclear fractions isolated from ΔIKK MEFs expressing vector (control) or hNIK and treated with TWEAK (10ng/ml) to induce NF-κB signaling. Blots were probed with the indicated antibodies.

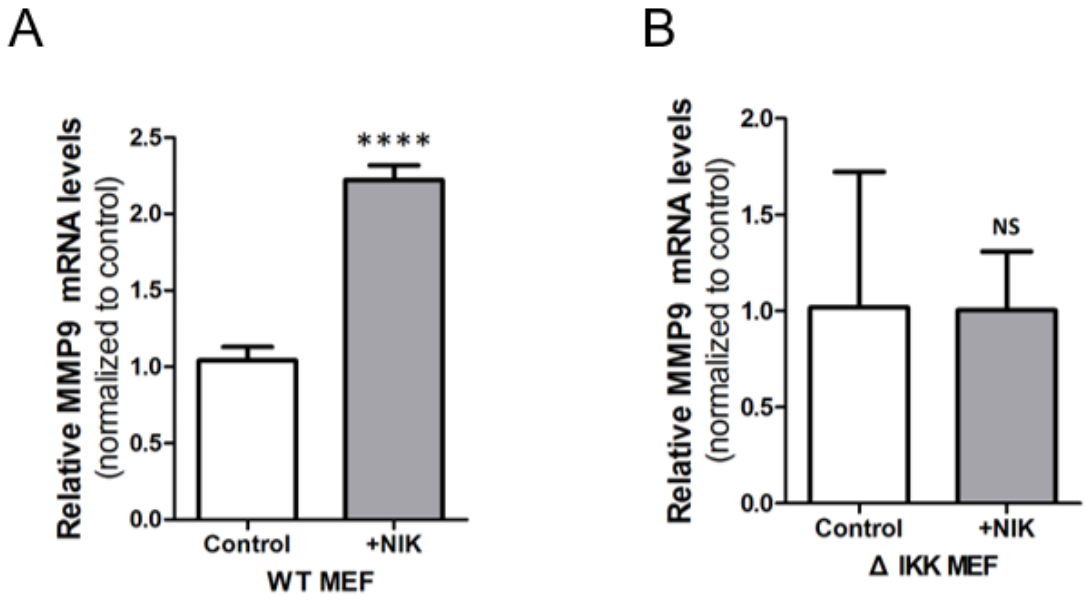

Figure 42. Overexpression of NIK in ΔIKK MEFs does not affect expression of the NF-κB target gene. (A) Quantitative RT-PCR (qPCR) analysis of MMP9 expression in untreated WT MEFs and ΔIKK MEFs expressing vector (control) or hNIK. **** $p<0.0001$ (n=3), unpaired t-test, NS: not significant.

3.3.8 NIK regulates mitochondrial morphology by recruiting Drp1 independently of IKK/NF-κB

To analyze mitochondrial morphology in MEFs, fluorescence microscopy was used to examine the morphology of mitochondria in ΔIKK MEFs, sgNIK-ΔIKK MEFs, ΔIKK MEFs+vector and ΔIKK MEFs+hNIK cells expressing a mito-RFP. The fluorescent images showed that loss of NIK in WT and ΔIKK MEFs resulted in collapsed, perinuclear mito-RFP staining (Fig. 43A and 44A), similar to BT25-sgNIK, Panc1-sgNIK and MDA-MB231-sgNIK cells (Fig. 8B, 14A, and 15A). Moreover, overexpression of NIK in both WT and ΔIKK MEFs increased the appearance of punctate mitochondria dispersed throughout the cytoplasm (Fig. 43A and 44B). Particle analysis of Mito-RFP staining using ImageJ revealed that although the number of mitochondria was significantly decreased in ΔIKK-MEFs compared to corresponding WT MEFs, mitochondria size was increased (Fig. 43B). Conversely, NIK overexpression in ΔIKK-MEFs (ΔIKK+hNIK) was associated with increased number and decreased size of mitochondria (Fig. 43B). Similar to BT25 cells, ΔIKK MEFs also exhibited co-localization of Drp1 with Mito-RFP, which was significantly diminished in sgNIK-ΔIKK MEFs (Fig. 45). Biochemical fractionation and immunoblot analyses confirmed loss of Drp1 protein specifically in the mitochondrial-enriched fraction of sgNIK-ΔIKK MEFs (Fig. 46). Together, these findings demonstrate that NIK regulates mitochondrial fission by increasing the mitochondrial recruitment of Drp1 independently of IKK/NF-κB.

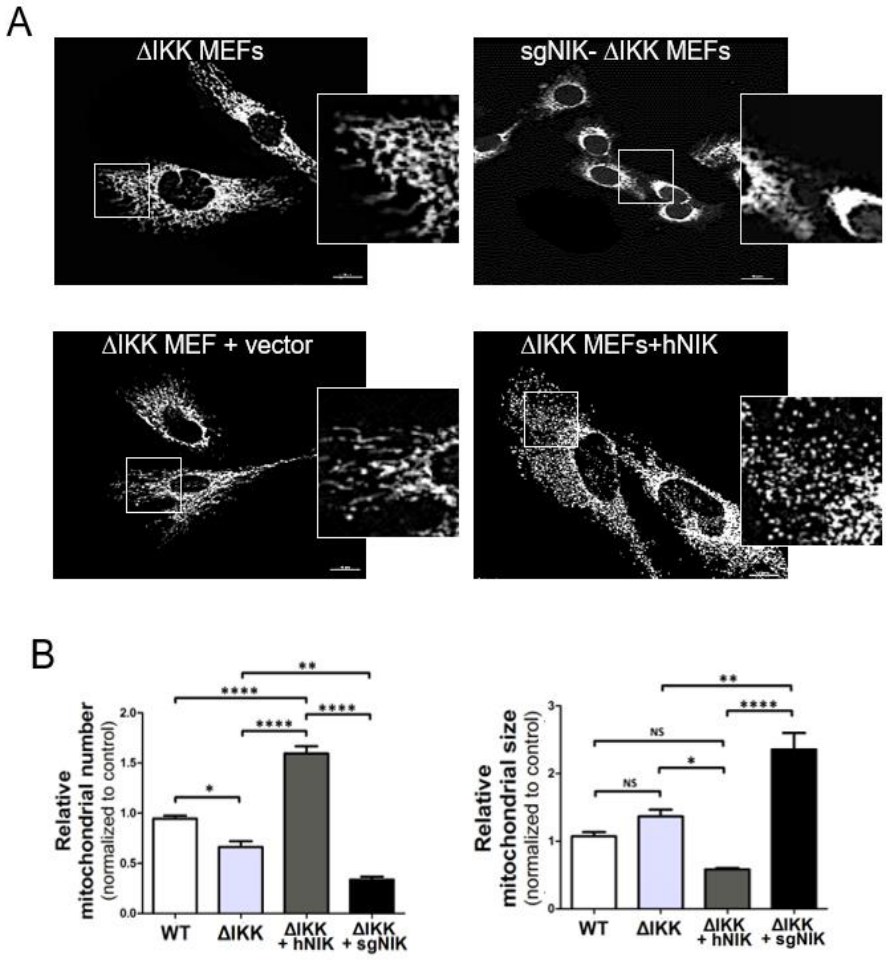

Figure 43. NIK regulates mitochondrial morphology of MEFs in the absence of IKK/NF-κB signaling. (A) Representative immunofluorescence confocal images of ΔIKK MEFs, ΔIKK MEFs+vector, sgNIK-ΔIKK MEFs and ΔIKK MEFs+hNIK that were transfected with Mito-RFP (grayscale) to visualize mitochondria. Images marked with white squares are amplified and shown in the right. Scale bar, 10 μm. (B) Mitochondrial number and size in WT MEFs, ΔIKK MEFs, ΔIKK MEFs+hNIK and sgNIK-ΔIKK MEFs were quantified using the Analyze Particles function in ImageJ software. Data are represented as mean ± SD (n>16). *p<0.05; **p<0.01; ***p<0.001; ****p<0.0001; one-way ANOVA).

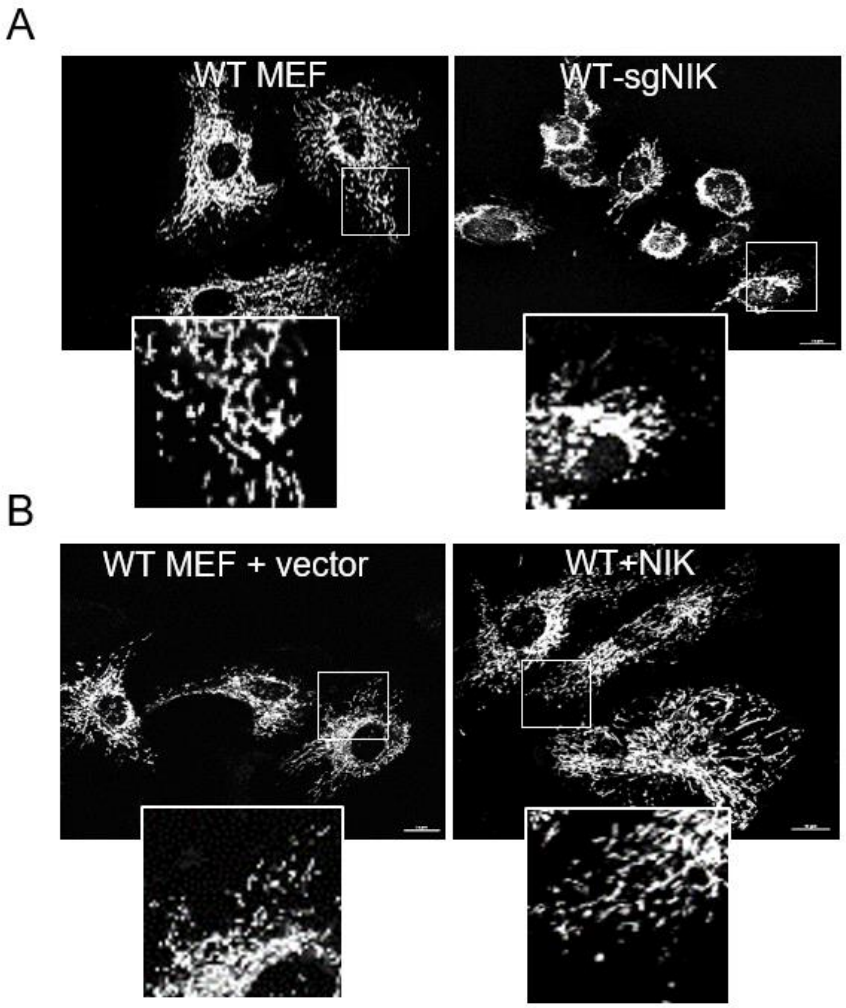

Figure 44. NIK promotes mitochondrial fragmentation in MEFs. (A) Representative immunofluorescence confocal images of WT MEFs and sgNIK MEFs and (B) WT MEFs and WT-hNIK that were transfected with Mito-RFP (grayscale) to visualize mitochondria. Images marked with white squares are amplified and shown in the right. Scale bar, 10 μm.

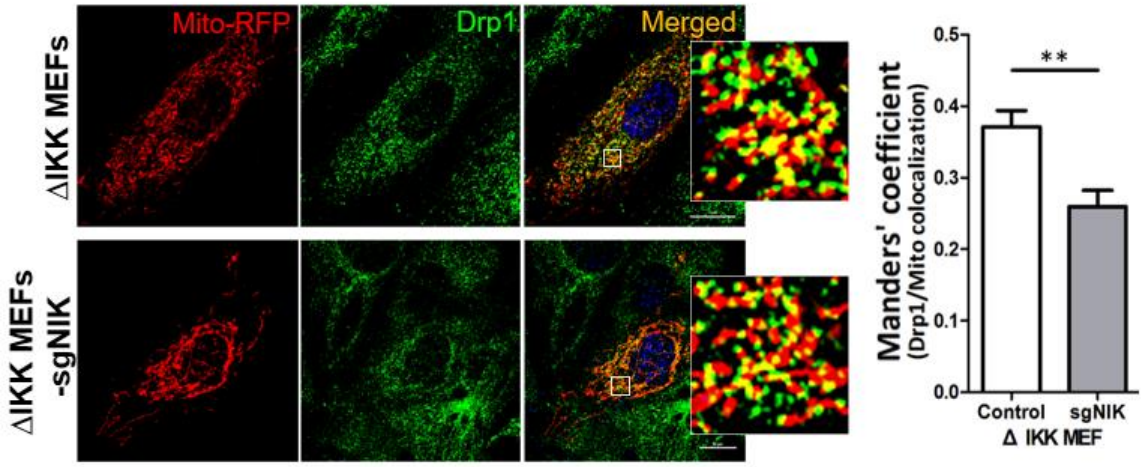

Figure 45. NIK contributes mitochondrial localization of Drp1 in IKK-knockout MEFs. ΔIKK MEFs and sgNIK-ΔIKK MEFs were transfected with Mito-RFP to visualize mitochondria (red) and immunostained for Drp1 (green), and DAPI (blue). Images marked with white squares are amplified and shown in the right. Scale bar, 10 μm. Right bar graph shows Manders' coefficients (fraction of Drp1 in co-localization with Mito-RFP) for co-localization of Drp1 and mitochondria. Data are mean ± SEM (n>14). ** $p<0.01$, unpaired t-test.

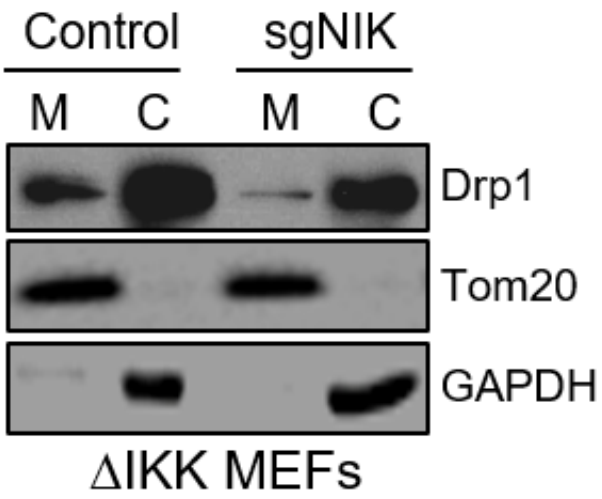

Figure 46. NIK enhances Drp1 recruitment to mitochondria in IKK-knockout MEFs. Immunoblot analysis of mitochondria-enriched (M) and cytosolic (C) fractions from ΔIKK MEFs and sgNIK-ΔIKK MEFs was performed with the indicated antibodies.

CHAPTER IV

NIK REGULATES DRP1 PHOSPHORYLATION AND IS LOCALIZED TO SITES OF MITOCHONDRIAL FISSION

4.1 Summary

Mitochondrial morphology is dynamically regulated by fusion and fission, and dysregulation of this process has been implicated in tumorigenesis. In chapter III, we found that a novel pool of NIK protein is localized to mitochondria and regulates mitochondrial recruitment of Drp1, a key fission regulator, to promotes mitochondrial fragmentation and glioma cell invasion. However, effects of NIK kinase activity on tumor progression and mitochondrial dynamics remains largely unknown. Here, we show that depletion of NIK in glioma cell results in diminished invasion and also results in entangled and clustered mitochondria in perinuclear regions, phenotypes that could be restored by reconstituting NIK wild-type, but not kinase-dead NIK mutant. In addition, impaired kinase activity of NIK reduces tumor growth in human glioma xenograft mouse models. Intriguingly, NIK is accumulated transiently on dividing mitochondria, where Drp1 is recruited to mitochondrial constriction sites for fission to occur. Kinase activity of NIK is critical to promote phosphorylation of Drp1 at serine 616 residue, but not to interact with Drp1. These results provide a cellular mechanism for kinase activity of NIK-mediated mitochondrial dynamics leads to constriction at the fission site and tumor growth.

4.2 Introduction

In non-canonical NF-κB pathway, the fundamental purpose of NIK as serine/threonine protein kinase is to phosphorylate IKKα, resulting proteasomal processing of p100 to p52 to

regulates the transcription of genes involved in inflammation, development, cell cycle, cell proliferation, and cell survival (Ge et al., 2016; McDaniel et al., 2016; Park and Hong, 2016; Sun, 2012). While most studies about NF-κB pathway focused on investigating how canonical NF-κB/p65-mediated signaling cascade regulates the activity of transcription factors associated with various cellular functions, our previous studies identified involvement of NIK-mediated non-canonical NF-κB pathway in pseudopodia formation, cell elongation, and invasion of glioma cell (Cherry et al., 2015; Duran et al., 2016). Particularly, overexpression of NIK led to accelerated tumor growth in a xenograft model, compared to control cells. (Cherry et al., 2015). In the previous chapter, we found that mitochondrial NIK is a novel pool of NIK protein in cancer cells that regulate mitochondrial dynamics, motility and cell invasion even in the absence of the IKK/NF-κB signaling cascade. However, it is still unclear whether kinase activity of NIK is required for regulating mitochondrial dynamics and glioma tumorigenesis.

Phosphorylation of mitochondrial fission regulators such as Drp1 are known to be required for their activity or recruitment to mitochondria (Kashatus et al., 2011; Taguchi et al., 2007). In fact, a phosphodefective mutant Drp1-S616A (serine at 616 was mutated to alanine) failed to promote mitochondria fission, which resulted in abnormal mitochondrial morphology (Cereghetti et al., 2008). Knockdown of Drp1 expression or the phosphorylation-deficient mutant of Drp1 was unable to promote tumor growth (Kashatus et al., 2015; Zhan et al., 2016). It strongly suggests that the effect of Drp1 activity involved in mitochondria dynamics and tumor progression may depend on upstream kinases (Chang and Blackstone, 2010; Hu et al., 2017). Considering that phosphorylation sites tend to be located on binding spots to regulate complex formation, activity of fusion and fission molecular machineries to control mitochondrial dynamics will be easily influenced by binding partners. Moreover, we identified several potential

phosphorylation sites of Drp1 for NIK through the PhosphoNET prediction database, Drp1 - S119, S248, S616, and S665 (Fig.47). Although we observed that NIK binds to Drp1 and enhances phosphorylation of the key fission regulator, it is still unclear how NIK and Drp1 collaborate to drive mitochondria division and whether NIK acts directly to phosphorylate Drp1. Here, we identified that the kinase activity of NIK maintains mitochondrial dynamics, drives cell invasion and tumor growth, and is required for the phosphorylation Drp1.

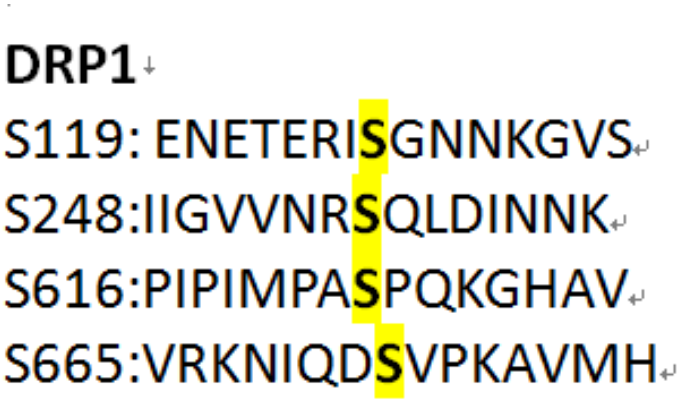

Figure 47. Potential phosphorylation motifs of Drp1 for serine/threonine protein kinase NIK. The potential phosphorylation sites (highlighted) were predicted using PhosphoNET prediction database.

4.3 Results

4.3.1 Kinase-dead NIK affects mitochondrial fission and invasion of glioma

To explore effects of NIK kinase activity on mitochondrial dynamics, we first made mouse NIK cDNA construct with point mutations K431A/K432A (corresponds to the K429A/K430A mutations in human NIK), which abrogate its kinase activity (de Leon-Boenig et al., 2012; Luftig et al., 2001; Tao and Ghosh, 2012). The human glioma BT25 cells lacking a functional NIK gene (BT25-sgNIK) were reconstituted with murine NIK wild-type (BT25-sgNIK+rescue) or kinase-dead mutant ($mNIK^{K431A/K432A}$; BT25-sgNIK+KD-rescue). The total protein levels of non-canonical NF-κB signaling in each BT25 cells were examined by western blot using specific antibodies for the subunits of non-canonical NF-κB. As expected, the kinase-dead mutant of NIK was not able to induce the phosphorylation of IKKα/β and the p100 processing to p52, while the expression levels of the non-canonical NF-κB subunits in BT25-sgNIK+rescue cells remained similar or higher than that of control cells (Fig. 48A). However, the results of experiments showing NIK immunostaining to examine whether kinase-dead mutant affects NIK localization reveal that kinase-dead NIK was successfully colocalized with Tim50 as a marker to establish the localization of NIK in the mitochondria, similar to wild-type NIK in BT25 control cells (Fig. 48B). Consistent with immunostaining results, kinase-dead NIK protein was present in both mitochondrial-enriched (M) and cytosolic (C) cell fractions as well as endogenous NIK (BT25 control) and reconstituted wild-type NIK (BT25-sgNIK+rescue), whereas NIK protein was not detected by immunostaining and immunoblot in either fraction from BT25-sgNIK cells (Fig. 48B and 49).

To determine whether kinase activity of NIK is required for glioma invasion, we performed three-dimensional collagen invasion assay. Depletion of NIK expression in BT25-

sgNIK cells significantly attenuates invasive potential in three-dimensional collagen matrices compared with control cells, and the decreased invasion was restored with reconstitution of murine wild-type NIK. Interestingly, reconstitution of kinase-dead NIK in BT25-sgNIK (BT25-sgNIK+KD-rescue) was unable to restore invasion ability compared to BT25-sgNIK+rescue (Fig. 50). We also examined changes in mitochondrial morphology due to loss of NIK kinase activity. Each structure obtained from Mito-GFP staining was outlined and the area was determined by ImageJ morphometric analysis (Fig. 51A). Consistent with previous observation, loss of NIK in glioma cell (BT25-sgNIK cells) results in increased mitochondrial size and decreased mitochondrial number compared to control cells (Fig. 51B). Importantly, the mitochondrial hyperfusion of BT25-sgNIK cells was rescued through reconstitution of wild-type NIK (BT25-sgNIK+rescue), but not kinase-dead NIK (BT25-sgNIK+KD-rescue) (Fig. 51B). Together, these data demonstrate that the kinase activity of NIK is important for invasion and mitochondrial dynamics in glioma cells.

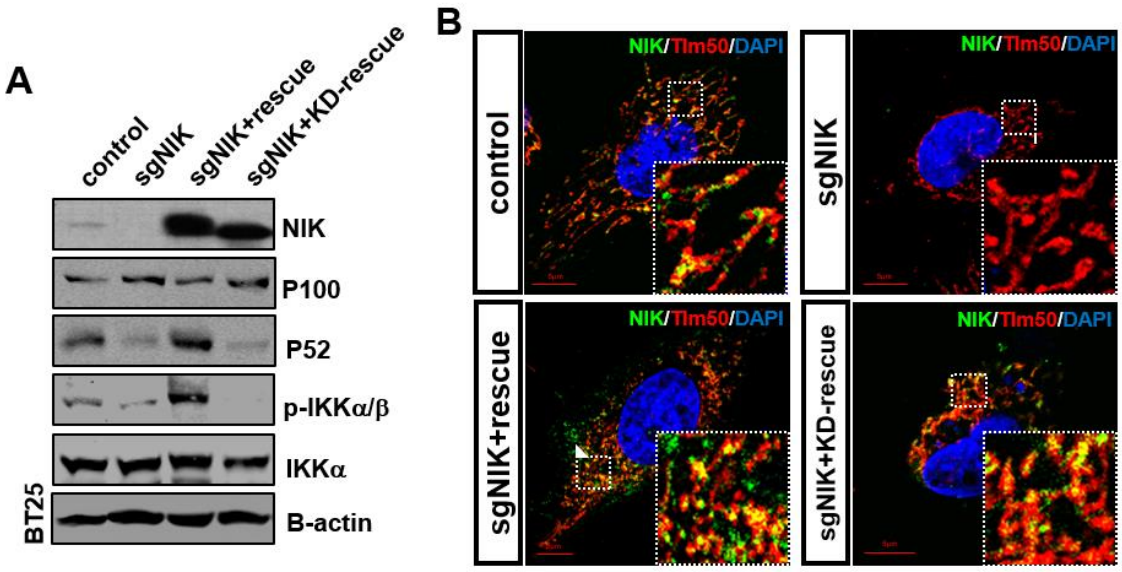

Figure 48. Kinase-dead mutant of NIK was not able to promote the non-canonical NF-κB pathway. (A) Immunoblot analysis of whole cell lysates prepared from BT25 control, BT25-sgNIK, BT25-sgNIK+rescue and BT25-sgNIK+KD-rescue cells pretreated with TWEAK (10 ng/ml) and MG132 (5 μM) to stabilize NIK for facile detection. Blots were probed with indicated antibodies. (B) Immunofluorescence images of BT25 control, BT25-sgNIK, BT25-sgNIK+rescue and BT25-sgNIK+KD-rescue cells immunostained for NIK (Red), Tim50 (green) and DAPI (blue). Images marked with white squares are amplified and shown in the insert. Scale bar, 5 μm.

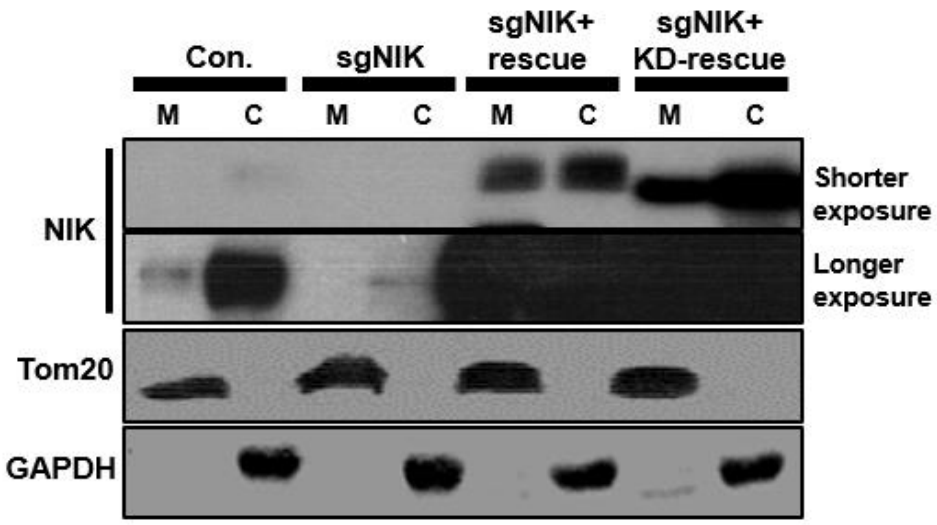

Figure 49. Loss of NIK kinase activity does not affect its mitochondrial localization. Immunoblot analysis of mitochondrial-enriched (M) and cytosolic (C) fractions prepared from BT25 control, BT25-sgNIK, BT25-sgNIK+rescue and BT25-sgNIK+KD-rescue cells pretreated with TWEAK (10 ng/ml) and MG132 (5 μM). Four times the volume equivalent of mitochondrial-enriched fraction versus cytosol fraction was loaded (mitochondrial-enriched/cytosol = 4:1). Blots were probed with indicated antibodies.

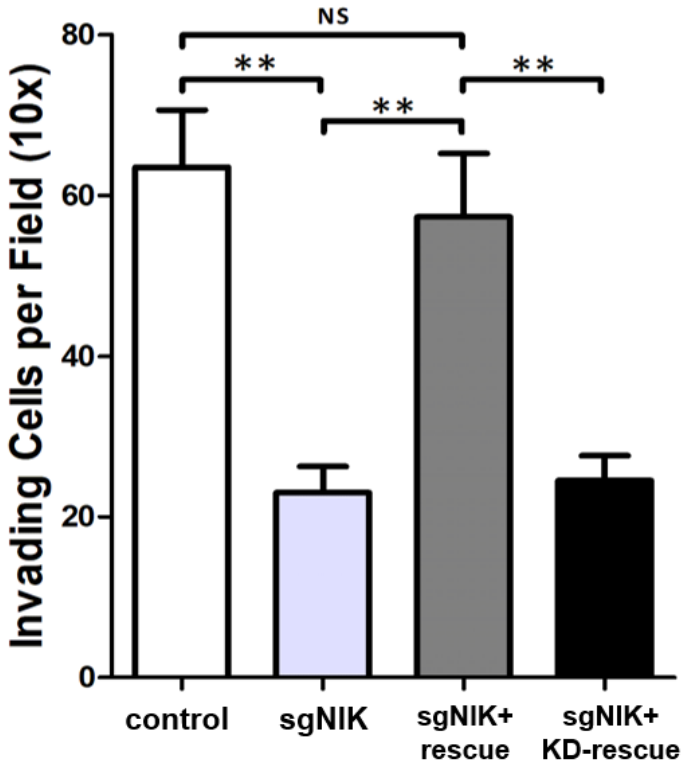

Figure 50. Loss of NIK kinase activity reduces their invasive potential in glioma cells. Quantification of three-dimensional collagen invasion assays comparing BT25 control, BT25-sgNIK, BT25-sgNIK+rescue and BT25-sgNIK+KD-rescue cells. Data are represented as mean ± SD. ** $p<0.01$ (n=6), one-way ANOVA; NS: not significant.

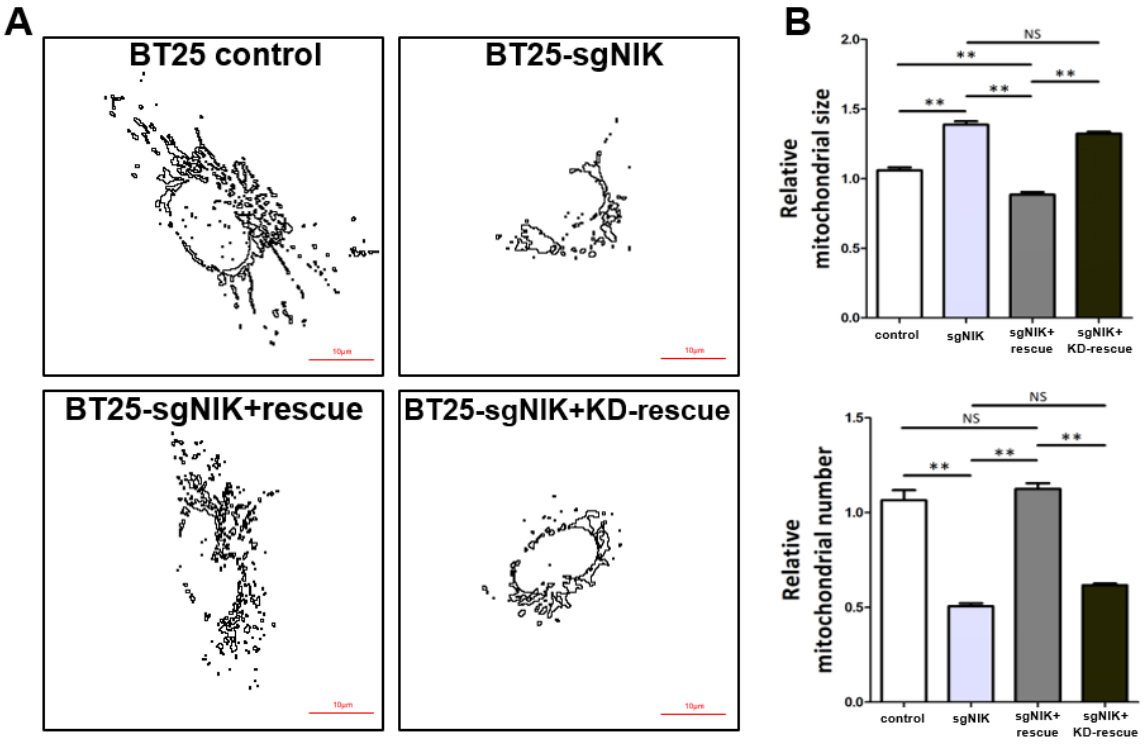

Figure 51. Kinase-dead mutant of NIK failed to restore mitochondria fission. (A) Mitochondrial number and size in BT25 control, BT25-sgNIK, BT25-sgNIK+rescue and BT25-sgNIK+KD-rescue cells were transfected with Mito-GFP (Outline), and (B) then quantified using the Analyze Particles function in ImageJ software. Data are represented as mean ± SD. ** $p<0.01$ for sgNIK vs. control; sgNIK vs. sgNIK+rescue; sgNIK+rescue vs. sgNIK+KD-rescue. one-way ANOVA ($n > 50$, respectively); NS: not significant. Scale bar, 10 μm.

4.3.2 Impaired kinase activity of NIK reduces tumor growth *in vivo* xenograft models of glioma

Previously we have reported that NIK overexpression in glioma positively regulates tumor growth in vivo (Cherry et al., 2015), suggesting that loss of NIK expression may inhibits tumor growth. To examine the roles of kinase activity of NIK in vivo, BT25 control, -sgNIK, -sgNIK+rescue and -sgNIK+KD-rescue cells were fluorescently labeled with a DiD-fluorescent probe to monitor tumor growth and injected intracranially into the brain of CD-1 nude mice. We found that suppression of NIK expression (BT25-sgNIK) significantly inhibited intracranial tumor growth compared with the mice injected with BT25 control cells (Fig. 52). Particularly, the three-dimensional tomographic reconstruction of fluorescent images obtained from in vivo imaging system (IVIS) showed that loss of NIK kinase activity (BT25-sgNIK+KD-rescue) resulted in reduced tumor size and less invasive tumors compared with BT25-sgNIK+rescue cells (Fig. 53). Unexpectedly, tumors derived from kinase-dead NIK cells had become much larger then NIK-knockout cells for unknown reasons, it was probably due to transduction-mediated overexpression of NIK proteins above the threshold value (Fig. 52 and 53). In addition, the hematoxylin and eosin (H&E) staining assay was performed to evaluate and to visualize the brain tumors. Consistent with results from IVIS analysis, we found that BT25-sgNIK+KD-rescue cells diminished tumor formation, by contrast, mice receiving BT25-sgNIK+rescue cells showed an increase in tumor size (Fig. 54). These results strongly suggest that NIK kinase activity is crucial for tumor growth.

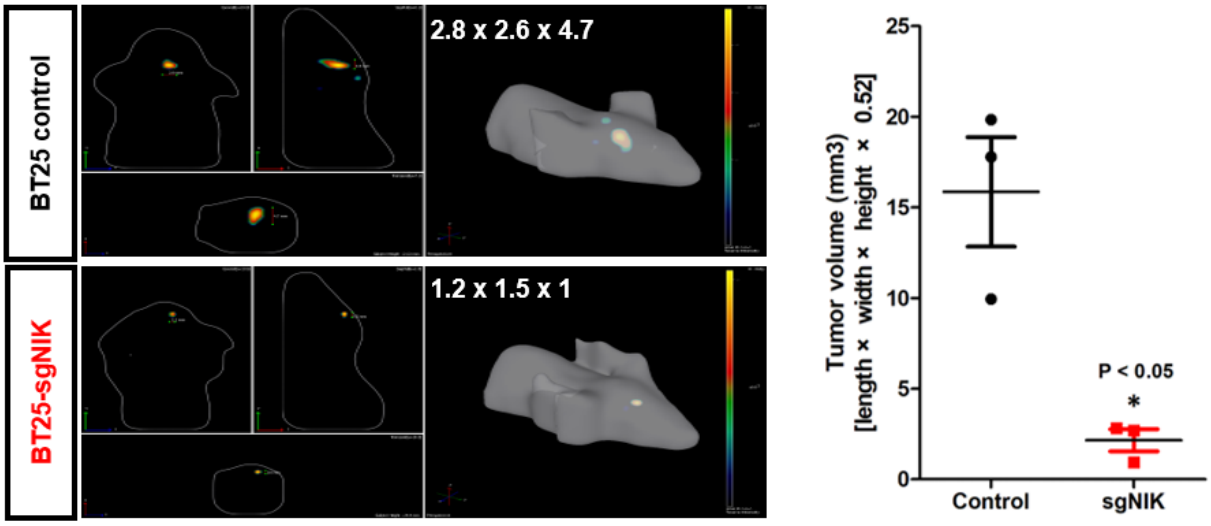

Figure 52. Loss of NIK reduces xenograft tumor growth. Representative IVIS images of three-dimensional rendering of tumors derived from DiD-labelled intracranial-injected BT25 control and BT25-sgNIK at 30 days post-injection (n=3 mice per group). Numbers indicate length of three dimension for each image. Right graph showing quantification of tumors size. Data represent average tumor volume ± S.E.M. *p < 0.05 for BT25 control vs. BT25-sgNIK; Unpaired Student's t-test.

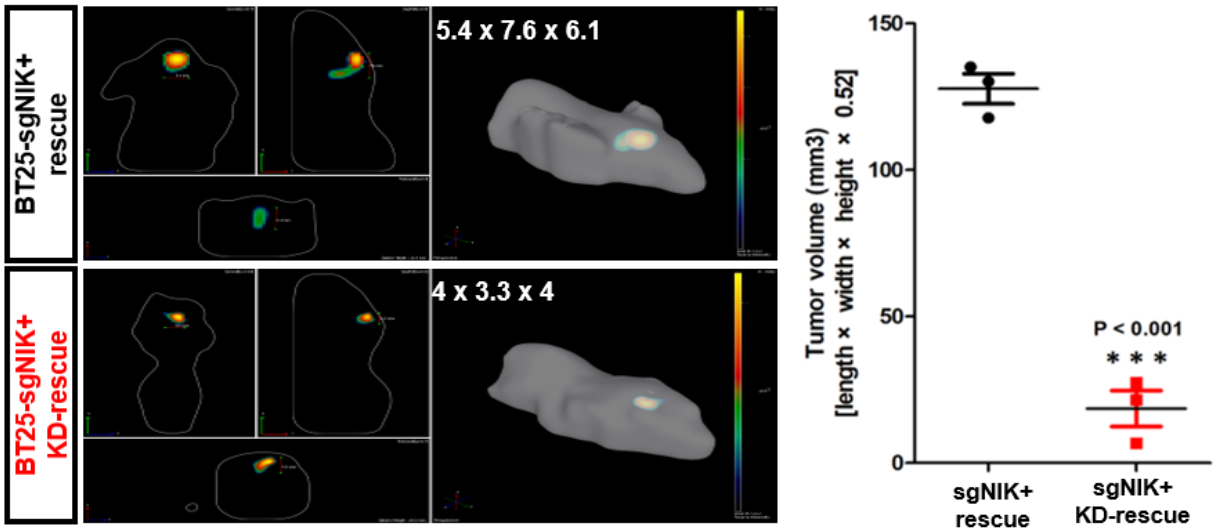

Figure 53. Kinase activity of NIK is required for xenograft tumor growth. Representative IVIS images of three-dimensional rendering of tumors derived from DiD-labelled intracranial-injected BT25-sgNIK+rescue and BT25-sgNIK+KD-rescue cells at 30 days post-injection (n=3 mice per group). Numbers indicate length of three dimension for each image. Right graph showing quantification of tumors size. Data represent average tumor volume ± S.E.M. *** $p < 0.001$ for BT25-sgNIK+rescue vs. BT25-sgNIK+KD-rescue. Unpaired Student's t-test.

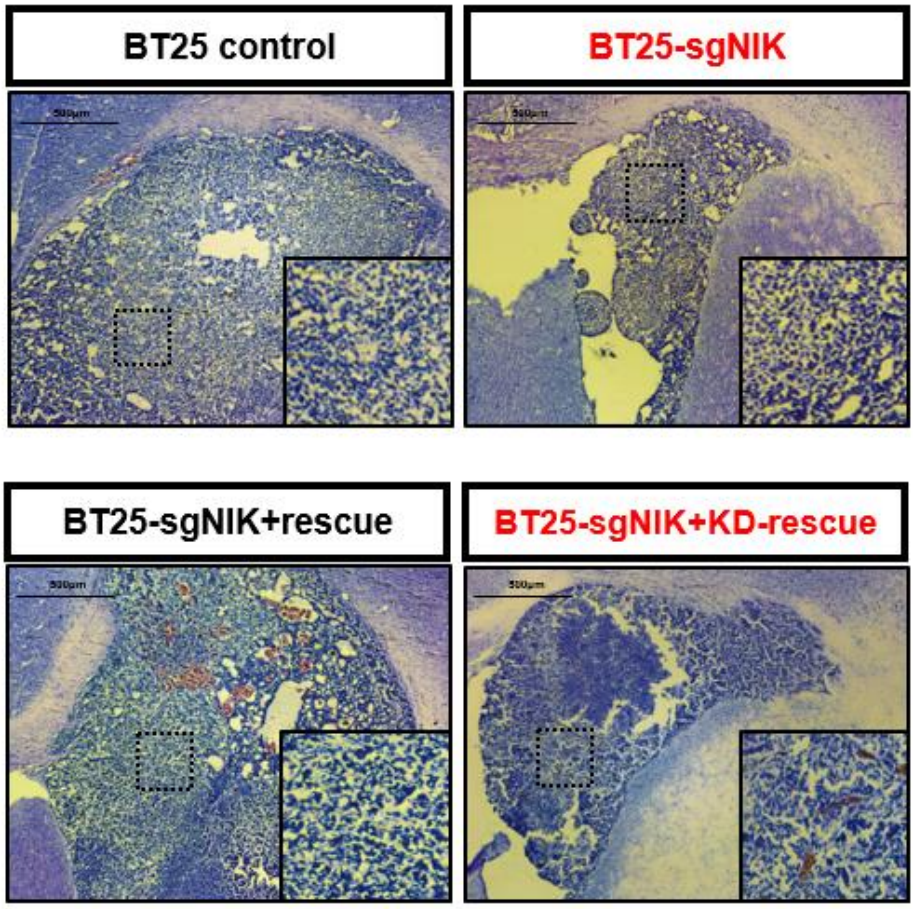

Figure 54. H&E staining of xenograft tumor. Representative hematoxylin and eosin (H&E) staining images of brain sections from BT25 control, BT25-sgNIK, BT25-sgNIK+rescue and BT25-sgNIK+KD-rescue xenograft tumors. Brains were harvested at 5 - 6 weeks after transplantation. Images marked with black squares are amplified and shown in the insert. Scale bars: 500 μm.

4.3.3 NIK-Drp1 interaction enriches at mitochondrial constriction sites

In chapter III, we have shown that NIK localizes to mitochondria and binds Drp1 as well as its potential to recruit Drp1 from the cytoplasm to mitochondria to promote mitochondrial fission. Thus, identifying an exact localization of NIK-Drp1 interaction in glioma cell is essential to finding mechanisms underlying mitochondrial fission. We performed live-cell imaging using a NIK green fluorescent protein (GFP)-fusion protein (GFP-NIK) to determine whether NIK localized at mitochondrial fission sites. First, functionality of the NIK protein after GFP-tagging was confirmed by western blot analysis that transiently expressed GFP-NIK activates non-canonical NF-κB pathway including p100 processing, p52 nuclear translocation and phosphorylation of IKKα/β, similar to non GFP-tagged NIK (Fig. 55). Time-lapse imaging assays revealed that GFP-NIK recruits and accumulates transiently at the outer surface of mitochondrial division sites from the non-constricted sites, and then released from the constriction sites immediately after fission (Fig. 56).

Considering that a key fission regulator Drp1 is primarily localized to the cytoplasm and recruited to mitochondrial constriction sites immediately prior to fission (Frank et al., 2001; Smirnova et al., 2001), NIK enrichment at construction sites is most likely necessary for Drp1 recruitment and interaction with Drp1. Therefore, an in situ proximity ligation assay (in situ PLA), a highly specific protein interaction screening method (Fredriksson et al., 2002), was employed to determine whether endogenous NIK binds Drp1 at mitochondria in glioma cell. The in situ PLA experiment showed that interactions between NIK and Drp1 were predominantly observed in mitochondria, as indicated by most PLA signals localized on mitochondrial marker Tom20, and are rarely found in cytosol (Fig. 57). To confirm that these signals were indeed specific, in situ PLA was performed using immunoglobulin G as a negative control or PGAM5,

which is known to interact with Drp1 (Xu et al., 2015), as a positive control. As expected, IgG control did not produce any PLA signals in the cells as well as BT25-sgNIK cells (Fig. 58A and C), while a number of distinct fluorescent dots are observed in assay using PGAM5 and Drp1 antibodies (Fig. 58B). This endogenous protein-protein interaction was also verified by immunofluorescence staining using NIK and Drp1 antibody and immunoprecipitation for Drp1 in TWEAK/MG132-treated BT25 cells (Fig. 59). Wild-type NIK, reconstituted NIK or kinase-dead mutant NIK all colocalized and associated with Drp1, indicating that NIK-Drp1 interaction was independent of kinase activity (Fig. 59). We further assessed the involvement of NIK and Drp1 on the division event by live-cell imaging using mCherry-tagged Drp1 (mch-Drp1) and GFP-NIK in glioma cells. We found that mCh-Drp1 puncta were recruited transiently at constriction site and colocalized with GFP-NIK around the outer surface of mitochondrial fission site (Solid arrows in Fig. 60). Particularly, GFP-NIK was recruited to future constriction sites prior to Drp1 recruitment to trigger mitochondrial constriction (hollow arrows in Fig. 60). Recruitment of NIK and Drp1 into mitochondrial fission sites was also observed in non-cancerous COS-7 cells (Fig. 61 and 62). These results suggest that NIK enriched at mitochondrial constriction site may play an important role in initiation of mitochondria fission through interaction with Drp1.

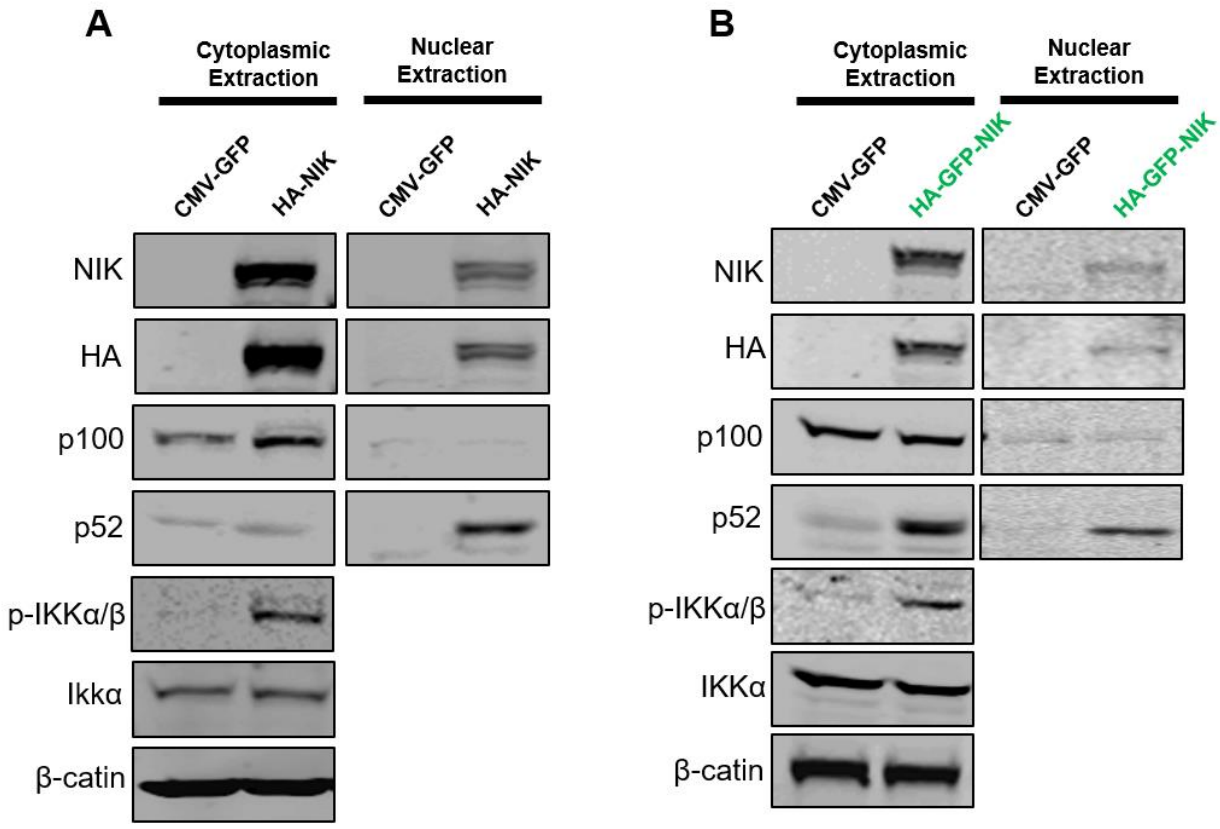

Figure 55. Validation of NIK-GFP fusion protein function. Western blot analysis of cytosolic and nuclear fractions isolated from 293T transiently expressing GFP-empty vector (control) and (A) HA-NIK or (B) GFP-NIK. Blots were probed with the indicated antibodies.

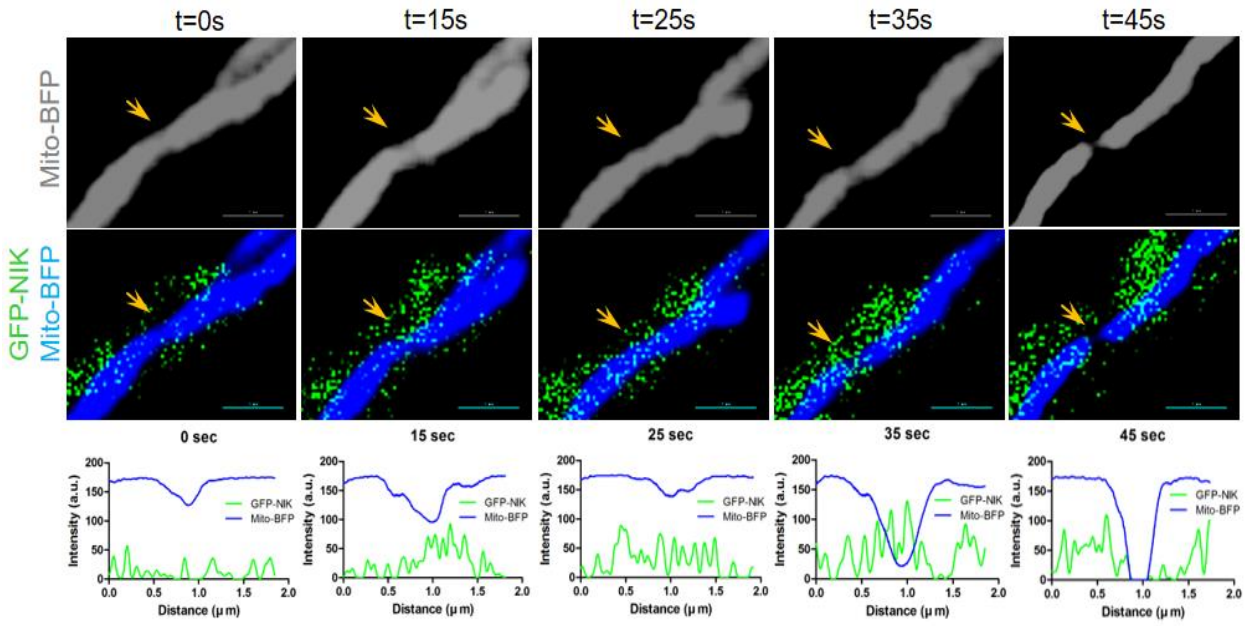

Figure 56. NIK accumulates at mitochondrial constriction sites in glioma cells. Time-lapse image of BT25 cell transiently expressing mito-BFP (blue) and GFP-NIK (green) acquired with every 5 sec intervals for 3 min. Line-scan analysis shows fluorescence intensity of GFP-NIK along a portion of indicated fission site. Images were threshold-adjusted by subtracting background GFP in the cytosol, followed by deconvolution. Yellow arrow indicates fission site. Scale bar, 1 μm.

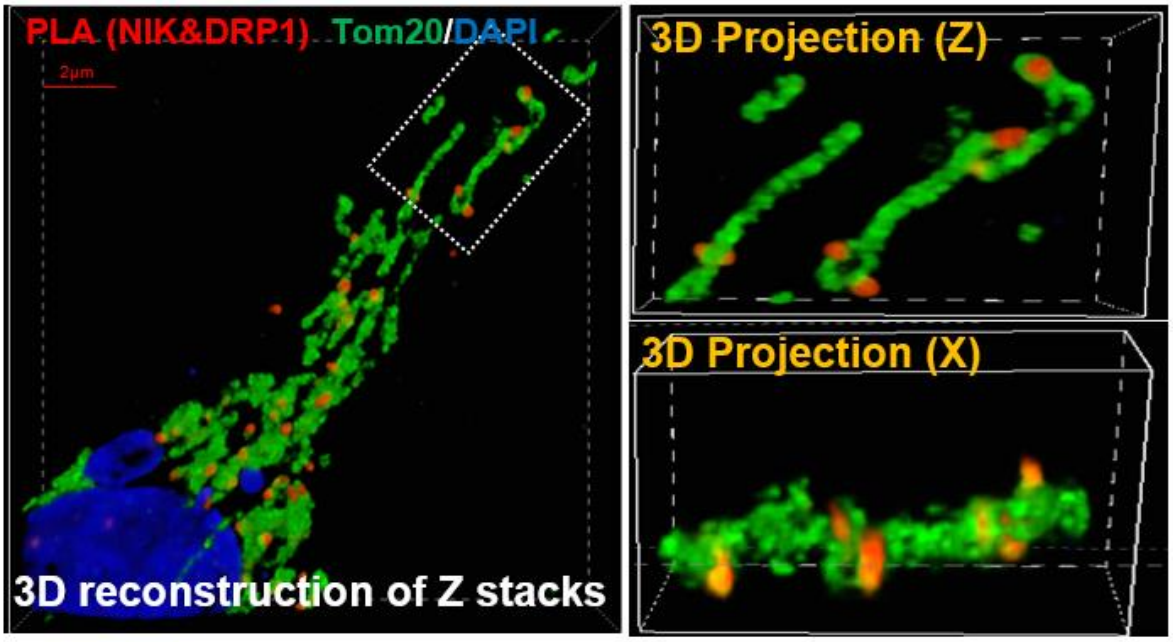

Figure 57. Interactions between NIK and Drp1 are predominantly localized in mitochondria. BT25 cells were stained for endogenous NIK and Drp1, followed by ligation and amplification (Red) of PLA probes minus and plus, and then immunostained for Tom20 (green) and DAPI (blue). Images marked with white squares are magnified and shown as three-dimensional projections (3D). Scale bar, 2 μm.

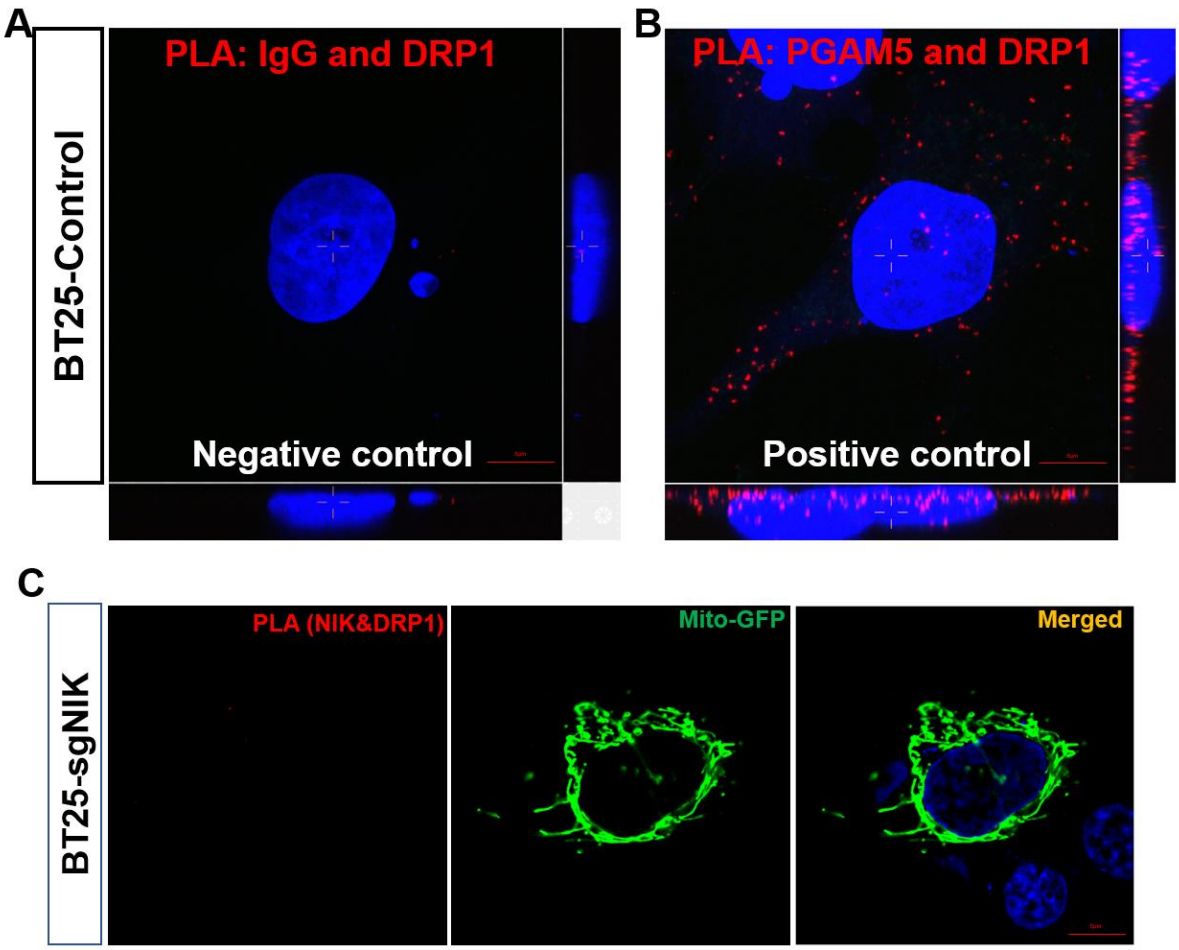

Figure 58. Validation of specificity of proximity ligation assay. (A) BT25 cells were stained with endogenous Drp1 and control IgG or PGAM5, followed by ligation and amplification (Red) of PLA probes minus and plus, and then immunostained for DAPI (blue) (B) Mito-GFP labelled BT25-sgNIK cells were subjected to in situ proximity ligation assay with NIK and Drp1 antibody. Scale bar, 5 μm.

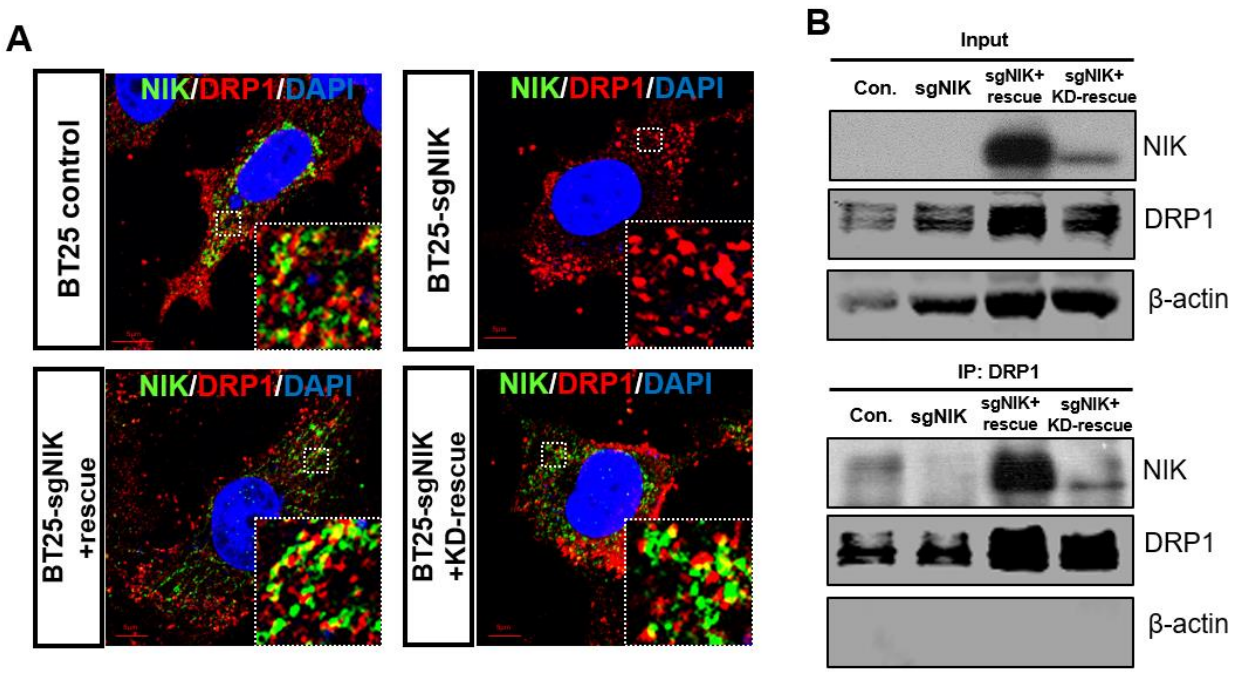

Figure 59. NIK–Drp1 interaction is independent of NIK kinase activity. (A) Immunofluorescence images of BT25 control, BT25-sgNIK, BT25-sgNIK+rescue and BT25-sgNIK+KD-rescue cells immunostained for NIK (Green), Drp1 (red) and DAPI (blue). Images marked with white squares are amplified and shown in the insert. Scale bar, 5 μm. (B) BT25 control, BT25-sgNIK, BT25-sgNIK+rescue and BT25-sgNIK+KD-rescue cell lysates were subjected to immunoprecipitation (IP) with control IgG or a Drp1 antibody, and then analyzed by immunoblotting with the indicated antibodies.

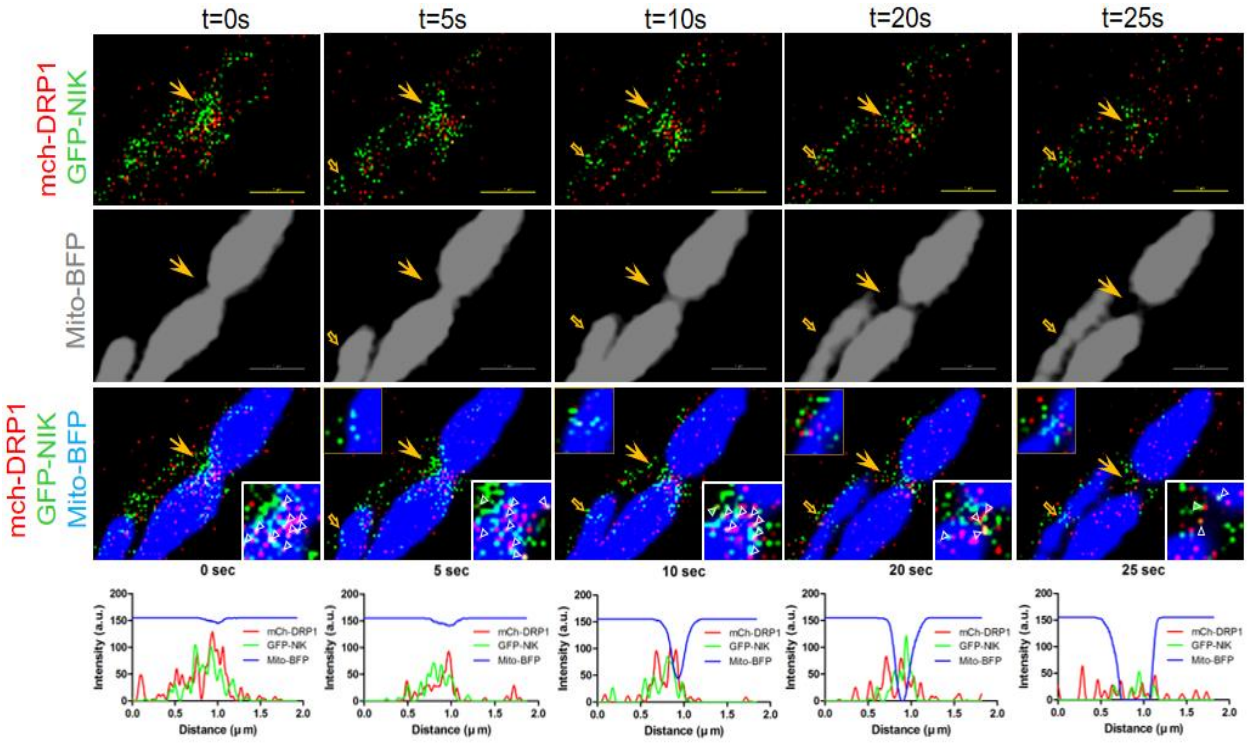

Figure 60. NIK-Drp1 interaction accumulates at mitochondrial constriction sites in glioma cells. Time-lapse image of BT25 cell transiently expressing mito-BFP (blue), mch-Drp1 (red) and GFP-NIK (green) acquired with every 5 sec intervals for 3 min. Line-scan analysis shows fluorescence intensity of mch-Drp1 and GFP-NIK along a portion of indicated fission site. Images were threshold-adjusted by subtracting background GFP in the cytosol, followed by deconvolution. Arrows denote: yellow arrows (fission site; amplified and shown in the lower right corner); hollow arrowheads (co-localization of mch-Drp1 and GFP-NIK); hollow arrow (beginning of constriction; amplified and shown in the upper left corner). Scale bar, 1 μm.

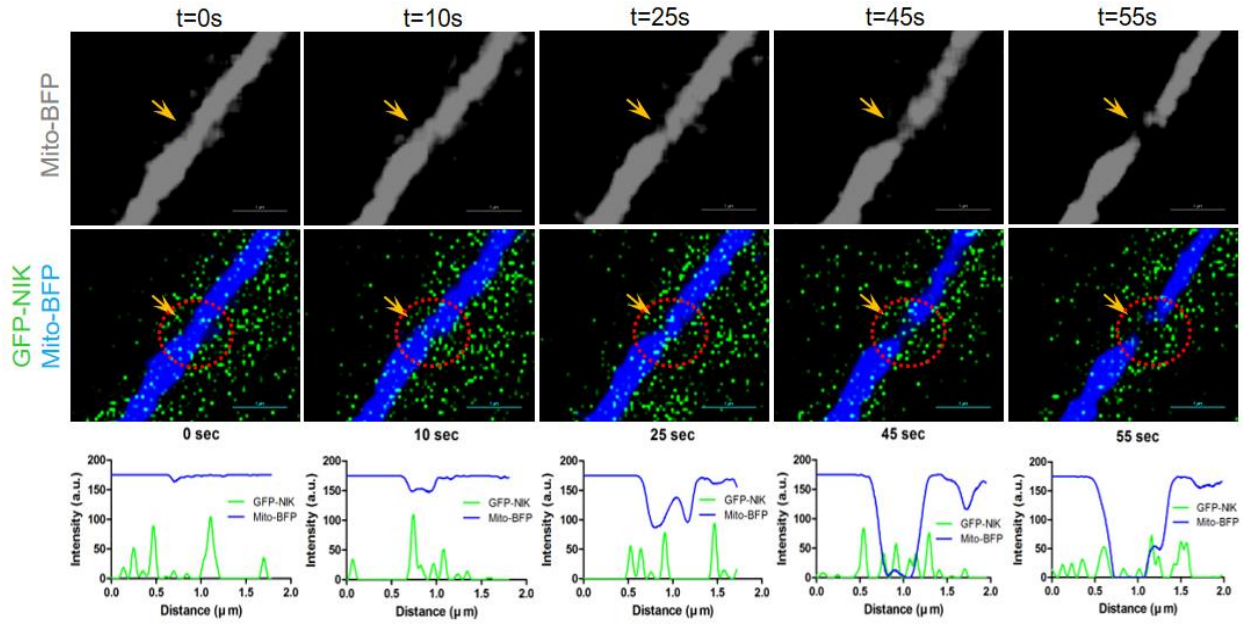

Figure 61. NIK recruits to mitochondrial constriction sites in COS-7 cells. Time-lapse image of COS-7 cell transiently expressing mito-BFP (blue) and GFP-NIK (green) acquired with every 5 sec intervals for 3 min. Line-scan analysis shows fluorescence intensity of GFP-NIK along a portion of indicated fission site. Images were threshold-adjusted by subtracting background GFP in the cytosol, followed by deconvolution. Yellow arrow with red circle indicates fission site. Scale bar, 1 μm.

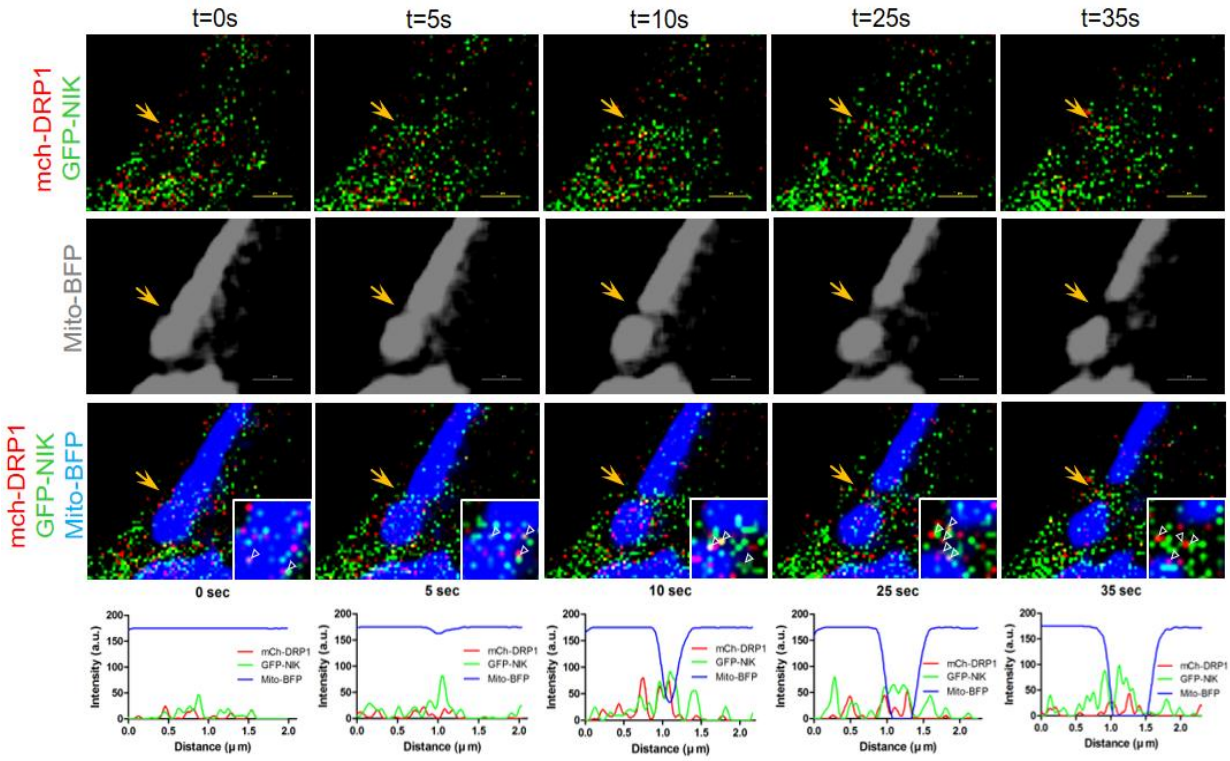

Figure 62. NIK recruits to mitochondria and interacts with Drp1 at constriction sites in COS-7 cells. Time-lapse image of COS-7 cell transiently expressing mito-BFP (blue), mch-Drp1(red) and GFP-NIK (green) acquired with every 5 sec intervals for 3 min. Line-scan analysis shows fluorescence intensity of GFP-NIK along a portion of indicated fission site. Images were threshold-adjusted by subtracting background GFP in the cytosol, followed by deconvolution. Images marked with yellow arrows are amplified and shown in the insert. Arrows denote: yellow arrows (fission site); arrowheads (co-localization of mch-Drp1 and GFP-NIK). Scale bar, 1 μm.

4.3.4 NIK promotes phosphorylation of Drp1

Drp1 activity is regulated by post-translational modification, particularly phosphorylation at serine residue 616 (S616) is necessary to promote mitochondrial fission (Jahani-Asl and Slack, 2007; Prieto et al., 2016; Taguchi et al., 2007). We therefore investigated whether NIK regulates Drp1 activity through phosphorylation of S616. Immunofluorescence analyses showed that puncta of Drp1 phosphorylation at S616 (p-S616) were localized mostly in the mitochondria in BT25 control cells (Fig. 63). The number of Drp1 p-S616 puncta were significantly decreased in BT25-sgNIK cells, but it was restored in BT25-sgNIK+rescue cells (Fig. 63). Interestingly, kinase-dead mutant of NIK (BT25-sgNIK+KD-rescue), unlike wild-type NIK, failed to restore the increased p-S616 staining (Fig. 63). Biochemical fractionation analyses also confirmed that the total level of Drp1 phosphorylation at S616 was decreased in BT25-sgNIK cells (Fig. 64). Compared to BT25-sgNIK+rescue cells, BT25-sgNIK+KD-rescue cells exhibited substantially diminished phosphorylation of Drp1-S616 (Fig. 63 and 64), but the kinase-dead mutant of NIK does not significantly affect the efficiency of Drp1 mitochondrial recruitment (Fig. 64, 65 and 66). Unpredictably, relatively lower levels of mitochondrial Drp1 phosphorylation at S616 was detected by fractionation analysis (Fig. 64), while immunostaining showed that Drp1 p-S616 staining is mostly colocalized with a mitochondria marker (Fig. 63). This discrepancy may be due to weak association of Drp1 with mitochondria membrane, which is easily lost during the fractionation procedure.

To test whether kinase activity of NIK is responsible for phosphorylation of Drp1-S616, we first performed an in vitro kinase assay using cell lysates as sources of the kinase. The cell extracts from 293T cells transfected with a construct expressing NIK wild-type or $NIK^{K429A/K430A}$ were incubated with purified glutathione S-transferase (GST)-Drp1 as a substrate, and we found

that only lysates of 293T cells transfected with NIK wild-type phosphorylates Drp1-S616 (Fig. 67A). Similar results were also observed with immunoprecipitates from the cell lysates. NIK proteins are isolated with antibody-coupled magnetic beads, and then performed in vitro kinase assay using the purified GST-Drp1. We observed that Drp1-S616 was phosphorylated by bead-bound NIK wild-type, but neither bead-bound $NIK^{K429A/K430A}$ nor bead control (Fig. 67B). Taken together, these results indicate that NIK is responsible for Drp1-S616 phosphorylation, which promotes mitochondrial fission.

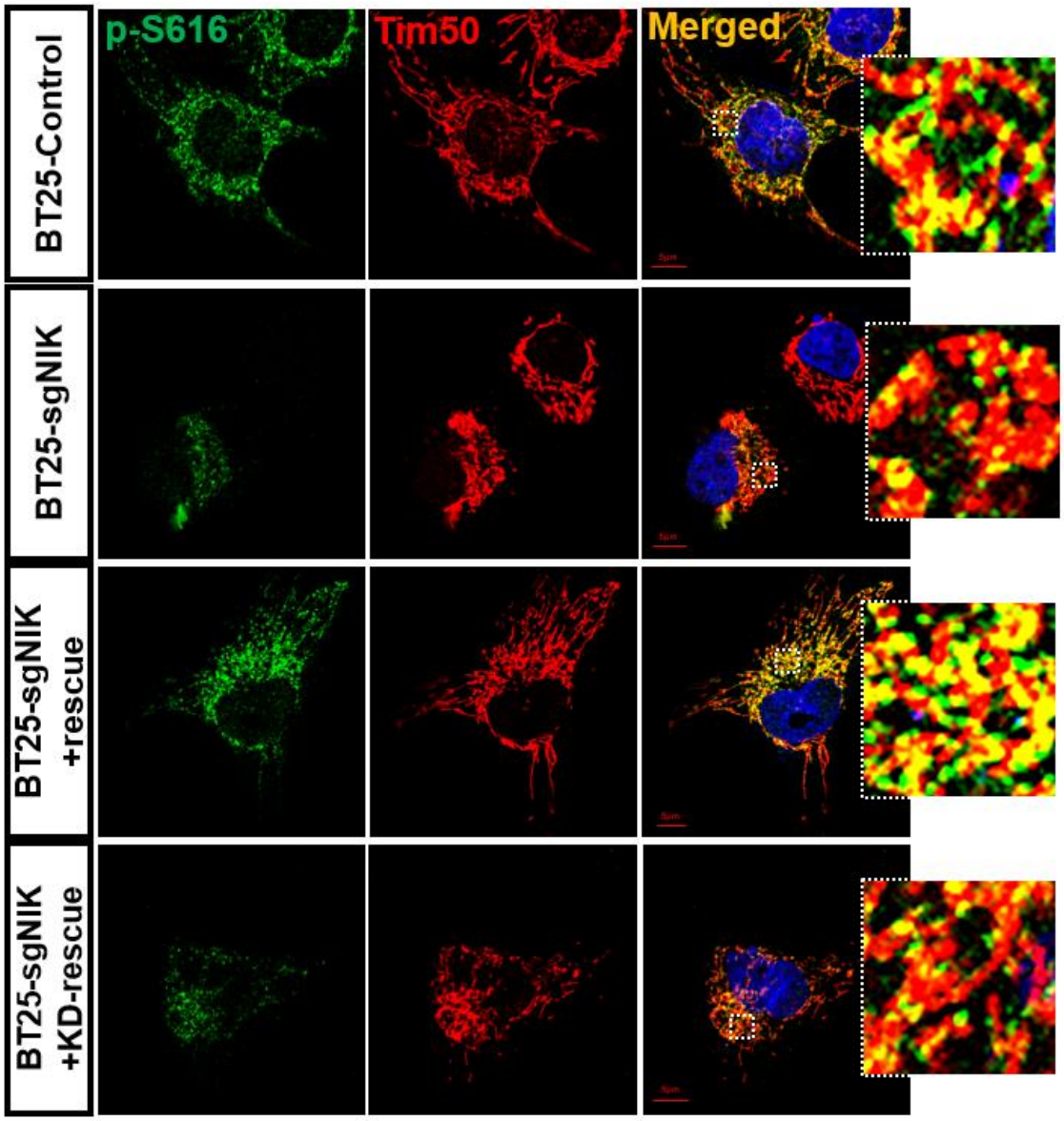

Figure 63. NIK influences phosphorylation of Drp1-S616. BT25 control, BT25-sgNIK, BT25-sgNIK+rescue and BT25-sgNIK+KD-rescue cells immunostained for p-Drp1 S616 (green), Tim50 (red) and DAPI (blue). Images marked with white squares are amplified and shown on the right. Scale bar, 5 μm.

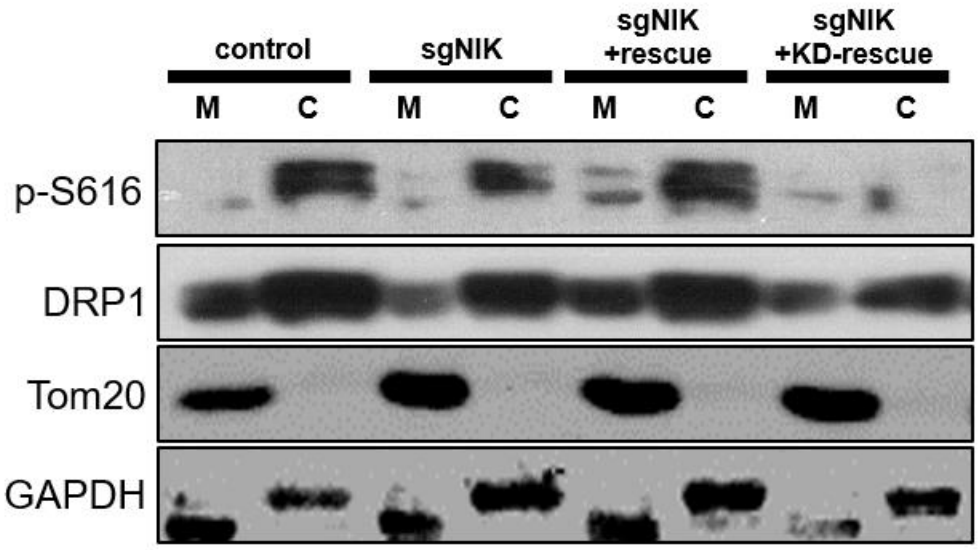

Figure 64. Kinase-dead mutant of NIK reduces phosphorylation of Drp1-S616. Immunoblot analysis of mitochondrial-enriched (M) and cytosolic (C) fractions prepared from BT25 control, BT25-sgNIK, BT25-sgNIK+rescue and BT25-sgNIK+KD-rescue cells were performed with indicated antibodies.

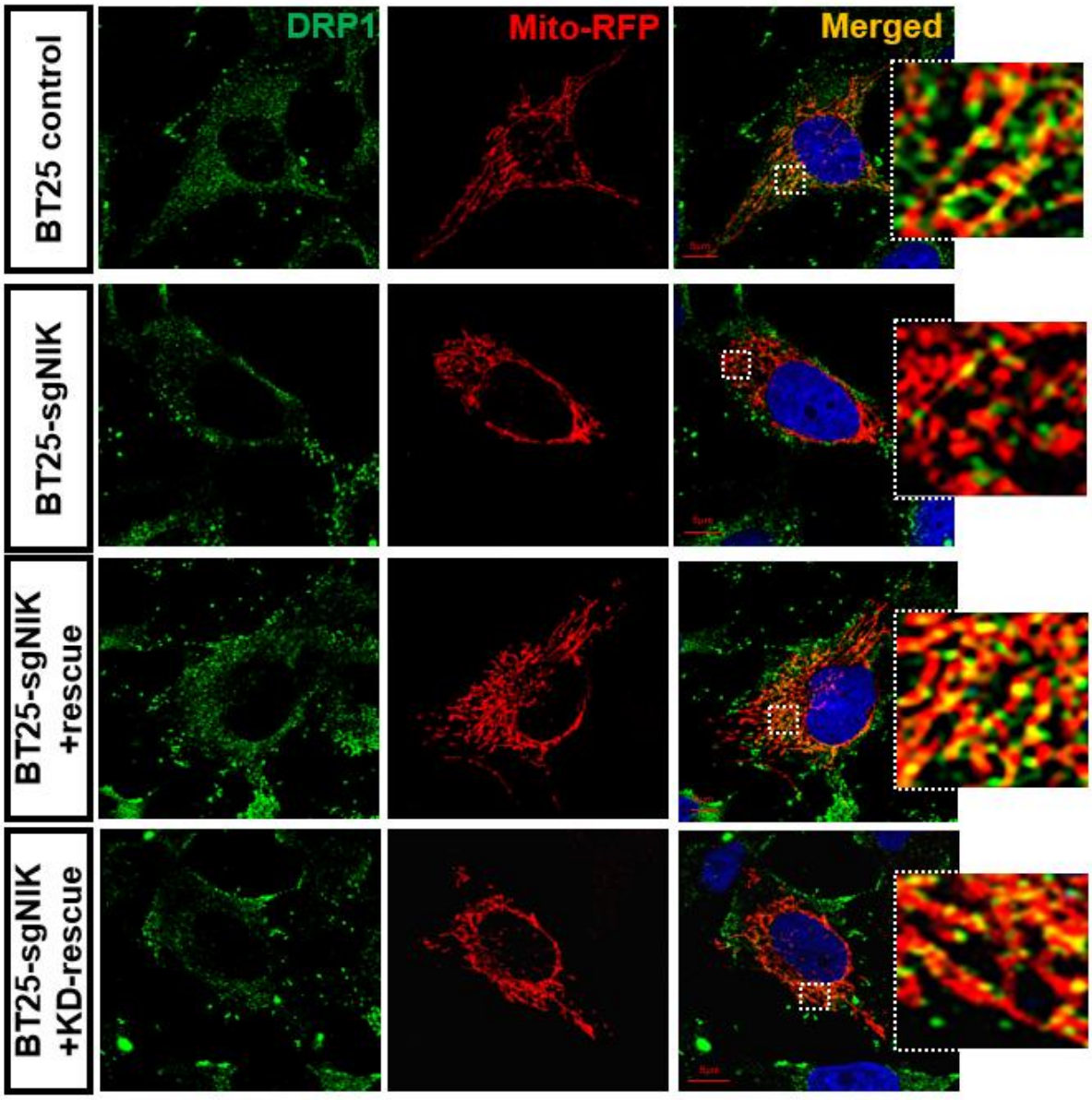

Figure 65. Kinase-dead mutant of NIK doesn't affect mitochondrial association of Drp1. BT25 control, BT25-sgNIK, BT25-sgNIK+rescue and BT25-sgNIK+KD-rescue cells were transfected with Mito-RFP to visualize mitochondria (red) and then immunostained for Drp1 (green), and DAPI (blue). Areas within white squares are amplified and shown on the right. Scale bar, 5 μm.

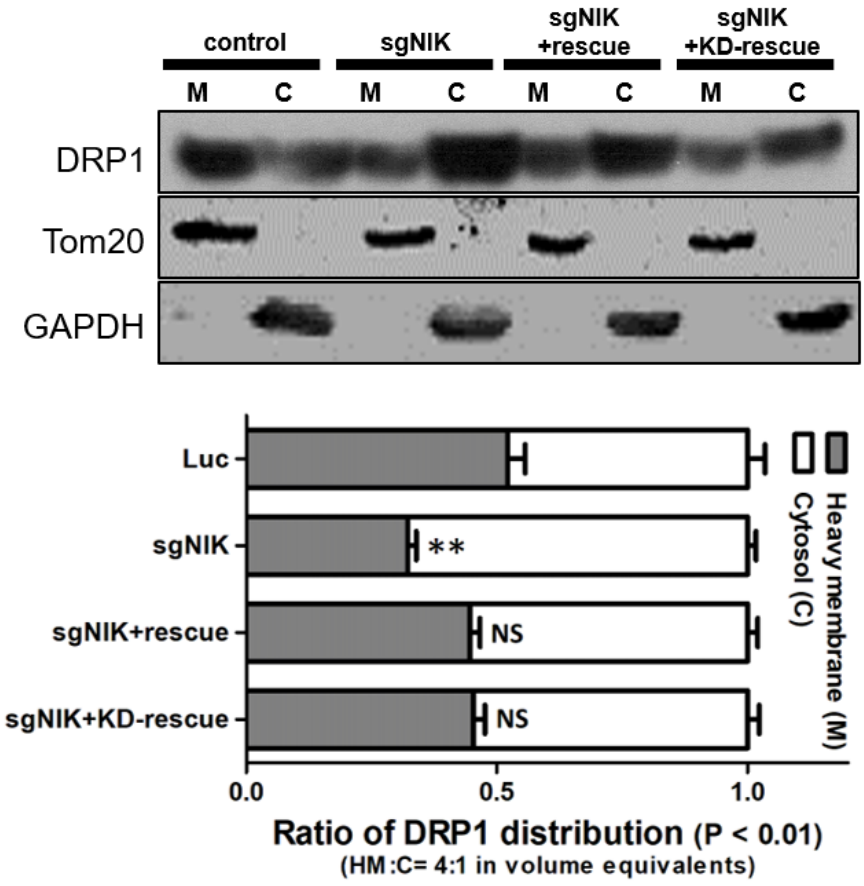

Figure 66. Kinase activity of NIK is not required for Drp1 mitochondrial recruitment. Immunoblot analysis of mitochondrial-enriched (M) and cytosolic (C) fractions prepared from BT25 control, BT25-sgNIK, BT25-sgNIK+rescue and BT25-sgNIK+KD-rescue cells was performed with indicated antibodies. Results are representative of 4 separate experiments. Bar graph shows quantification of the ratio of Drp1 in cytosolic and mitochondria-enriched fractions. Mean ± SD. ** $p<0.01$ for control vs. sgNIK; NS (not significant) for control vs. sgNIK+rescue and control vs. sgNIK+KD-rescue, one-way ANOVA.

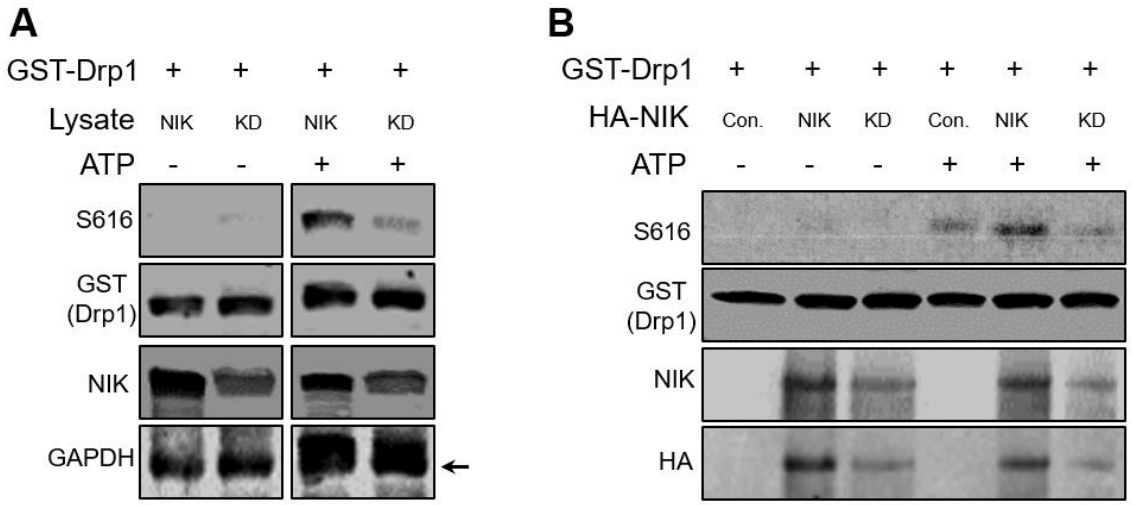

Figure 67. NIK phosphorylates Drp1 in vitro. 293T cells were transfected with HA-NIK wild-type (WT) or kinase-dead mutant $^{K429A/K430A}$ (KD) expression vectors. Cell lysates were immunoprecipitated with anti-HA antibody, and the whole cell lysates (A) or immunocomplexes (B) as a source of kinase were subjected to the in vitro kinase assay with GST-Drp1 in the absence or presence of 20μM ATP for 15 min at 37 °C. Blots were probed with the indicated antibodies.

CHAPTER V

CONCLUSIONS AND FUTURE DIRECTIONS*

5.1 NIK promotes tumor cell invasion by regulating mitochondrial dynamics

The present study establishes several novel features of NIK in cancer cells. We identify a previously unrecognized pool of NIK protein in mitochondria and demonstrate that NIK regulates Drp1 activity and distribution to control mitochondria dynamics, and ultimately, cancer cell morphology and invasiveness. Moreover, these functions and localization of NIK in mitochondria do not require the known NIK targets IKKα and IKKβ, and hence, are very likely independent of NF-κB signaling.

Based on biochemical cell fractionation and immunofluorescence staining experiments, we propose that NIK exists in at least two protein pools: a proteasome-associated cytosolic pool primarily mediating IKK/NF-κB signaling and a mitochondrial pool regulating Drp1 recruitment and mitochondrial dynamics (Fig. 68). The discovery of a discrete mitochondria-associated fraction of NIK was unexpected, given that NIK has been described primarily as cytosolic protein that is constitutively degraded in the absence of stimuli (Sun, 2012). Indeed, this property renders endogenous NIK difficult to detect by immunoblot under basal conditions and in the absence of proteasome inhibition (Fig. 12D and 39B). Regardless, distinct NIK immunostaining is observed in mitochondria, even under unstimulated conditions in different cancer cell lines, as

*Part of this chapter is reprinted with permission from "NIK/MAP3K14 Regulates Mitochondrial Dynamics and Trafficking to Promote Cell Invasion." By Jung JU, Ravi S, Lee DW, McFadden K, Kamradt ML, Toussaint LG, Sitcheran R, 2016. Current Biology, 26, 3288-3302, Copyright 2016 by Elsevier Ltd.

well as immortalized MEFs. NIK mitochondrial localization was observed in MEFs and all cancer cells examined using two different antibodies (Fig. 10), and their specificity was verified by loss of signal in NIK knockout cells. Most importantly, both the mitochondrial defects and NIK mitochondrial localization in NIK knockout cells were rescued by expression of mNIK. We surmise that the discrepancy between immunoblot analysis, which detects both cytosolic and mitochondrial NIK, and immunofluorescence, may be due to differences in the ability of the antibodies to interact with the NIK epitope in its native confirmation in different cellular compartments. For example, factors present in the cytosol, but absent in mitochondria, might associate with NIK and either alter its conformation or sequester its epitope, thereby preventing interaction between the antibody and NIK. In support of this interpretation, one Drp1-specific antibody also recognizes only mitochondria-associated, but not cytosolic, Drp1 (Fig. 24). Alternatively, the majority of soluble, cytosolic NIK may be lost during the immunostaining procedure. NIK detection in the mitochondria by immunofluorescence may also be enhanced by its oligomerization at this site. Similar to Drp1, whose oligomerization is critical for its fission-promoting activity (Ji et al., 2015), NIK is capable of forming homotypic oligomers (Lin et al., 1998), for which a biological function has not yet been established. While our studies have unambiguously identified a pool of NIK in mitochondria, we can not rule out the possibility that some NIK protein may localize with other organelles, such as peroxisomes, the ER, the mitochondria-associated membrane (MAM) (Schrader et al., 2015) or mitochondrial-derived vesicles (MDV) (Sugiura et al., 2014). In this context, we note that a relatively small fraction of NIK was reported to co-localize with Rab5+ endosomes in human endothelial cells (Jane-wit et al., 2015). However, in cancer cells, NIK does not co-localize with Rab5 (Fig. 11), or ER

markers (Fig. 10A and 11A). Thus, it is possible that NIK has distinct roles and subcellular localizations in different cell types.

Because NIK lacks a mitochondrial targeting sequence (MTS), it is likely recruited to, and retained in, the mitochondria through interactions with a protein containing an MTS (Omura, 1998). Potential candidates include the mitochondrial Hsp90, which is not only a known chaperone of NIK (Qing et al., 2007), but was also found to deliver proteins to mitochondrial import receptors (Fan et al., 2006; Young et al., 2003). Alternatively, mitochondrial localization of NIK may involve localized, co-translational mitochondrial import (Lesnik et al., 2015), which would potentially facilitate its protection from being immediately ubiquitinated and degraded. Localization of NIK to mitochondria, its presence in a complex with Drp1, and its regulatory role in Drp1 activity and mitochondrial localization suggests that NIK functions as a novel fission "sensor". Thus, it will be interesting to determine whether the association of NIK with mitochondria is dynamic, and possibly induced by specific signals known to promote fission (Frank et al., 2001; Taguchi et al., 2007; Wang et al., 2012; Willems et al., 2015).

Our imaging studies have identified a role for NIK in regulating the velocity and anterograde movement of mitochondria towards the periphery of migrating cells, suggesting that increased fission, mitochondrial motility and cell invasion are functionally linked. This hypothesis is supported by the striking phenotype of diverse cancer cells and MEFs lacking NIK, which exhibit less fragmented mitochondria that are concentrated in the perinuclear region (Fig. 8B, 14A, 15A, 16B, 19B, 36A, 43A, 44A). It remains to be investigated whether NIK may regulate the motor proteins on the mitochondrial surface, such as kinesin and Miro (Wang and Schwarz, 2009). Additionally, in light of recent findings demonstrating a critical role for ER-associated actin in regulating mitochondrial fission (Friedman et al., 2011; Ji et al., 2015), future

studies are necessary to address whether NIK is involved in establishing contacts between mitochondria and the ER at sites of fission, or regulating calcium flux, which was recently demonstrated to be required for cancer cell migration (Tosatto et al., 2016).

The recruitment of Drp1 to mitochondria is mediated by several mitochondrial outer membrane proteins including mitochondrial fission factors Mff and Fis1 (Loson et al., 2013; Otera et al., 2010; Yamada et al., 2016). *Mff*-null and *Fis1*-null cells appear interconnected, yet elongated (Liu and Chan, 2015), while mitochondria in cells lacking NIK appear tangled and collapsed within the perinuclear region, similar to *Drp1*-null cells (Fig. 8B and 35B). We also note the presence of circularized mitochondria in glioma cells lacking NIK (Fig. 19B), which is indicative of mitochondrial damage and stress (Ahmad et al., 2013). These results suggest that NIK may regulate other mitochondrial functions, and indeed, we have observed that loss of NIK decreases ROS and oxygen consumption, similar to cells lacking Drp1 (Fig. 28 and 29).

Although we found that NIK forms a complex with Drp1 and affects Drp1 phosphorylation (Fig. 27 and 32), it remains unclear exactly how NIK mediates Drp1 phosphorylation. It was recently reported that Erk2 (also known as MAPK1) promotes tumorigenesis through phosphorylation of Drp1 S616, resulting in increased mitochondrial fission activity (Kashatus et al., 2015). Thus, it's possible that NIK as a serine/threonine protein kinase may regulate Drp1 phosphorylation directly through its interaction or indirectly through its ability to phosphorylate Erk (Nemoto et al., 1998). Additionally, the increase of Drp1-P637 observed in BT25-sgNIK cells suggests that NIK may regulate a phosphatase that dephosphorylates Drp1. Indeed, a recent study of the NIK interactome identified several mitochondrial membrane proteins, including PGAM5, a Drp1-P637 phosphatase (Willmann et al., 2016). Alternatively, NIK may regulate Drp1 at other steps, such as oligomeric maturation (Ji

et al., 2015), or GTP hydrolysis (Francy et al., 2015). Future studies are needed to clarify these molecular mechanisms.

Lastly, we propose that NIK's function in mitochondria is independent of IKK/NF-κB signaling because it supports an expansive mitochondria network, promotes Drp1 mitochondrial recruitment and enhances invasive potential in the absence of IKKα or IKKβ (Fig. 38, 40, and 42). To our knowledge, this is the first report of IKK-independent functions for NIK in cancer. However, our data do not exclude the possibility that other mitochondrial functions of NIK may involve regulation by the IKK/NF-κB axis, particularly in light of previous studies identifying other NF-κB proteins localized to mitochondria (Cogswell et al., 2003), NF-κB-dependent control of mitochondrial biogenesis (Bakkar et al., 2012; Zeng et al., 2015), IKKα-dependent regulation of the fusion protein Opa1 (Laforge et al., 2016), and NIK-IKKα association with mitochondrial antiviral signaling (MAVS) in response to viral infection (Liu et al., 2008). In this study, we have uncovered new roles for NIK in regulating mitochondrial dynamics and tumor cell invasion independently of IKK/NF-κB, highlighting the emerging importance of NIK signaling in cancer.

5.2 NIK regulates Drp1 phosphorylation and is recruited to mitochondria constriction sites

In chapter IV, we investigated the molecular mechanism by which NIK regulates mitochondria fission and tumor growth. We found first that kinase deficiency mutation of NIK ($mNIK^{K431A/K432A}$) in patient-derived glioma cells decreased the mitochondria fission as well as NIK-deficient cells. Second, the kinase-dead mutant NIK was unable to rescue the tumorigenic phenotypes of NIK, which promote invasion into three-dimensional collagen I matrices and

xenograft tumor growth of glioma cells, compared with wild-type NIK. Third, NIK interacted with Drp1 predominantly in mitochondria constriction sites, where NIK may regulate Drp1 phosphorylation and thus promoting mitochondria fission.

Abolishment of non-canonical NF-κB activation in reconstitution of $mNIK^{K431A/K432A}$ in NIK-deficient glioma cells (BT25-sgNIK+KD-rescue cells) was remarkably similar to that of loss of function model derived by NIK knock-out (BT25-sgNIK cell) (Fig. 48A), supporting the view for NIK as a critical kinase in the non-canonical NF-κB pathway (de Leon-Boenig et al., 2012; Luftig et al., 2001). The mitochondria morphology in BT25-sgNIK+KD-rescue cells also resembles hyperfused mitochondria features of BT25-sgNIK cells, which appeared more tangled and fused within the perinuclear region (Fig. 48B). Intriguingly, NIK was successfully colocalized with mitochondria marker and detected in the mitochondrial fraction, regardless its kinase activity (Fig. 48 and 49). However, NIK kinase-dead mutant failed to restore normal mitochondria morphology in BT25-sgNIK, while wild-type NIK was able to re-establish that increase in number and decrease in size of mitochondria, compare to BT25-sgNIK and BT25-sgNIK+KD-rescue cells (Fig. 51). These observations suggest that NIK regulates mitochondria fission of glioma cells through its kinase activity resided in mitochondria.

In addition to aberrant mitochondrial dynamics, the BT25-sgNIK+KD-rescue cells display loss of tumorigenic phenotypes that were observed in BT25 control and BT25-sgNIK+rescue cells. We previously observed a reduced invasive potential in NIK-deficient glioma cells, by contrast, overexpression of NIK increased glioma cell invasion (Cherry et al., 2015; Duran et al., 2016). The invasion ability of glioma cells was significantly diminished in BT25-sgNIK+KD-rescue cells, but not BT25-sgNIK+rescue cells, suggesting that loss of NIK kinase activity contributes to this deficit (Fig. 50). Therefore, similar results observed in BT25-

sgNIK cells that may be caused fundamentally by absence of serine/threonine protein kinase function of NIK (Fig. 50).

Previously, studies have demonstrated that targeting Drp1 using genetic or pharmacological inhibition constrained tumorigenesis of glioma, melanoma, and breast cancer (Wieder et al., 2015; Xie et al., 2015; Zhao et al., 2013). Similar results were also observed in BT25-sgNIK cells (Fig. 52). Nevertheless, the biological significance of NIK kinase activity in regulation of tumor progression is poorly understood. Interestingly, the kinase-dead mutant of NIK resulted in significant reduction of tumor volume in a glioma xenograft model in mice compared with BT25-sgNIK cells expressing wild-type NIK, indicating that loss of NIK kinase activity is accompanied by a reduced intracranial tumorigenesis in vivo (Fig. 53 and 54). However, these results do not exclude IKK/NF-κB axis's contribution in tumorigenic features including invasion and growth of tumor. In fact, non-canonical NF-κB pathway including IKKα and RelB have been shown to contribute to development of tumors (Cao et al., 2007; Wang et al., 2016). Considering the previous observation that overexpression of NIK in cells lacking IKKα and IKKβ, key downstream targets of NIK, increased mitochondria fission and cell invasion (Fig. 40 and 43), kinase activity of NIK must be at least necessary not only for activation of NF-κB signaling, but also for additional factors involved in these events to promote malignancy. We thus propose that kinase activity of NIK is required for tumorigenesis in glioma cells.

Intriguingly, NIK is accumulated to mitochondria constriction sites prior to division event, strongly suggesting a potential involvement of NIK in mitochondria fission (Fig. 56 and 61). The fission event requires the function of Drp1, which is translocated from the cytosol to the pre-determined sites on mitochondria that subsequently generates the mechanical force to

promote membrane scission (Otera et al., 2013; Smirnova et al., 2001). Indeed, live cell imaging revealed that Drp1 and NIK puncta were recruited and accumulated transiently at constriction site (Fig. 60 and 62), particularly NIK is recruited to the pre-determined sites, which is followed by subsequent Drp1 undergoes mitochondrial recruitment and transiently colocalized to NIK within the constriction sites (Fig. 60). This result is supported by biochemical cell fractionation and in situ PLA experiments that NIK enhances mitochondrial recruitment of Drp1 and the NIK-Drp1 interactions are predominantly localized in mitochondria (Fig. 25 and 57), whereas NIK does not bind to Drp1-related mitochondrial dynamic regulators and MIM protein (Fig. 33). We also speculate that NIK might be required for Drp1-independent initial constriction events, because NIK undergoes mitochondrial recruitment prior to recruitment of Drp1 (hollow arrows in Fig. 60). This view is in line with some studies that Drp1 recruitment and mitochondrial constriction are distinct processes (Legesse-Miller et al., 2003), and inverted formin-2 (INF2) on the ER membrane drives initial constriction of mitochondria through promoting actin polymerization (Friedman et al., 2011; Korobova et al., 2013). The actin polymerization promotes myosin II recruitment and constriction, resulting in Drp1 accumulation and fission (Korobova et al., 2014). Therefore, as suggested by the previous chapter, further investigations are necessary to address the possible hypothesis that NIK may regulate ER-associated actin in driving constriction.

To date, many studies have been identified multiple serine/threonine protein kinases such as PKA, CDK, and Erk2 for Drp1 phosphorylation (Chang and Blackstone, 2007a; Cho et al., 2014; Cribbs and Strack, 2007; Prieto et al., 2016; Strack et al., 2013). Phosphorylation at Ser616 of Drp1 has been implicated in promoting mitochondrial fission and tumor growth (Kashatus et al., 2015). In this study, we observed a marked decrease in phosphorylation at S616

in glioma cells lacking NIK (BT25-sgNIK) or expressing NIK kinase-dead mutant (BT25-sgNIK+KD-rescue) (Fig. 63 and 64). Unexpectedly, the results obtained from two different analyses showed the different quantitative patterns of phosphorylation of Drp1-S616 that puncta of Drp1-S616 phosphorylation in immunofluorescence staining were largely localized in mitochondria, while high levels of the phosphorylated protein were detected in cytosolic fractions by biochemical fractionation analysis (Fig. 63 and 64). These differences are likely related to a transient recruitment of Drp1, which probably bind transiently to the MOM (Otera et al., 2010; Otsuga et al., 1998; Smirnova et al., 1998). Consequently, mitochondrial phosphorylated Drp1 may be unstable after mitochondria fission events and may easily lose its association with the mitochondria. NIK-mediated Drp1 activation is also confirmed by in vitro kinase assay using the purified Drp1 as a substrate, showing that the purified protein is phosphorylated at serine 616 by wild-type NIK, but not by kinase-dead mutant NIK (Fig. 67). Importantly, the kinase-dead NIK protein can still associate with Drp1 (Fig. 59), thus excluding the possibility that its incapability to regulate phosphorylation of S616 is due to lack of association with Drp1. We therefore propose that the kinase activity of NIK is responsible for phosphorylation of Drp1-S616.

In light of these observations, we suggest that NIK-Drp1 interaction may result in enrichment of active Drp1 in mitochondrial constriction sites and influence mitochondria dynamics to promote tumorigenic potential of glioma. So, it would be interesting in future studies to investigate which domain or motif in NIK interacts with Drp1 and how the interaction is regulated for mitochondria dynamics.

In conclusion, my dissertation studies demonstrate the novel mechanisms of NIK-mediated tumor progression. We propose a working model that NIK kinase activity in glioma

cells is required for tumorigenesis through regulating phosphorylation of Drp1, which activates mitochondrial fission (Fig. 68B). These findings may help to explain the complexity of NIK behavior in promoting tumor progression and establish therapeutic interventions to malignant tumors.

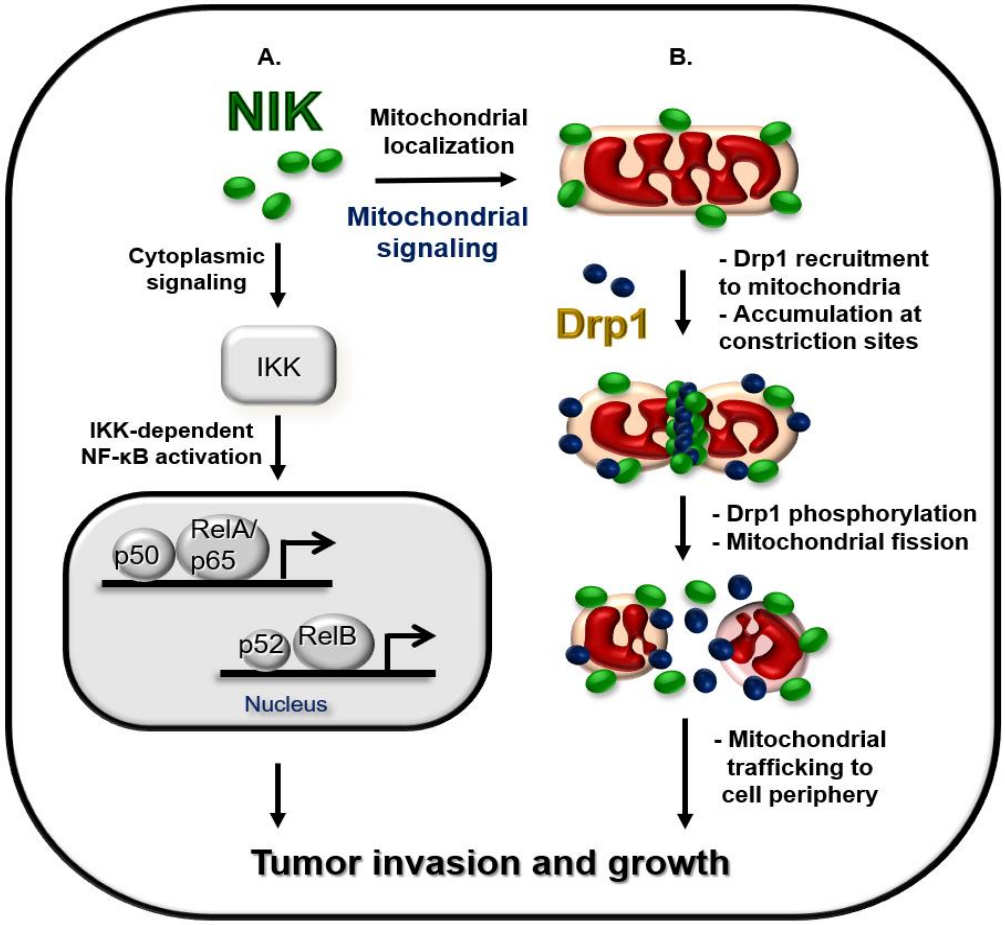

Figure 68. Model depicting NIK function in mitochondria. Model depicts two distinct pools of NIK protein that regulate IKK-dependent NF-κB signaling and IKK-independent mitochondrial dynamics. (A) Cytosolic NIK is constitutively degraded in resting cells, while signal-induced stabilization regulates downstream IKK complexes to activate NF-κB signaling. (B) NIK is localized to mitochondria and regulates Drp1 phosphorylation and recruitment to mitochondria constriction sites, resulting in increased mitochondrial fission, motility and distribution throughout the cell, as well as enhanced tumorigenesis, in a manner that is independent of IKK/NF-κB signaling.

REFERENCES

Aggarwal, B.B. (2004). Nuclear factor-kappaB: the enemy within. Cancer Cell *6*, 203-208.

Ahmad, T., Aggarwal, K., Pattnaik, B., Mukherjee, S., Sethi, T., Tiwari, B.K., Kumar, M., Micheal, A., Mabalirajan, U., Ghosh, B., *et al.* (2013). Computational classification of mitochondrial shapes reflects stress and redox state. Cell Death Dis *4*, e461.

Annunziata, C.M., Davis, R.E., Demchenko, Y., Bellamy, W., Gabrea, A., Zhan, F., Lenz, G., Hanamura, I., Wright, G., Xiao, W., *et al.* (2007). Frequent engagement of the classical and alternative NF-kappaB pathways by diverse genetic abnormalities in multiple myeloma. Cancer Cell *12*, 115-130.

Arismendi-Morillo, G. (2009). Electron microscopy morphology of the mitochondrial network in human cancer. Int J Biochem Cell Biol *41*, 2062-2068.

Attanasio, F., Caldieri, G., Giacchetti, G., van Horssen, R., Wieringa, B., and Buccione, R. (2011). Novel invadopodia components revealed by differential proteomic analysis. Eur J Cell Biol *90*, 115-127.

Bakkar, N., Ladner, K., Canan, B.D., Liyanarachchi, S., Bal, N.C., Pant, M., Periasamy, M., Li, Q., Janssen, P.M., and Guttridge, D.C. (2012). IKKalpha and alternative NF-kappaB regulate PGC-1beta to promote oxidative muscle metabolism. J Cell Biol *196*, 497-511.

Baldwin, A.S., Jr. (1996). The NF-kappa B and I kappa B proteins: new discoveries and insights. Annu Rev Immunol *14*, 649-683.

Ben-Neriah, Y., and Karin, M. (2011). Inflammation meets cancer, with NF-kappaB as the matchmaker. Nat Immunol *12*, 715-723.

Benard, G., Bellance, N., Jose, C., Melser, S., Nouette-Gaulain, K., and Rossignol, R. (2010). Multi-site control and regulation of mitochondrial energy production. Biochim Biophys Acta *1797*, 698-709.

Bennett, L., Quinn, J., McCall, P., Mallon, E.A., Horgan, P.G., McMillan, D.C., Paul, A., and Edwards, J. (2017). High IKKalpha expression is associated with reduced time to recurrence and cancer specific survival in oestrogen receptor (ER)-positive breast cancer. Int J Cancer *140*, 1633-1644.

Betts, J.C., and Nabel, G.J. (1996). Differential regulation of NF-kappaB2(p100) processing and control by amino-terminal sequences. Mol Cell Biol *16*, 6363-6371.

Bhargava, P., and Schnellmann, R.G. (2017). Mitochondrial energetics in the kidney. Nat Rev Nephrol *13*, 629-646.

Boland, M.L., Chourasia, A.H., and Macleod, K.F. (2013). Mitochondrial dysfunction in cancer. Front Oncol *3*, 292.

Caino, M.C., and Altieri, D.C. (2015). Cancer cells exploit adaptive mitochondrial dynamics to increase tumor cell invasion. Cell Cycle *14*, 3242-3247.

Calderwood, S.K. (2013). Tumor heterogeneity, clonal evolution, and therapy resistance: an opportunity for multitargeting therapy. Discov Med *15*, 188-194.

Cao, Y., Luo, J.L., and Karin, M. (2007). IkappaB kinase alpha kinase activity is required for self-renewal of ErbB2/Her2-transformed mammary tumor-initiating cells. Proc Natl Acad Sci U S A *104*, 15852-15857.

Cereghetti, G.M., Stangherlin, A., Martins de Brito, O., Chang, C.R., Blackstone, C., Bernardi, P., and Scorrano, L. (2008). Dephosphorylation by calcineurin regulates translocation of Drp1 to mitochondria. Proc Natl Acad Sci U S A *105*, 15803-15808.

Chan, D.C. (2006). Mitochondrial fusion and fission in mammals. Annu Rev Cell Dev Biol *22*, 79-99.

Chang, C.R., and Blackstone, C. (2007a). Cyclic AMP-dependent protein kinase phosphorylation of Drp1 regulates its GTPase activity and mitochondrial morphology. J Biol Chem *282*, 21583-21587.

Chang, C.R., and Blackstone, C. (2007b). Drp1 phosphorylation and mitochondrial regulation. EMBO Rep *8*, 1088-1089; author reply 1089-1090.

Chang, C.R., and Blackstone, C. (2010). Dynamic regulation of mitochondrial fission through modification of the dynamin-related protein Drp1. Ann N Y Acad Sci *1201*, 34-39.

Cherry, E.M., Lee, D.W., Jung, J.U., and Sitcheran, R. (2015). Tumor necrosis factor-like weak inducer of apoptosis (TWEAK) promotes glioma cell invasion through induction of NF-kappaB-inducing kinase (NIK) and noncanonical NF-kappaB signaling. Mol Cancer *14*, 9.

Cho, B., Cho, H.M., Kim, H.J., Jeong, J., Park, S.K., Hwang, E.M., Park, J.Y., Kim, W.R., Kim, H., and Sun, W. (2014). CDK5-dependent inhibitory phosphorylation of Drp1 during neuronal maturation. Exp Mol Med *46*, e105.

Cogswell, P.C., Guttridge, D.C., Funkhouser, W.K., and Baldwin, A.S., Jr. (2000). Selective activation of NF-kappa B subunits in human breast cancer: potential roles for NF-kappa B2/p52 and for Bcl-3. Oncogene *19*, 1123-1131.

Cogswell, P.C., Kashatus, D.F., Keifer, J.A., Guttridge, D.C., Reuther, J.Y., Bristow, C., Roy, S., Nicholson, D.W., and Baldwin, A.S., Jr. (2003). NF-kappa B and I kappa B alpha are found in the mitochondria. Evidence for regulation of mitochondrial gene expression by NF-kappa B. J Biol Chem *278*, 2963-2968.

Cribbs, J.T., and Strack, S. (2007). Reversible phosphorylation of Drp1 by cyclic AMP-dependent protein kinase and calcineurin regulates mitochondrial fission and cell death. EMBO Rep *8*, 939-944.

Dagda, R.K., Cherra, S.J., 3rd, Kulich, S.M., Tandon, A., Park, D., and Chu, C.T. (2009). Loss of PINK1 function promotes mitophagy through effects on oxidative stress and mitochondrial fission. J Biol Chem *284*, 13843-13855.

de Leon-Boenig, G., Bowman, K.K., Feng, J.A., Crawford, T., Everett, C., Franke, Y., Oh, A., Stanley, M., Staben, S.T., Starovasnik, M.A., *et al.* (2012). The crystal structure of the catalytic domain of the NF-kappaB inducing kinase reveals a narrow but flexible active site. Structure *20*, 1704-1714.

Desai, S.P., Bhatia, S.N., Toner, M., and Irimia, D. (2013). Mitochondrial localization and the persistent migration of epithelial cancer cells. Biophys J *104*, 2077-2088.

Dolfi, S.C., Chan, L.L., Qiu, J., Tedeschi, P.M., Bertino, J.R., Hirshfield, K.M., Oltvai, Z.N., and Vazquez, A. (2013). The metabolic demands of cancer cells are coupled to their size and protein synthesis rates. Cancer Metab *1*, 20.

Doppler, H., Liou, G.Y., and Storz, P. (2013). Downregulation of TRAF2 mediates NIK-induced pancreatic cancer cell proliferation and tumorigenicity. PLoS One *8*, e53676.

Duran, C.L., Lee, D.W., Jung, J.U., Ravi, S., Pogue, C.B., Toussaint, L.G., Bayless, K.J., and Sitcheran, R. (2016). NIK regulates MT1-MMP activity and promotes glioma cell invasion independently of the canonical NF-kappaB pathway. Oncogenesis *5*, e231.

Elgass, K., Pakay, J., Ryan, M.T., and Palmer, C.S. (2013). Recent advances into the understanding of mitochondrial fission. Biochim Biophys Acta *1833*, 150-161.

Enzler, T., Bonizzi, G., Silverman, G.J., Otero, D.C., Widhopf, G.F., Anzelon-Mills, A., Rickert, R.C., and Karin, M. (2006). Alternative and classical NF-kappa B signaling retain autoreactive B cells in the splenic marginal zone and result in lupus-like disease. Immunity *25*, 403-415.

Fagarasan, S., Shinkura, R., Kamata, T., Nogaki, F., Ikuta, K., Tashiro, K., and Honjo, T. (2000). Alymphoplasia (aly)-type nuclear factor kappaB-inducing kinase (NIK) causes defects in secondary lymphoid tissue chemokine receptor signaling and homing of peritoneal cells to the gut-associated lymphatic tissue system. J Exp Med *191*, 1477-1486.

Fan, A.C., Bhangoo, M.K., and Young, J.C. (2006). Hsp90 functions in the targeting and outer membrane translocation steps of Tom70-mediated mitochondrial import. J Biol Chem *281*, 33313-33324.

Fan, C.M., and Maniatis, T. (1991). Generation of p50 subunit of NF-kappa B by processing of p105 through an ATP-dependent pathway. Nature *354*, 395-398.

Ferreira-da-Silva, A., Valacca, C., Rios, E., Populo, H., Soares, P., Sobrinho-Simoes, M., Scorrano, L., Maximo, V., and Campello, S. (2015). Mitochondrial dynamics protein Drp1 is

overexpressed in oncocytic thyroid tumors and regulates cancer cell migration. PLoS One *10*, e0122308.

Francy, C.A., Alvarez, F.J., Zhou, L., Ramachandran, R., and Mears, J.A. (2015). The mechanoenzymatic core of dynamin-related protein 1 comprises the minimal machinery required for membrane constriction. J Biol Chem *290*, 11692-11703.

Frank, S., Gaume, B., Bergmann-Leitner, E.S., Leitner, W.W., Robert, E.G., Catez, F., Smith, C.L., and Youle, R.J. (2001). The role of dynamin-related protein 1, a mediator of mitochondrial fission, in apoptosis. Dev Cell *1*, 515-525.

Fredriksson, S., Gullberg, M., Jarvius, J., Olsson, C., Pietras, K., Gustafsdottir, S.M., Ostman, A., and Landegren, U. (2002). Protein detection using proximity-dependent DNA ligation assays. Nat Biotechnol *20*, 473-477.

Friedman, J.R., Lackner, L.L., West, M., DiBenedetto, J.R., Nunnari, J., and Voeltz, G.K. (2011). ER tubules mark sites of mitochondrial division. Science *334*, 358-362.

Fukuyama, R., Ng, K.P., Cicek, M., Kelleher, C., Niculaita, R., Casey, G., and Sizemore, N. (2007). Role of IKK and oscillatory NFkappaB kinetics in MMP-9 gene expression and chemoresistance to 5-fluorouracil in RKO colorectal cancer cells. Mol Carcinog *46*, 402-413.

Galluzzi, L., Larochette, N., Zamzami, N., and Kroemer, G. (2006). Mitochondria as therapeutic targets for cancer chemotherapy. Oncogene *25*, 4812-4830.

Ge, Q.L., Liu, S.H., Ai, Z.H., Tao, M.F., Ma, L., Wen, S.Y., Dai, M., Liu, F., Liu, H.S., Jiang, R.Z., *et al.* (2016). RelB/NF-kappaB links cell cycle transition and apoptosis to endometrioid adenocarcinoma tumorigenesis. Cell Death Dis *7*, e2402.

Ghosh, S., May, M.J., and Kopp, E.B. (1998). NF-kappa B and Rel proteins: evolutionarily conserved mediators of immune responses. Annu Rev Immunol *16*, 225-260.

Grandemange, S., Herzig, S., and Martinou, J.C. (2009). Mitochondrial dynamics and cancer. Semin Cancer Biol *19*, 50-56.

Grupp, K., Jedrzejewska, K., Tsourlakis, M.C., Koop, C., Wilczak, W., Adam, M., Quaas, A., Sauter, G., Simon, R., Izbicki, J.R., *et al.* (2013). High mitochondria content is associated with prostate cancer disease progression. Mol Cancer *12*, 145.

Guertin, D.A., and Sabatini, D.M. (2007). Defining the role of mTOR in cancer. Cancer Cell *12*, 9-22.

Hacker, H., Chi, L., Rehg, J.E., and Redecke, V. (2012). NIK prevents the development of hypereosinophilic syndrome-like disease in mice independent of IKKalpha activation. J Immunol *188*, 4602-4610.

Hahn, M., Macht, A., Waisman, A., and Hovelmeyer, N. (2016). NF-kappaB-inducing kinase is essential for B-cell maintenance in mice. Eur J Immunol *46*, 732-741.

Hayden, M.S., and Ghosh, S. (2012). NF-kappaB, the first quarter-century: remarkable progress and outstanding questions. Genes Dev *26*, 203-234.

Heusch, M., Lin, L., Geleziunas, R., and Greene, W.C. (1999). The generation of nfkb2 p52: mechanism and efficiency. Oncogene *18*, 6201-6208.

Hu, C., Huang, Y., and Li, L. (2017). Drp1-Dependent Mitochondrial Fission Plays Critical Roles in Physiological and Pathological Progresses in Mammals. Int J Mol Sci *18*.

Inoue-Yamauchi, A., and Oda, H. (2012). Depletion of mitochondrial fission factor DRP1 causes increased apoptosis in human colon cancer cells. Biochem Biophys Res Commun *421*, 81-85.

Jahani-Asl, A., and Slack, R.S. (2007). The phosphorylation state of Drp1 determines cell fate. EMBO Rep *8*, 912-913.

Jane-wit, D., Surovtseva, Y.V., Qin, L., Li, G., Liu, R., Clark, P., Manes, T.D., Wang, C., Kashgarian, M., Kirkiles-Smith, N.C., *et al.* (2015). Complement membrane attack complexes activate noncanonical NF-kappaB by forming an Akt+ NIK+ signalosome on Rab5+ endosomes. Proc Natl Acad Sci U S A *112*, 9686-9691.

Ji, W.K., Hatch, A.L., Merrill, R.A., Strack, S., and Higgs, H.N. (2015). Actin filaments target the oligomeric maturation of the dynamin GTPase Drp1 to mitochondrial fission sites. Elife *4*, e11553.

Johnson, R.F., Witzel, II, and Perkins, N.D. (2011). p53-dependent regulation of mitochondrial energy production by the RelA subunit of NF-kappaB. Cancer Res *71*, 5588-5597.

Jost, P.J., and Ruland, J. (2007). Aberrant NF-kappaB signaling in lymphoma: mechanisms, consequences, and therapeutic implications. Blood *109*, 2700-2707.

Kageyama, Y., Zhang, Z., Roda, R., Fukaya, M., Wakabayashi, J., Wakabayashi, N., Kensler, T.W., Reddy, P.H., Iijima, M., and Sesaki, H. (2012). Mitochondrial division ensures the survival of postmitotic neurons by suppressing oxidative damage. J Cell Biol *197*, 535-551.

Kajiura, F., Sun, S., Nomura, T., Izumi, K., Ueno, T., Bando, Y., Kuroda, N., Han, H., Li, Y., Matsushima, A., *et al.* (2004). NF-kappa B-inducing kinase establishes self-tolerance in a thymic stroma-dependent manner. J Immunol *172*, 2067-2075.

Karbowski, M., Cleland, M.M., and Roelofs, B.A. (2014). Photoactivatable green fluorescent protein-based visualization and quantification of mitochondrial fusion and mitochondrial network complexity in living cells. Methods Enzymol *547*, 57-73.

Karin, M. (2006). Nuclear factor-kappaB in cancer development and progression. Nature *441*, 431-436.

Kashatus, D.F., Lim, K.H., Brady, D.C., Pershing, N.L., Cox, A.D., and Counter, C.M. (2011). RALA and RALBP1 regulate mitochondrial fission at mitosis. Nat Cell Biol *13*, 1108-1115.

Kashatus, J.A., Nascimento, A., Myers, L.J., Sher, A., Byrne, F.L., Hoehn, K.L., Counter, C.M., and Kashatus, D.F. (2015). Erk2 phosphorylation of Drp1 promotes mitochondrial fission and MAPK-driven tumor growth. Mol Cell *57*, 537-551.

Keats, J.J., Fonseca, R., Chesi, M., Schop, R., Baker, A., Chng, W.J., Van Wier, S., Tiedemann, R., Shi, C.X., Sebag, M., *et al.* (2007). Promiscuous mutations activate the noncanonical NF-kappaB pathway in multiple myeloma. Cancer Cell *12*, 131-144.

Kelly, J.J., Stechishin, O., Chojnacki, A., Lun, X., Sun, B., Senger, D.L., Forsyth, P., Auer, R.N., Dunn, J.F., Cairncross, J.G., *et al.* (2009). Proliferation of human glioblastoma stem cells occurs independently of exogenous mitogens. Stem Cells *27*, 1722-1733.

Khacho, M., Clark, A., Svoboda, D.S., Azzi, J., MacLaurin, J.G., Meghaizel, C., Sesaki, H., Lagace, D.C., Germain, M., Harper, M.E., *et al.* (2016). Mitochondrial Dynamics Impacts Stem Cell Identity and Fate Decisions by Regulating a Nuclear Transcriptional Program. Cell Stem Cell *19*, 232-247.

Kilgore, J.A., Dolman, N.J., and Davidson, M.W. (2013). A review of reagents for fluorescence microscopy of cellular compartments and structures, Part II: reagents for non-vesicular organelles. Curr Protoc Cytom *66*, Unit 12 31.

Korobova, F., Gauvin, T.J., and Higgs, H.N. (2014). A role for myosin II in mammalian mitochondrial fission. Curr Biol *24*, 409-414.

Korobova, F., Ramabhadran, V., and Higgs, H.N. (2013). An actin-dependent step in mitochondrial fission mediated by the ER-associated formin INF2. Science *339*, 464-467.

Laforge, M., Rodrigues, V., Silvestre, R., Gautier, C., Weil, R., Corti, O., and Estaquier, J. (2016). NF-kappaB pathway controls mitochondrial dynamics. Cell Death Differ *23*, 89-98.

Lawrence, M.S., Stojanov, P., Polak, P., Kryukov, G.V., Cibulskis, K., Sivachenko, A., Carter, S.L., Stewart, C., Mermel, C.H., Roberts, S.A., *et al.* (2013). Mutational heterogeneity in cancer and the search for new cancer-associated genes. Nature *499*, 214-218.

Lee, D.W., Ramakrishnan, D., Valenta, J., Parney, I.F., Bayless, K.J., and Sitcheran, R. (2013). The NF-kappaB RelB protein is an oncogenic driver of mesenchymal glioma. PLoS One *8*, e57489.

Legesse-Miller, A., Massol, R.H., and Kirchhausen, T. (2003). Constriction and Dnm1p recruitment are distinct processes in mitochondrial fission. Mol Biol Cell *14*, 1953-1963.

Lehninger, A.L. (1964). The mitochondrion; molecular basis of structure and function (New York,: W. A. Benjamin).

Lesnik, C., Golani-Armon, A., and Arava, Y. (2015). Localized translation near the mitochondrial outer membrane: An update. RNA Biol *12*, 801-809.

Li, H., Mittal, A., Paul, P.K., Kumar, M., Srivastava, D.S., Tyagi, S.C., and Kumar, A. (2009). Tumor necrosis factor-related weak inducer of apoptosis augments matrix metalloproteinase 9 (MMP-9) production in skeletal muscle through the activation of nuclear factor-kappaB-inducing kinase and p38 mitogen-activated protein kinase: a potential role of MMP-9 in myopathy. J Biol Chem *284*, 4439-4450.

Li, Q., Estepa, G., Memet, S., Israel, A., and Verma, I.M. (2000). Complete lack of NF-kappaB activity in IKK1 and IKK2 double-deficient mice: additional defect in neurulation. Genes Dev *14*, 1729-1733.

Liao, G., Zhang, M., Harhaj, E.W., and Sun, S.C. (2004). Regulation of the NF-kappaB-inducing kinase by tumor necrosis factor receptor-associated factor 3-induced degradation. J Biol Chem *279*, 26243-26250.

Liesa, M., Palacin, M., and Zorzano, A. (2009). Mitochondrial dynamics in mammalian health and disease. Physiol Rev *89*, 799-845.

Lin, X., Mu, Y., Cunningham, E.T., Jr., Marcu, K.B., Geleziunas, R., and Greene, W.C. (1998). Molecular determinants of NF-kappaB-inducing kinase action. Mol Cell Biol *18*, 5899-5907.

Ling, L., Cao, Z., and Goeddel, D.V. (1998). NF-kappaB-inducing kinase activates IKK-alpha by phosphorylation of Ser-176. Proc Natl Acad Sci U S A *95*, 3792-3797.

Liu, C.Y., Lee, C.F., Hong, C.H., and Wei, Y.H. (2004). Mitochondrial DNA mutation and depletion increase the susceptibility of human cells to apoptosis. Ann N Y Acad Sci *1011*, 133-145.

Liu, J., Sudom, A., Min, X., Cao, Z., Gao, X., Ayres, M., Lee, F., Cao, P., Johnstone, S., Plotnikova, O., *et al.* (2012). Structure of the nuclear factor kappaB-inducing kinase (NIK) kinase domain reveals a constitutively active conformation. J Biol Chem *287*, 27326-27334.

Liu, P., Li, K., Garofalo, R.P., and Brasier, A.R. (2008). Respiratory syncytial virus induces RelA release from cytoplasmic 100-kDa NF-kappa B2 complexes via a novel retinoic acid-

inducible gene-I{middle dot}NF- kappa B-inducing kinase signaling pathway. J Biol Chem *283*, 23169-23178.

Liu, R., and Chan, D.C. (2015). The mitochondrial fission receptor Mff selectively recruits oligomerized Drp1. Mol Biol Cell *26*, 4466-4477.

Longo, D.L. (2012). Tumor heterogeneity and personalized medicine. N Engl J Med *366*, 956-957.

Loson, O.C., Song, Z., Chen, H., and Chan, D.C. (2013). Fis1, Mff, MiD49, and MiD51 mediate Drp1 recruitment in mitochondrial fission. Mol Biol Cell *24*, 659-667.

Luftig, M.A., Cahir-McFarland, E., Mosialos, G., and Kieff, E. (2001). Effects of the NIK aly mutation on NF-kappaB activation by the Epstein-Barr virus latent infection membrane protein, lymphotoxin beta receptor, and CD40. J Biol Chem *276*, 14602-14606.

Margulis, L. (1970). Origin of eukaryotic cells; evidence and research implications for a theory of the origin and evolution of microbial, plant, and animal cells on the Precambrian earth (New Haven,: Yale University Press).

May, M.J., and Ghosh, S. (1998). Signal transduction through NF-kappa B. Immunol Today *19*, 80-88.

Maycotte, P., Marin-Hernandez, A., Goyri-Aguirre, M., Anaya-Ruiz, M., Reyes-Leyva, J., and Cortes-Hernandez, P. (2017). Mitochondrial dynamics and cancer. Tumour Biol *39*, 1010428317698391.

McDaniel, D.K., Eden, K., Ringel, V.M., and Allen, I.C. (2016). Emerging Roles for Noncanonical NF-kappaB Signaling in the Modulation of Inflammatory Bowel Disease Pathobiology. Inflamm Bowel Dis *22*, 2265-2279.

Mierke, C.T., Kollmannsberger, P., Zitterbart, D.P., Diez, G., Koch, T.M., Marg, S., Ziegler, W.H., Goldmann, W.H., and Fabry, B. (2010). Vinculin facilitates cell invasion into three-dimensional collagen matrices. J Biol Chem *285*, 13121-13130.

Millet, P., McCall, C., and Yoza, B. (2013). RelB: an outlier in leukocyte biology. J Leukoc Biol *94*, 941-951.

Mils, V., Bosch, S., Roy, J., Bel-Vialar, S., Belenguer, P., Pituello, F., and Miquel, M.C. (2015). Mitochondrial reshaping accompanies neural differentiation in the developing spinal cord. PLoS One *10*, e0128130.

Moynagh, P.N. (2005). The NF-kappaB pathway. J Cell Sci *118*, 4589-4592.
Nadiminty, N., Chun, J.Y., Lou, W., Lin, X., and Gao, A.C. (2008). NF-kappaB2/p52 enhances androgen-independent growth of human LNCaP cells via protection from apoptotic cell death and cell cycle arrest induced by androgen-deprivation. Prostate *68*, 1725-1733.

Natoli, G., Costanzo, A., Moretti, F., Fulco, M., Balsano, C., and Levrero, M. (1997). Tumor necrosis factor (TNF) receptor 1 signaling downstream of TNF receptor-associated factor 2. Nuclear factor kappaB (NFkappaB)-inducing kinase requirement for activation of activating protein 1 and NFkappaB but not of c-Jun N-terminal kinase/stress-activated protein kinase. J Biol Chem *272*, 26079-26082.

Nemoto, S., DiDonato, J.A., and Lin, A. (1998). Coordinate regulation of IkappaB kinases by mitogen-activated protein kinase kinase kinase 1 and NF-kappaB-inducing kinase. Mol Cell Biol *18*, 7336-7343.

Ni, H.M., Williams, J.A., and Ding, W.X. (2015). Mitochondrial dynamics and mitochondrial quality control. Redox Biol *4*, 6-13.

Odqvist, L., Sanchez-Beato, M., Montes-Moreno, S., Martin-Sanchez, E., Pajares, R., Sanchez-Verde, L., Ortiz-Romero, P.L., Rodriguez, J., Rodriguez-Pinilla, S.M., Iniesta-Martinez, F., *et al.* (2013). NIK controls classical and alternative NF-kappaB activation and is necessary for the survival of human T-cell lymphoma cells. Clin Cancer Res *19*, 2319-2330.

Oeckinghaus, A., and Ghosh, S. (2009). The NF-kappaB family of transcription factors and its regulation. Cold Spring Harb Perspect Biol *1*, a000034.

Oeckinghaus, A., Hayden, M.S., and Ghosh, S. (2011). Crosstalk in NF-kappaB signaling pathways. Nat Immunol *12*, 695-708.

Omura, T. (1998). Mitochondria-targeting sequence, a multi-role sorting sequence recognized at all steps of protein import into mitochondria. J Biochem *123*, 1010-1016.

Otera, H., Ishihara, N., and Mihara, K. (2013). New insights into the function and regulation of mitochondrial fission. Biochim Biophys Acta *1833*, 1256-1268.

Otera, H., Wang, C., Cleland, M.M., Setoguchi, K., Yokota, S., Youle, R.J., and Mihara, K. (2010). Mff is an essential factor for mitochondrial recruitment of Drp1 during mitochondrial fission in mammalian cells. J Cell Biol *191*, 1141-1158.

Otsuga, D., Keegan, B.R., Brisch, E., Thatcher, J.W., Hermann, G.J., Bleazard, W., and Shaw, J.M. (1998). The dynamin-related GTPase, Dnm1p, controls mitochondrial morphology in yeast. J Cell Biol *143*, 333-349.

Palmer, C.S., Elgass, K.D., Parton, R.G., Osellame, L.D., Stojanovski, D., and Ryan, M.T. (2013). Adaptor proteins MiD49 and MiD51 can act independently of Mff and Fis1 in Drp1 recruitment and are specific for mitochondrial fission. J Biol Chem *288*, 27584-27593.

Park, M.H., and Hong, J.T. (2016). Roles of NF-kappaB in Cancer and Inflammatory Diseases and Their Therapeutic Approaches. Cells *5*.

Perkins, N.D. (2012). The diverse and complex roles of NF-kappaB subunits in cancer. Nat Rev Cancer *12*, 121-132.

Prieto, J., Leon, M., Ponsoda, X., Sendra, R., Bort, R., Ferrer-Lorente, R., Raya, A., Lopez-Garcia, C., and Torres, J. (2016). Early ERK1/2 activation promotes DRP1-dependent mitochondrial fission necessary for cell reprogramming. Nat Commun *7*, 11124.

Qing, G., Yan, P., Qu, Z., Liu, H., and Xiao, G. (2007). Hsp90 regulates processing of NF-kappa B2 p100 involving protection of NF-kappa B-inducing kinase (NIK) from autophagy-mediated degradation. Cell Res *17*, 520-530.

Ramakrishnan, P., Wang, W., and Wallach, D. (2004). Receptor-specific signaling for both the alternative and the canonical NF-kappaB activation pathways by NF-kappaB-inducing kinase. Immunity *21*, 477-489.

Raychaudhuri, B., Han, Y., Lu, T., and Vogelbaum, M.A. (2007). Aberrant constitutive activation of nuclear factor kappaB in glioblastoma multiforme drives invasive phenotype. J Neurooncol *85*, 39-47.

Razani, B., Reichardt, A.D., and Cheng, G. (2011). Non-canonical NF-kappaB signaling activation and regulation: principles and perspectives. Immunol Rev *244*, 44-54.

Rehman, J., Zhang, H.J., Toth, P.T., Zhang, Y., Marsboom, G., Hong, Z., Salgia, R., Husain, A.N., Wietholt, C., and Archer, S.L. (2012). Inhibition of mitochondrial fission prevents cell cycle progression in lung cancer. FASEB J *26*, 2175-2186.

Saitoh, Y., Martinez Bruyn, V.J., Uota, S., Hasegawa, A., Yamamoto, N., Imoto, I., Inazawa, J., and Yamaoka, S. (2010). Overexpression of NF-kappaB inducing kinase underlies constitutive NF-kappaB activation in lung cancer cells. Lung Cancer *70*, 263-270.

Saotome, M., Safiulina, D., Szabadkai, G., Das, S., Fransson, A., Aspenstrom, P., Rizzuto, R., and Hajnoczky, G. (2008). Bidirectional Ca2+-dependent control of mitochondrial dynamics by the Miro GTPase. Proc Natl Acad Sci U S A *105*, 20728-20733.

Sasaki, Y., Calado, D.P., Derudder, E., Zhang, B., Shimizu, Y., Mackay, F., Nishikawa, S., Rajewsky, K., and Schmidt-Supprian, M. (2008). NIK overexpression amplifies, whereas ablation of its TRAF3-binding domain replaces BAFF:BAFF-R-mediated survival signals in B cells. Proc Natl Acad Sci U S A *105*, 10883-10888.

Schrader, M., Godinho, L.F., Costello, J.L., and Islinger, M. (2015). The different facets of organelle interplay-an overview of organelle interactions. Front Cell Dev Biol *3*, 56.

Sen, R., and Baltimore, D. (1986). Multiple nuclear factors interact with the immunoglobulin enhancer sequences. Cell *46*, 705-716.

Senft, D., and Ronai, Z.A. (2016). Regulators of mitochondrial dynamics in cancer. Curr Opin Cell Biol *39*, 43-52.

Senftleben, U., Cao, Y., Xiao, G., Greten, F.R., Krahn, G., Bonizzi, G., Chen, Y., Hu, Y., Fong, A., Sun, S.C., *et al.* (2001). Activation by IKKalpha of a second, evolutionary conserved, NF-kappa B signaling pathway. Science *293*, 1495-1499.

Serasinghe, M.N., Wieder, S.Y., Renault, T.T., Elkholi, R., Asciolla, J.J., Yao, J.L., Jabado, O., Hoehn, K., Kageyama, Y., Sesaki, H., *et al.* (2015). Mitochondrial division is requisite to RAS-induced transformation and targeted by oncogenic MAPK pathway inhibitors. Mol Cell *57*, 521-536.

Sheng, L., Zhou, Y., Chen, Z., Ren, D., Cho, K.W., Jiang, L., Shen, H., Sasaki, Y., and Rui, L. (2012). NF-kappaB-inducing kinase (NIK) promotes hyperglycemia and glucose intolerance in obesity by augmenting glucagon action. Nat Med *18*, 943-949.

Shih, V.F., Tsui, R., Caldwell, A., and Hoffmann, A. (2011). A single NFkappaB system for both canonical and non-canonical signaling. Cell Res *21*, 86-102.

Shinkura, R., Kitada, K., Matsuda, F., Tashiro, K., Ikuta, K., Suzuki, M., Kogishi, K., Serikawa, T., and Honjo, T. (1999). Alymphoplasia is caused by a point mutation in the mouse gene encoding Nf-kappa b-inducing kinase. Nat Genet *22*, 74-77.

Siebenlist, U., Franzoso, G., and Brown, K. (1994). Structure, regulation and function of NF-kappa B. Annu Rev Cell Biol *10*, 405-455.

Singh, K.K., Ayyasamy, V., Owens, K.M., Koul, M.S., and Vujcic, M. (2009). Mutations in mitochondrial DNA polymerase-gamma promote breast tumorigenesis. J Hum Genet *54*, 516-524.

Smirnova, E., Griparic, L., Shurland, D.L., and van der Bliek, A.M. (2001). Dynamin-related protein Drp1 is required for mitochondrial division in mammalian cells. Mol Biol Cell *12*, 2245-2256.

Smirnova, E., Shurland, D.L., Ryazantsev, S.N., and van der Bliek, A.M. (1998). A human dynamin-related protein controls the distribution of mitochondria. J Cell Biol *143*, 351-358.

Strack, S., Wilson, T.J., and Cribbs, J.T. (2013). Cyclin-dependent kinases regulate splice-specific targeting of dynamin-related protein 1 to microtubules. J Cell Biol *201*, 1037-1051.

Sugiura, A., McLelland, G.L., Fon, E.A., and McBride, H.M. (2014). A new pathway for mitochondrial quality control: mitochondrial-derived vesicles. EMBO J *33*, 2142-2156.

Sun, S.C. (2010). Controlling the fate of NIK: a central stage in noncanonical NF-kappaB signaling. Sci Signal *3*, pe18.

Sun, S.C. (2011). Non-canonical NF-kappaB signaling pathway. Cell Res *21*, 71-85.

Sun, S.C. (2012). The noncanonical NF-kappaB pathway. Immunol Rev *246*, 125-140.

Sun, S.C. (2017). The non-canonical NF-kappaB pathway in immunity and inflammation. Nat Rev Immunol *17*, 545-558.

Swietach, P., Vaughan-Jones, R.D., and Harris, A.L. (2007). Regulation of tumor pH and the role of carbonic anhydrase 9. Cancer Metastasis Rev *26*, 299-310.

Sylla, B.S., Hung, S.C., Davidson, D.M., Hatzivassiliou, E., Malinin, N.L., Wallach, D., Gilmore, T.D., Kieff, E., and Mosialos, G. (1998). Epstein-Barr virus-transforming protein latent infection membrane protein 1 activates transcription factor NF-kappaB through a pathway that includes the NF-kappaB-inducing kinase and the IkappaB kinases IKKalpha and IKKbeta. Proc Natl Acad Sci U S A *95*, 10106-10111.

Taguchi, N., Ishihara, N., Jofuku, A., Oka, T., and Mihara, K. (2007). Mitotic phosphorylation of dynamin-related GTPase Drp1 participates in mitochondrial fission. J Biol Chem *282*, 11521-11529.

Tao, Z., and Ghosh, G. (2012). Understanding NIK regulation from its structure. Structure *20*, 1615-1617.

Tchoghandjian, A., Jennewein, C., Eckhardt, I., Rajalingam, K., and Fulda, S. (2013). Identification of non-canonical NF-kappaB signaling as a critical mediator of Smac mimetic-stimulated migration and invasion of glioblastoma cells. Cell Death Dis *4*, e564.

Thu, Y.M., and Richmond, A. (2010). NF-kappaB inducing kinase: a key regulator in the immune system and in cancer. Cytokine Growth Factor Rev *21*, 213-226.

Thu, Y.M., Su, Y., Yang, J., Splittgerber, R., Na, S., Boyd, A., Mosse, C., Simons, C., and Richmond, A. (2012). NF-kappaB inducing kinase (NIK) modulates melanoma tumorigenesis by regulating expression of pro-survival factors through the beta-catenin pathway. Oncogene *31*, 2580-2592.

Tosatto, A., Sommaggio, R., Kummerow, C., Bentham, R.B., Blacker, T.S., Berecz, T., Duchen, M.R., Rosato, A., Bogeski, I., Szabadkai, G., *et al.* (2016). The mitochondrial calcium uniporter regulates breast cancer progression via HIF-1alpha. EMBO Mol Med *8*, 569-585.

Twig, G., Elorza, A., Molina, A.J., Mohamed, H., Wikstrom, J.D., Walzer, G., Stiles, L., Haigh, S.E., Katz, S., Las, G., *et al.* (2008). Fission and selective fusion govern mitochondrial segregation and elimination by autophagy. EMBO J *27*, 433-446.

Uno, M., Saitoh, Y., Mochida, K., Tsuruyama, E., Kiyono, T., Imoto, I., Inazawa, J., Yuasa, Y., Kubota, T., and Yamaoka, S. (2014). NF-kappaB inducing kinase, a central signaling component of the non-canonical pathway of NF-kappaB, contributes to ovarian cancer progression. PLoS One *9*, e88347.

Vaira, S., Johnson, T., Hirbe, A.C., Alhawagri, M., Anwisye, I., Sammut, B., O'Neal, J., Zou, W., Weilbaecher, K.N., Faccio, R., *et al.* (2008). RelB is the NF-kappaB subunit downstream of NIK responsible for osteoclast differentiation. Proc Natl Acad Sci U S A *105*, 3897-3902.

Valastyan, S., and Weinberg, R.A. (2011). Tumor metastasis: molecular insights and evolving paradigms. Cell *147*, 275-292.

van der Bliek, A.M., Shen, Q., and Kawajiri, S. (2013). Mechanisms of mitochondrial fission and fusion. Cold Spring Harb Perspect Biol *5*.

van Zijl, F., Krupitza, G., and Mikulits, W. (2011). Initial steps of metastasis: cell invasion and endothelial transmigration. Mutat Res *728*, 23-34.

Wang, J., Yi, S., Zhou, J., Zhang, Y., and Guo, F. (2016). The NF-kappaB subunit RelB regulates the migration and invasion abilities and the radio-sensitivity of prostate cancer cells. Int J Oncol *49*, 381-392.

Wang, W., Wang, Y., Long, J., Wang, J., Haudek, S.B., Overbeek, P., Chang, B.H., Schumacker, P.T., and Danesh, F.R. (2012). Mitochondrial fission triggered by hyperglycemia is mediated by ROCK1 activation in podocytes and endothelial cells. Cell Metab *15*, 186-200.

Wang, X., and Schwarz, T.L. (2009). The mechanism of Ca2+ -dependent regulation of kinesin-mediated mitochondrial motility. Cell *136*, 163-174.

Warburg, O.H., Dickens, F., and Kaiser-Wilhelm-Institut für Biologie. (1931). The metabolism of tumours (New York,: R. R. Smith).

Weinberg, F., Hamanaka, R., Wheaton, W.W., Weinberg, S., Joseph, J., Lopez, M., Kalyanaraman, B., Mutlu, G.M., Budinger, G.R., and Chandel, N.S. (2010). Mitochondrial metabolism and ROS generation are essential for Kras-mediated tumorigenicity. Proc Natl Acad Sci U S A *107*, 8788-8793.

Wertz, I.E., and Dixit, V.M. (2010). Signaling to NF-kappaB: regulation by ubiquitination. Cold Spring Harb Perspect Biol *2*, a003350.

Wieder, S.Y., Serasinghe, M.N., Sung, J.C., Choi, D.C., Birge, M.B., Yao, J.L., Bernstein, E., Celebi, J.T., and Chipuk, J.E. (2015). Activation of the Mitochondrial Fragmentation Protein DRP1 Correlates with BRAF(V600E) Melanoma. J Invest Dermatol *135*, 2544-2547.

Willems, P.H., Rossignol, R., Dieteren, C.E., Murphy, M.P., and Koopman, W.J. (2015). Redox Homeostasis and Mitochondrial Dynamics. Cell Metab *22*, 207-218.

Willmann, K.L., Sacco, R., Martins, R., Garncarz, W., Krolo, A., Knapp, S., Bennett, K.L., and Boztug, K. (2016). Expanding the Interactome of the Noncanonical NF-kappaB Signaling Pathway. J Proteome Res *15*, 2900-2909.

Xia, Y., Shen, S., and Verma, I.M. (2014). NF-kappaB, an active player in human cancers. Cancer Immunol Res *2*, 823-830.

Xie, Q., Wu, Q., Horbinski, C.M., Flavahan, W.A., Yang, K., Zhou, W., Dombrowski, S.M., Huang, Z., Fang, X., Shi, Y., *et al.* (2015). Mitochondrial control by DRP1 in brain tumor initiating cells. Nat Neurosci *18*, 501-510.

Xu, W., Jing, L., Wang, Q., Lin, C.C., Chen, X., Diao, J., Liu, Y., and Sun, X. (2015). Bax-PGAM5L-Drp1 complex is required for intrinsic apoptosis execution. Oncotarget *6*, 30017-30034.

Yamada, T., Adachi, Y., Iijima, M., and Sesaki, H. (2016). Making a Division Apparatus on Mitochondria. Trends Biochem Sci *41*, 209-210.

Yamaguchi, N., Ito, T., Azuma, S., Ito, E., Honma, R., Yanagisawa, Y., Nishikawa, A., Kawamura, M., Imai, J., Watanabe, S., *et al.* (2009). Constitutive activation of nuclear factor-kappaB is preferentially involved in the proliferation of basal-like subtype breast cancer cell lines. Cancer Sci *100*, 1668-1674.

Yamamoto, K., Gandin, V., Sasaki, M., McCracken, S., Li, W., Silvester, J.L., Elia, A.J., Wang, F., Wakutani, Y., Alexandrova, R., *et al.* (2014). Largen: a molecular regulator of mammalian cell size control. Mol Cell *53*, 904-915.

Yamamoto, M., Taguchi, Y., Ito-Kureha, T., Semba, K., Yamaguchi, N., and Inoue, J. (2013). NF-kappaB non-cell-autonomously regulates cancer stem cell populations in the basal-like breast cancer subtype. Nat Commun *4*, 2299.

Yang, C., McCoy, K., Davis, J.L., Schmidt-Supprian, M., Sasaki, Y., Faccio, R., and Novack, D.V. (2010). NIK stabilization in osteoclasts results in osteoporosis and enhanced inflammatory osteolysis. PLoS One *5*, e15383.

Yin, L., Wu, L., Wesche, H., Arthur, C.D., White, J.M., Goeddel, D.V., and Schreiber, R.D. (2001). Defective lymphotoxin-beta receptor-induced NF-kappaB transcriptional activity in NIK-deficient mice. Science *291*, 2162-2165.

Young, J.C., Hoogenraad, N.J., and Hartl, F.U. (2003). Molecular chaperones Hsp90 and Hsp70 deliver preproteins to the mitochondrial import receptor Tom70. Cell *112*, 41-50.

Yu, D., and Hung, M.C. (2000). Overexpression of ErbB2 in cancer and ErbB2-targeting strategies. Oncogene *19*, 6115-6121.

Zeng, R., Faccio, R., and Novack, D.V. (2015). Alternative NF-kappaB Regulates RANKL-Induced Osteoclast Differentiation and Mitochondrial Biogenesis via Independent Mechanisms. J Bone Miner Res *30*, 2287-2299.

Zhan, L., Cao, H., Wang, G., Lyu, Y., Sun, X., An, J., Wu, Z., Huang, Q., Liu, B., and Xing, J. (2016). Drp1-mediated mitochondrial fission promotes cell proliferation through crosstalk of p53 and NF-kappaB pathways in hepatocellular carcinoma. Oncotarget *7*, 65001-65011.

Zhang, Y., and Chan, D.C. (2007). New insights into mitochondrial fusion. FEBS Lett *581*, 2168-2173.

Zhao, J., Zhang, J., Yu, M., Xie, Y., Huang, Y., Wolff, D.W., Abel, P.W., and Tu, Y. (2013). Mitochondrial dynamics regulates migration and invasion of breast cancer cells. Oncogene *32*, 4814-4824.